T.R.
ONDOKUZ MAYIS UNIVERSITY
INSTITUTE OF GRADUATE STUDIES
DEPARTMENT OF NANOSCIENCE AND NANOTECHNOLOGY

SYNTHESIS AND CHARACTERIZATION OF SILVER-DOXORUBICIN NANOPARTICLE SYSTEM FOR PH-DEPENDENT RELEASE IN CANCEROUS CELL

Ph.D. Thesis

Güliz AKYÜZ

Supervisor
Prof. Dr. Ömer ANDAÇ

SAMSUN
2022

T.R.
ONDOKUZ MAYIS UNIVERSITY
INSTITUTE OF GRADUATE STUDIES
DEPARTMENT OF NANOSCIENCE AND NANOTECHNOLOGY

SYNTHESIS AND CHARACTERIZATION OF SILVER-DOXORUBICIN NANOPARTICLE SYSTEM FOR PH-DEPENDENT RELEASE IN CANCEROUS CELL

Ph.D. Thesis

Güliz AKYÜZ

Supervisor

Prof. Dr. Ömer ANDAÇ

This thesis was supported by Ondokuz Mayıs University with project number PYO.FEN.1901.18.008.

SAMSUN
2022

ACCEPTANCE AND APPROVAL OF THE THESIS

The study entitled **"SYNTHESIS AND CHARACTERIZATION OF SILVER-DOXORUBICIN NANOPARTICLE SYSTEM FOR PH-DEPENDENT RELEASE IN CANCEROUS CELL"** prepared by **Güliz AKYÜZ**, and supervised by **Prof. Dr. Ömer ANDAÇ**, was found successful and unanimously accepted by committee members as Ph.D. thesis, following the examination on the date 19.7.2022 .

	Title Name SURNAME University Department/Art	**Signature**	**Final Decision**
Chairman	Prof. Dr. Ömer ANDAÇ Ondokuz Mayıs University Department of Chemistry		☒ Accept ☐ Reject
Member	Prof. Dr. Oğuzhan YAVUZ Çukurova University Department of Pharmacology and Toxicology		☒ Accept ☐ Reject
Member	Assoc. Prof. Dr. Begüm YURDAKÖK DİKMEN Ankara University Department of Pharmacology and Toxicology		☒ Accept ☐ Reject
Member	Assoc. Prof. Dr. İsmail ÖÇSOY Erciyes University Department of Analytical Chemistry		☒ Accept ☐ Reject
Member	Assist. Prof. Dr. Aydemir Güralp URAL Samsun University Department of Aerospace Engineering		☒ Accept ☐ Reject

This thesis has been approved by the committee members that already stated above and determined by the Institute Executive Board.

.

APPROVAL
… / … / …
Prof. Dr. Ali BOLAT
Head of Institute of Graduate Studies

.

DECLARATION OF COMPLIANCE WITH SCIENTIFIC ETHIC

I hereby declare and undertake that I complied with scientific ethics and academic rules in all stages of my Master's Thesis , that I have referred to each quotation that I use directly or indirectly in the study and that the works I have used consist of those shown in the sources, that it was written in accordance with the institute writing guide and that the situations stated in the article 3, section 9 of the Regulation for TÜBİTAK Research and Publication Ethics Board were not violated.

Is Ethics Committee Necessary?

Yes ☐ (If it necessary, please add appendices.)

No ☒

15 /08 / 2022

Güliz AKYÜZ

DECLARATION OF THE THESIS STUDY ORIGINALITY REPORT

Thesis Title: SYNTHESIS AND CHARACTERIZATION OF SILVER-DOXORUBICIN NANOPARTICLE SYSTEM FOR PH-DEPENDENT RELEASE IN CANCEROUS CELL

As a result of the originality report taken by me from the plagiarism detection program on 15 /08 / 2022 for the thesis titled above;

Similarity ratio : % 22

Single resource rate : % 2 has been released.

15 /08 / 2022

Prof. Dr. Ömer ANDAÇ

ÖZET

GÜMÜŞ-DOKSORUBİSİN NANOPARÇACIK SİSTEMİNİN SENTEZİ, KARAKTERİZASYONU VE KANSERLİ HÜCREDE PH KONTROLLÜ SALIMININ İNCELENMESİ

Güliz AKYÜZ
Ondokuz Mayıs Üniversitesi
Lisansüstü Eğitim Enstitüsü
Nanobilim ve Nanoteknoloji Ana Bilim Dalı
Doktora, Ağustos/2022
Danışman: Prof. Dr. Ömer ANDAÇ

Bu çalışmada, doksorubisinin (DOX) kemoterapötik etkinliğini artırmak için pH'a duyarlı güdümlü ilaç taşıma sisteminin geliştirilmesi amaçlanmıştır. DOX'un hücre içine taşınmasında işlevsel gümüş nanoparçacıklar (AgNP) kullanılarak ilaç taşıma sistemi (AgNP/HS-PEG5K-NH_2/PAMAMG4/DOX) oluşturulmuştur. Küresel şekilli AgNPler, yeşil sentez yolu ile *Laurocerasus officinalis* Roemer (Rosaceae), yaprakları kullanılarak sentezlenmiş ve belirli koşullar altında optimize edilmiştir. Daha sonra AgNPler, tiyollü ve aminli polietilen glikol (HS-PEG5K-NH_2) ile fonksiyonelleştirilerek AgNP/HS-PEG5K-NH_2 yapısı elde edilmiş ve bu nano-yapı poliamidoamin (PAMAM) G4 dendrimer ile kovalent olarak bağlanmıştır. Son aşamada, DOX amid bağı ile PAMAMG4 ile bağ yapmış ve sonuç olarak AgNP/HS-PEG5K-NH_2/PAMAMG4/DOX pH'a duyarlı güdümlü ilaç taşıma sistemi elde edilmiştir. UV-Vis, FTIR, AAS, XRD, SEM, TEM ve EDS kullanılarak sentezlenen nano yapıların karakterizasyonları tamamlanmıştır. Nano yapının kolloidal stabilitesi için pH ve tuz testi gerçekleştirilmiştir. TEM analizi sonucunda elde edilen görüntülerden AgNP/HS-PEG5K-NH_2/PAMAMG4/DOX'un ortalama boyutu 74 nm olarak hesaplanmıştır. Ayrıca, DOX'un % 80'inin AgNP/HS-PEG5K-NH_2/PAMAMG4'e yüklendiği görülmüştür. DOX salım testleri, fizyolojik pH'da DOX salımının önemsiz derecede olduğunu göstermiştir. Bununla birlikte, pH 6,6 ve pH 4,0'da salımı önemli ölçüde artmıştır. DOX'un 10 günde %33,28, %21,52 ve %7,75'inin sırasıyla pH 4,0, pH 6,6 ve pH 7,4'te salımı *in vitro* olarak gerçekleştirilmiştir. Ayrıca, serbest DOX'un pH 4,0 ve pH 6,6'da 24 saat içinde % 100 salındığı gözlemlenmiştir. Serbest DOX'un pH 7,4'de 10 günün sonunda %71,8 salındığı kaydedilmiştir. AgNP/HS-PEG5K-NH_2/PAMAMG4/DOX'un sitotoksisitesi insan serviks adenokarsinoma hücre hattı (HeLa) üzerinde test edilmiştir. Güdümlü ilaç taşıma sisteminin 24 saat sonunda göstermiş olduğu IC50 değeri 1,66 µg/mL iken serbest DOX IC50 değeri 2,58 µg/mL olarak bulunmuştur. 48 saatlik maruziyetten sonra, AgNP/HS-PEG5K-NH_2/PAMAMG4/DOX için IC50 değeri 1,04 µg/ml ve serbest DOX için 1,34 µg/mL olarak bulunmuştur. Bu sonuçlar, pH'a duyarlı güdümlü ilaç taşıma sisteminin DOX'un etkinliğini artırdığını göstermektedir. Böylelikle, AgNP/HS-PEG-NH_2/PAMAMG4/DOX güdümlü ilaç taşıma sistemi, kanserli bölgedeki DOX'un hücre içi salımına yeni bir bakış getirmektedir.

Anahtar Sözcükler: Gümüş nanoparçacık, Yeşil sentez, Güdümlü ilaç, Kanser tedavisi, HeLa hücresi.

ABSTRACT

SYNTHESIS AND CHARACTERIZATION OF SILVER-DOXORUBICIN NANOPARTICLE SYSTEM FOR PH-DEPENDENT RELEASE IN CANCEROUS CELL

Güliz AKYÜZ
Ondokuz Mayıs University
Institute of Graduate Studies
Department of Nanoscience and Nanotechnology
Ph.D, August/2022
Supervisor: Prof. Dr. Ömer ANDAÇ

A pH responsive targeted drug delivery system has been designed to change the cellular uptake and chemotherapeutic efficiency of doxorubicin (DOX). The nano-system contains of multifunctional silver nanoparticles (AgNPs) based drug carrier system (AgNP/HS-PEG5K-NH_2/PAMAMG4/DOX) as a new aspect for intracellular transport of doxorubicin (DOX). AgNPs were produced by a green chemistry pathway using *Laurocerasus officinalis* Roemer (Rosaceae) leaves and, optimized under certain conditions. Then, AgNPs was functionalized with thiolated polyethylene glycol (HS-PEG5K-NH_2). In the next step, AgNP/HS-PEG5K-NH_2 was covalently conjugated with a polyamidoamine (PAMAM)G4 dendrimer. Moreover, conjugation of DOX to the PAMAMG4 via amide bond outcomed in AgNP/HS-PEG5K-NH_2/PAMAMG4/DOX pH sensitive targeted drug delivery system. Characterization studies were conducted by UV-Vis, FTIR, AAS, XRD, SEM, TEM and EDS. The pH and salt test were also, carried out for the colloidal stability of nano-structure. The average diameter of the AgNP/HS-PEG5K-NH_2/PAMAMG4/DOX was found to be 74 nm. Also, 80 % of DOX was loaded into the AgNP/HS-PEG5K-NH_2/PAMAMG4. Acellular DOX release tests showed that drug released from AgNP/HS-PEG5K-NH_2/PAMAMG4/DOX at pH 7.4 was insignificant. However, it was remarkably increased at a pH 6.6 and pH 4.0. *In vitro* drug release studies indicated that 33.28 %, 21.52 % and 7.75 % of the conjugated DOX was released from the nano system for pH 4.0, pH 6.6 and pH 7.4, respectively, in ten days. Whereas, 100 % of free DOX was released in the 24 hours for pH 4.0 and pH 6.6. In the pH 7. 4, only 71.8 % of free-DOX was released at the end of the 10 days. The cytotoxicity of AgNP/HS-PEG5K-NH_2/PAMAMG4/DOX was tested on Human cervix adenocarcinoma cell line (HeLa). The nano system possessed the IC50 of 1.66 µg/mL in 24 hours, notably lower than that of the free DOX which had the IC50 of 2.58 µg/mL in 24 hours. After 48 hours of exposure, the AgNP/HS-PEG5K-NH_2/PAMAMG4/DOX showed the IC50 of 1.04 µg/ml compared to 1.34 µg/mL for the free DOX. These results indicate that the pH sensitive targeted drug delivery system upgrades the efficacy of the free DOX. Thus, the AgNP/HS-PEG-NH_2/PAMAMG4/DOX targeted drug delivery system could allow a new principle for the intracellular release of DOX at the cancerous area.

Keywords: Silver nanoparticles, Green synthesis, Targeted drug delivery, Cancer therapy, HeLa Cell.

To my family

ACKNOWLEDGEMENT

I would like to express my deepest gratitude to my supervisor Prof. Dr. Ömer ANDAÇ for his academic support that made this thesis possible, for his suggestions, encouraging guidance, criticism and for keeping me focused throughout the study. Also, I appreciate the opportunity to be a part of an amazing research group headed by Prof. Dr. Ömer ANDAÇ.

Also, I want to specially thank to Prof. Dr. Müberra ANDAÇ for her support, kindness and valuable advices during my academic career.

I would like to thank the jury members, Prof. Dr. Oğuzhan YAVUZ, Assist. Prof. Dr. Aydemir Güralp URAL, Assoc. Prof. Dr. Begüm YURDAKÖK DİKMEN and Assoc. Prof. Dr. İsmail ÖÇSOY who took their most valuable time to read this study. It is an honour to receive suggestions and criticisms from them about my research.

My thanks go to Prof. Dr. Sadettin TURHAN, Assoc. Prof. Dr. Nebahat Şule ÜSTÜN, Assoc. Prof. Dr. Hilal AY and Prof. Dr. Metin AYDIN for their support, guidance and for providing me facilities during my career.

Also, I would like to thank to Prof. Dr. Hasan KORKMAZ who identified the plant material for the study.

My thanks are extended to my research colleague Dr. Orhan TOKUR who helped and contributed cell experiments with a pleasant brain storms.

My special thanks also go to Assoc. Prof. Dr. Ayça GENÇ and Assist. Prof. Dr. Sema BAYRAKTAR who have made my life easier with their encouraging attitude, friendship and the precious times we have spent together.

I would sincerely thank to Dr. Yasemin AK for her endless encouragement and helps in all parts of my life.

I would also like to express my warmest thanks to my sister Gülin Deniz for sharing with me priceless engineering ideas and always being there for me. Finally, I would like to dedicate this work to my dear mom and dad for their endless love, support, belief and patience in me and for making those tough times much easier. Words are incapable to express my deepest gratitude and my infinite love to my family. I am so lucky to have them.

I would like to acknowledge the 100/2000 YOK National PhD Scholarship Program for supporting me in the field of Targeted Drugs.

I would also like to acknowledge the Scientific and Technological Research Council of Turkey (TÜBİTAK) for their support within the scope of the 2211-C TÜBITAK National PhD Scholarship Program in the Priority Fields in Science and Technology.

This study was supported by Ondokuz Mayıs University Research Foundation (BAP) Project (PYO.FEN.1901.18.008).

Güliz AKYÜZ

CONTENTS

SYMBOLS AND ABBREVIATIONS

AAS	: Atomic Absorption Spectroscopy
$AgNO_3$	: Silver Nitrate
AgNP	: Silver Nanoparticle
ANOVA	: Analysis of Variance
DIPEA	: N,N-Diisopropyl Ethylamine
DOX	: Doxorubicin Hydrochloride
E	: Extract
EDC.HCl	: 1-Ethyl-3-(3-Dimethylaminopropyl) Carbodimide
EDS	: Energy Dispersive Spectroscopy
EMEM	: Eagle's Minimum Essential Medium
EPR	: Enhanced Permeability and Retention
FBS	: Fetal Bovine Serum
FTIR	: Fourier Transform Infrared Spectroscopy
HeLa	: Human Cervix Adenocarcinoma Cell Line
H_2O	: Water
HS-PEG5K-NH_2	: Thiol-PEG-Amine
IC	: Inhibitor Concentrations
M	: Maturity of the *L. officinalis* Leaves
Ma	: Mature
Mi	: Mixed
NaCl	: Sodium Chloride
NaOH	: Sodium Hydroxide
NEAA	: Non-Essential Amino Acids
NHS	: N-Hydroxysulfosuccinimide
PAMAM	: Polyamidoamine
PBS	: Phosphate Buffered Saline
PEG	: Polyethylene Glycol
RES	: Reticuloendothelial System
SEM	: Scanning Electron Microscopy
T	: Extraction Temperature
TEM	: Transmission Electron Microscopy

WST-8	: 2-(2-Methoxy-4-Nitrophenyl)-3-(4-Nitrophenyl)-5-(2,4-Disulfophenyl)-2h TetrazoliumMono-SodiumSalt
X	: Volume of the Water Used for Extraction
XRD	: X-ray powder diffraction
Y	: Young

FIGURES LEGENDS

TABLES LEGENDS

1. INTRODUCTION

Cancer is generic term for the uncontrolled growth of abnormal cells in the body and, it can progress rapidly and uncontrollably. Various treatment methods such as chemotherapy, photothermal, photodynamic, hormone and gene therapy, surgery and radiation are preferred options for cancer cases (Bray et al., 2018; Fadaka et al., 2017; Siegel, Miller, FuchsandJemal, 2021). However, these strategies fail to control advanced metastatic tumours and also toxic adverse effects inevitably occur in healthy cells, tissues and organs during the treatment (Huda, AlamandSharma, 2020; Kumari, GhoshandBiswas, 2016; Tian, Xin, Wu, GuanandZhou, 2022). Further, multidrug resistance, low circulation half-life, less therapeutic index, biodistribution problems and low selectivity for cancerous cells can be listed as critical disadvantages of conventional treatments (Manchun, DassandSriamornsak, 2012; Z. Wang et al., 2018; Zou et al., 2020). Therefore, research for alternative therapeutic approaches are necessary.

In the recent years, novel nanotechnological applications in various biomedical fields are used to enhance the efficacy of the cancer therapy. Changing the pharmacodynamics and pharmacokinetics of active drugs via nanoscience is an important aspect. Drug delivery systems have led to a new strategy for targeting tumours by development of nanotechnology. Drug delivery systems reach the target and, cancer drug releases under certain conditions. As a result, efficacy of the drug increases (Raj et al., 2021; Z. Wang et al., 2018).

Moreover, nanoparticle-based drug delivery systems are used for their good carrier properties and, their extending time in the blood circulation can be prolonged with modifications (B. Bahrami et al., 2017; Kumari et al., 2016; Raj et al., 2021; Z. Wang et al., 2018). Also, concentration of the drug in the cancerous area can be adjusted with the modified nanoparticles. If drug releases too slow, cancer cells may gain the resistance to the cancer drug. When there is a fast drug release before reaching the cancer cells, the toxic side effects can be occurred. (Blanco, ShenandFerrari, 2015; El-HammadiandArias, 2022). For this reason, the controlled release becomes one of the major important factors of the targeted drug delivery systems. (Blanco et al., 2015; El-HammadiandArias, 2022; Raj et al., 2021; Z. Wang et al., 2018). The controlled release of the drug in the target area has been a subject extensively researched in the recent years.

Drug delivery systems which are sensitive to external factors (electrochemical triggers, temperature, light and ultrasound) or sensitive to cancer microenvironment (redox properties, pH and enzyme activity) are being investigated to overcome their release problems (Cao et al., 2019; Corma, BotellaandRivero-Buceta, 2022; El-HammadiandArias, 2022; Y. Wang, Shim, Levinson, SungandXia, 2014).

Reshma et al., (2019) synthesized paclitaxel-loaded galactoxyloglucan nanoparticles and, tested them to prevent drug resistance caused by lung cancer cells. Drug release from the system was studied in the different pH ranges at pH 7.4, pH 6.4 and pH 5.4. Also, cell experiments showed that the prepared nanoparticle-based system prevented multidrug resistance and caused apoptotic cell death. The system has been shown more effective on resistant cancer cells than a single usage of paclitaxel (Reshma et al., 2019). Bahrami et al., (2020) synthesized two different nano-silica which are sensitive to hydrogen peroxide (ROS component) and dithiothreitol (redox agent) in the cancer cell environment. Hyaluronic acid was used as a functionalizing and targeting agent. Results showed that the selective drug release to stimuli in the cancer cell environment is 50 % higher than the release in the environment without redox features. It has been reported that the release ratio of doxorubicin (DOX) varies depending on the concentrations of the components in the cell medium (F. Bahrami, Abdekhodaie, BehrooziandMehrvar, 2020). Chiang et al., (2015) studied the loaded anticancer drug camptothecin (CPT) into micelles sensitive to glutathione (GSH) and reactive oxygen species (ROS). CPT release was performed in cancer cells media rich in H_2O_2 or GSH. Results showed that CPT-loaded double redox-sensitive micelles remained stable at low levels of GSH and ROS in the bloodstream. CPT-loaded double redox-sensitive micelles were found to have high *in vivo* antitumor activity. GSH and ROS dual redox-sensitive micelles have been reported to have potential use in various cancer therapies (Chiang, YenandLo, 2015). Banghbani and Moztarzadeh (2017) synthesized a nano-alginate drug delivery system for doxorubicin/turmeric delivery to cancer cells. Drug release from the system was triggered by sonication. The release of DOX-curcumin from the nanosystem showed cytotoxicity on ovarian cancer cells. Tumor shrinkage has been reported in advanced stages (BaghbaniandMoztarzadeh, 2017). As seen in these studies, the effectiveness of cancer treatment is increased with the development of controlled release systems. Also, targeting mechanisms are used for the reaching the cancer region of the body and the drug releases in a controlled

manner. Release mechanisms of cancer drug from the drug delivery system are classified as physical, active and passive targeting.

In physical targeting, it is possible to direct nano drug delivery systems to a specific target region with external factors. External stimulation, such as radiation and magnetic fields are used for physical targeting. Using external magnets, some superparamagnetic iron oxide nanoparticles are studied for physical targeting. It is possible to navigate the nanoparticles to a specific site (Danhier, FeronandPreat, 2010; Yu et al., 2016). Xie et al., (2014) developed magnetic nanocrystals. Simultaneous diagnosis and therapy of tumours using magnetic field (ACMF) and magnetic resonance have been investigated. Mn-Zn ferrite nanosystem modified with PEG phospholipids was synthesized. The nanosystem was administered to mice with breast cancer cells by injection at 18 mg Fe/kg mouse body weight. It was applied to the tumour area at 43 °C for 30 minutes (ACMF: 390 kHz, 12 A). It has been reported that the application can suppress tumour growth over a certain period of time (Xie et al., 2014).

In the active targeting mechanism, there are three stages. In the first step, the nano-system recognizes the target, in the second step it binds to the target, and in the last step, controlled drug release is performed (Dutta, BarickandHassan, 2021). The drug delivery system is further enhanced by the ligand-receptor interaction after reaching the target area via enhanced permeability and retention (EPR) effect from the bloodstream. The method performed by using the key-lock relationship between ligand and receptors is called active targeting. Features such as excess vascular permeability, rapid growth of tumour vessels, and poor structural integrity distinguish the physiology of most tumours from those of normal tissues and organs. Thus, nano-structured drug delivery systems leak the region through permeable tumour vessels and adhere to the tumour bed due to low lymphatic drainage. So, this process is called the EPR effect (Dutta et al., 2021; Helmy et al., 2021; Nandi, OnyesomandDouroumis, 2021). In the previous studies, the activities of small molecules, proteins, aptamers, cell penetration peptides, sugars, monoclonal antibodies and their specific receptors as active targeting ligands have been reported on many cancer cells. For example, folic acid, transferrin, arginine-glycine-aspartate (RGD/integrin receptor), lactobionic acid (acialoglycoprotein receptor) and AS1411 aptamer ligands were modified to the surface of the nanosystems and, used as active targeting agents (GochevaandIvanova,

2019; Nandi et al., 2021; Prabhuraj, Bomb, SrivastavaandBandyopadhyaya, 2020).

In the passive targeting mechanism, the EPR effect is primarily used. As it is well known, most of the solid tumours possess remarkable number of tumour vascular permeability factor, low structural integrity of tumour blood vessels and the fast growth (Kalyane et al., 2019; Theek et al., 2014; Tsujimoto et al., 2021). Also, the growing solid tumour vascular permeability has a pore cut-off-size of 200 nm to 1.2 μm (Fan Yuan, 1995a; Susan K. Hobbs, 1998; Z. Wang et al., 2018). This physiological difference provides lots of nutrients and oxygen for the cancer cells. However, the nanoparticle based targeted drug delivery systems have a diameter in range of 60 to 500 nm (Huang, Sun, HuangandChen, 2021; Z. Wang et al., 2018). So, nanoparticle-based drug delivery systems are small enough to pass through cancerous cell membranes. They can carry drugs to the target cells via EPR effect and, drug releases through changes in the cell microenvironment (pH, redox or enzymatic) (Cao et al., 2019; Kalyane et al., 2019; Theek et al., 2014; Tsujimoto et al., 2021; Y. Wang et al., 2014).

Recent studies in the literature, especially targeted drug delivery systems which possess pH responsive nanomaterials have been attracted much attention among these stimulus sensitive systems (Bami, Raeisi Estabragh, Khazaeli, OhadiandDehghannoudeh, 2021; Cao et al., 2019; Z. Wang et al., 2018). The release of the drug from the pH responsive system can be triggered by the low pH values of the cancer cells because cancer cell energy generation pathway is partly different from that of the healthy cells. The energy is mainly derived from glycolysis. It is the main source for the energy production and, lactic acid can be produced by the cancer cells even in normoxic condition (Diaz-Ruiz, RigouletandDevin, 2011; Fadaka et al., 2017; Warburg, 1956a). Thus, the abnormality of extreme glycolysis causes the acidic pH (Fadaka et al., 2017). The interstitial cells of the cancer tissue are weakly acidic (lower than pH 7.0). However, the healthy cells, tissue and the extracellular pH in the blood remains constant at physiological pH (almost pH 7.4) (Fadaka et al., 2017; J. Haveman and H. S. Reinhold J. L. Wike-Hooley, 1984; Z. Wang et al., 2018). After the drug delivery system reach the target side via the EPR effect, the drug is carried through the endosomes (pH 5.5 – 6.0)/lysosomal (pH 5.0) transportation (Constantin et al., 2021; Z. Wang et al., 2018). In this process, drug delivery system responses to acidic condition and, drug releases.

Using passive targeting, Long et al., (2020) modified the drug delivery system consisting of MoS_2 (Molybdenum disulfide) nanoparticles with hydrazine groups that can form bonds with PEG and DOX. Drug release was tested at pH 5.4 and pH 7.2 for 72 hours (Long et al., 2020). It has been reported that the slow release of DOX from the system can kill cancer cells. Besides, Li et al., (2020) reported that multiporous silica nanoparticles (MSN-NH_2) loaded with 5-fluorouracil (5-FU). For 5-FU encapsulation, the system was coated with pullulan using the Schiff base reaction. Since the bond between MSN and pullulan tends to hydrolyze under acidic conditions, the encapsulated 5-FU was easily released from the structure in acidic conditions. Drug release was achieved at pH 5.5, pH 6.8 and pH 7.4 (37 °C) (S. Li et al., 2020).

Nano sized drug delivery systems are also designed and improved by conjugation or encapsulation of active cancer drugs with a nanoparticle. The basic aim in the development of targeted nanocarriers are certain drug targeting and delivery, greater safety and biocompatibility and developed pharmacokinetic behaviour. In the literature, there are also combinations with systems containing metal nanoparticles are used in cancer treatment. Mn (H. Ma et al., 2022), Ru(II) (M. Yang et al., 2021), Cu (Nakhaeepour, Mashreghi, Matin, NakhaeiPourandHousaindokht, 2019), Au (KhutaleandCasey, 2017), Mn-Zn (Xie et al., 2014) and Ag (F. Benyettou, 2013; Hepokur et al., 2019; L. Yang et al., 2018) are some of the metals that have been used for drug delivery studies.

Recently, silver nanoparticles (AgNPs) have attracted great attention for drug delivery systems because of their special properties such as antineoplastic, antibacterial, antifungal and antiviral effects. In particular, pH-sensitive drug delivery systems using passive targeting are being investigated for AgNP based drug delivery systems. Benyettou et al., (2013) applied microwave in the synthesis of AgNPs. Bisphosphonate and rhodamine were used for functionalization of AgNPs. The system was tested on HeLa cell line by loading DOX and alendronate (Ald) (F. Benyettou, 2013). The imine bond in DOX-modified nanoparticles was used for the release of DOX in acid medium. It has been reported that the anticancer activity of the nano system is higher than the use of DOX and Ald alone (S. Iravani, 2014). Also, Sakr et al., (2018) synthesized AgNPs reduced by polyethylene glycol with the I-131 radionuclide tumor probe. It has been reported that the system didn't show a toxic effect on healthy cells but showed accumulation of radioactivity in tumor areas (Sakr

et al., 2018). Hepokur et al., (2019) evaluated the effect of capecitabine-loaded silver particles on human breast cancer cells (MCF-7). They synthesized the AgNPs in different sizes (5, 10, 15 and 30 nm). The ones with a size of 10 nm show the lowest toxic effect. IC 50 value was found to be 31.25 μg/mL against on MCF-7 cells after 24 hours (Hepokur et al., 2019).

There are physical, chemical, and biological synthesis routes for the production of AgNPs. Evaporation-condensation applications are examples of physical production methods. The physical synthesis of AgNPs using a tube furnace at atmospheric pressure for evaporation-condensation has some drawbacks. For instance, the tube furnace covers a large area, consumes a large quantity of energy, raises the ambient temperature around the source material and wants much time to reach thermal stability (S. Iravani, 2014). It is also possible to obtain AgNPs by chemical synthesis using organic and inorganic reducing agents. For this purpose, different reducing agents such as sodium citrate, sodium borohydrid, elemental hydrogen, tollens reagent and N,N-dimethylformamide are used to reduce the silver ion (S. Iravani, 2014). There are some difficulties in the density of toxic components in the synthesis medium and their removal from the system.

For this reasons, green synthesis method has attracted attention under the title of biological synthesis applications, which is an alternative production method in the recent years. This method does not require the use of toxic chemicals and solvents for AgNP synthesis (Hekmati, Hasanirad, KhalediandEsmaeili, 2020; TamilarasiandMeena, 2020).

With the green synthesis method, AgNPs with antineoplastic, antibacterial, antifungal and antiviral properties are easily obtained as a system carrier. It is also possible to eliminate the toxic effect caused by chemical methods and the loss of energy and time in physical methods (Mehta, ChhajlaniandShrivastava, 2017; MelkamuandBitew, 2021; Rajkumar, EzhumalaiandGnanadesigan, 2021; Rolim et al., 2019; Tailor, Yadav, Chaudhary, JoshiandSuvalka, 2020; Yousaf, Mehmood, AhmadandRaffi, 2020; Zarei, RazmjoueandKarimi, 2020) .

Biological systems (microorganisms etc.) and plant extracts are used for producing AgNPs. For preparing plant extracts; peels, fruits, rhizomes, leaves or whole plant can be used easily. The extract and silver nitrate solution are mixed under optimized conditions. AgNPs are occurred by the reducing from Ag^{+} to Ag^{0}. The

formation of AgNPs is followed by a colour change (Banala, NagatiandKarnati, 2015; Díaz-Cruz, Alonso Nuñez, Espinoza-GómezandFlores-López, 2016; DuttandUpadhyay, 2018; Guan et al., 2022; Jagpreet Singh, 2016; Kambale et al., 2020; Krishnaraj, Ramachandran, MohanandKalaichelvan, 2012).

AgNPs need to be keep away from the blood circulation before reaching the target. Hence, one of the most significant roles of the nanosized drug delivery systems is the enhanced circulation time in the blood. The most common method is using a surface modification of nanoparticles by a biocompatible polymer, such as polyethyleneglycol (PEG). So, it can be possible to avoid the detection and removing of the nanoparticle by the reticuloendothelial system (RES) (B. Bahrami et al., 2017; Kumari et al., 2016; Raj et al., 2021; Z. Wang et al., 2018). PEG is flexible, hydrophilic and neutral polymer that can act as a dispersant because of its ability to bind water. PEG protect the AgNPs from phagocytosis. It reduces the toxicity and increases the lifetime of the drug delivery system in the blood circulation. Besides, it enhances the nanoparticle penetration into the mucus layer (Bastos et al., 2016; Díaz-Cruz et al., 2016; He et al., 2014; HuckabyandLai, 2018; Knop, Hoogenboom, FischerandSchubert, 2010; Mishra, NayakandDey, 2016; Rolim et al., 2019). So, the pharmacokinetic behaviour of the drug delivery system is improved. In addition, modifying AgNPs with a biocompatible polymer prevents charge-dependent interactions with molecules such as proteins in the body (Jokerst, Lobovkina, ZareandGambhir, 2011).

After functionalization of the nanoparticle with polymers, the drug is loaded into the structure and is expected to be released effectively. At this stage, structures are preferred suitable for branched and covalently bonding also, responsive to low pH properties. Dendrimers are the one of the promising structures for this purpose. They are highly branched three-dimensional structures which are synthesized by mono dispersed of macro molecules. These unique molecules have great functions owing to their great molecular structure. They can be used wide range of biomedical and industrial applications. In general, dendrimers are good and efficient choices for the drug loading step (R. Ahmed, Aucamp, EbrahimandSamsodien, 2021; Ciolkowski et al., 2012; Elfiyani, SrifianaandAl Rasyied, 2018; Jiang et al., 2010; Tsujimoto et al., 2021; ZhaoandLi, 2011). Pan et al., reported that functionalized of activated PEG2000 with polyamidoamine (PAMAM) G3 dendrimer. Besides, they encapsulated

methotrexate into the synthesized structure and drug release study was investigated at 37 C in a tube containing 30 mL of a Tris-HCl-buffer (pH 7.4) (Pan, Lemmouchi, AkalaandBakare, 2016). Also, Kurtoglu et al. (2010), reported the ibuprofen release from PAMAMG4 dendrimer. Ibuprofen was bonded via amide, ester and peptide linkers. Additionally, a linear PEG5000–ibuprofen structure was investigated on drug release kinetics (Kurtoglu, Mishra, KannanandKannan, 2010).

In the literature novel nano-structures with functionalization applications and targeted drug delivery systems of those with different release mechanisms have been studied (F. Benyettou, 2013; Jose et al., 2019; Mohamed, 2020; Xie et al., 2014; L. Yang et al., 2018). Especially, for cancer cell targeting, pH responsive nano-drug delivery systems which contain passive targeting mechanism have attracted attention (KhutaleandCasey, 2017; Miranda, SampaioandZucolotto, 2022; Saravanakumar et al., 2021; Z. Wang et al., 2018; Xie et al., 2018). However potential disadvantages such as the possible toxicity of the synthesis methods, and the biocompatibility of the nano structures are questionable. Therefore, in this thesis, it was aimed to use green chemistry approach which is less costly with fewer side effects and different from the existing examples in the literature.

It was planned to design, synthesize and characterize silver-PAMAM-Doxorubicin pH-responsive drug delivery system. AgNPs were synthesized by fresh *Laurocerasus officinalis* Roemer (Rosaceae) leaves extract and this study is original by producing the AgNPs via green synthesis pathway in the pH-targeted drug delivery systems. It was reported that *L. officinalis* leaves extract had antispasmodic, analgesic, anti-nausea and cough suppressant properties (EMEA, 2000). Jeong et al., (2009) tested low-dose quercetin for cancer cell inhibition. They reported that quercetin induced the p21 CDK inhibitor with a simultaneous decrease in the phosphorylation of pRb, inhibiting the G1/S cell cycle by capturing E2F1 (Jeong, An, Kwon, RheeandLee, 2009). On the other hand, anticancer mechanism of kaempferol, data on the regulation of apoptosis, and its effectiveness in various cancer cell lines such as colon and leukemia have been reported (KimandChoi, 2013). It was planned to use the advantageous effect of the *L. officinalis* leaves extract composition, in which silver nanoparticles were synthesized, on cancerous cells.

It has also been revealed that AgNPs can significantly induce apoptosis or necrosis in different cell types (Hussain, Hess, Gearhart, GeissandSchlager, 2005; J.

Ma, LuandHuang, 2011; Nirmala et al., 2012). Structural changes in DNA caused by the synergistic effects of AgNPs and DOX were investigated on human breast cancer cell lines (T47D and MCF7). DOX and AgNPs appeared to interact more strongly with DNA compared to AgNPs or DOX alone. It has also been reported that this combination is not toxic to human endometrial stem cell proliferation (Hekmat, SabouryandDivsalar, 2012).

In this thesis, the anticancer efficiency of the drug delivery system aimed to increase via the synergistic effect of AgNPs and DOX. AgNP-PEG-PAMAMG4-DOX structure is used in pH-responsive drug delivery system first time. It was also planned that AgNPs were functionalized with a biocompatible polymer HS-PEG5K-NH_2. After this process, PAMAMG4 dendrimers was added into the prepared system. Then, DOX was covalently bonded via amide linkage with PAMAMG4 dendrimers. Characterization of the drug delivery system was performed. Also, the efficiency of drug binding was calculated. The pH and salt studies were carried out to test the colloidal stability of drug delivery system. In the next step, the pH dependent *in vitro* drug release was verified using in phosphate buffer solutions at pH 4.0, pH 6.6 and pH 7.4. The drug release was monitored as a function of time for 240 hours. Besides, drug release profile was observed in cancerous cell line. HeLa (human cervical adenocarcinoma) cell lines were used in cell culture applications. As known, HeLa cells have resemblance and commonality of marker chromosomes with the bona fide breast cancer cell lines. HeLa cells were found to be extremely durable and productive. Thus, it is used extensively in scientific researches (Pathak, 2021). Cell stocks that came in frozen form were properly thawed and sub-cultured. After sufficient cell production, the efficacy of nanoparticle-drug combinations was determined by the WST-8 cell viability test.

Overall, it is planned that the system will take the place of other nanoparticle-based pH-targeted methods and make it possible to use it in the treatment process in the future.

2. SUMMARY OF LITERATURE REVIEW

Herein, latest advances of medicine in nanotechnology, nanomaterials, design and synthesis of targeted drug delivery systems were highlighted.

2.1. Nanotechnological Approaches for Cancer Treatment

Currently first line options for cancer treatment are surgery, radiotherapy and chemotherapy or followed by combination of them (Delaney, Jacob, FeatherstoneandBarton, 2005; Dos Santos, De Almeida, Terra, BaptistaandLabriola, 2019; Elnair, ChoateandJamous, 2018; Maes-Carballo et al., 2020; Schirrmacher, 2019).

Patient preferences, tumour-subtype and anatomic cancer stage are the important factors for the optimal treatment. For example, debulking surgery, neoadjuvant therapy, chemotherapeutic agents, intraperitoneal chemotherapy and vitamin-D are the standard therapies for ovarian cancer (Stewart, RalyeaandLockwood, 2019). For breast cancer, surgery, radiation, endocrine therapy and chemotherapy or their combinations are preferred (WaksandWiner, 2019). Pancreatic cancer treatment includes pre-operative biliary drainage, anastomotic technique, minimally invasive surgery, vascular resection, adjuvant chemotherapy, neo-adjuvant therapy (McGuigan et al., 2018). Further, surgery, radiation, androgen deprivation therapy, vaccines and traditional hormonal therapy are used for prostate cancer (LitwinandTan, 2017). However, these therapies are failing to cure metastatic tumours which have occurred in distant organs. Also, nonspecific targeting properties of traditional cancer therapies cause adverse effects on the healthy tissues (Schirrmacher, 2019). Even though concentration, solubility, biodistribution, toxicity problems and multiple drug resistance are the challenges of the conventional cancer drugs (KhutaleandCasey, 2017; Kumari et al., 2016). Therefore, alternative cancer therapeutics which are selective to target and, have the controlled release mechanisms are necessity.

Use of nanotechnology especially in the drug delivery applications has attracted much attention. The medical application of nanotechnology for diagnosis and treatment of cancer is mostly at the development stage. However, there are several nanomedicines in the market and many more have phase studies (Sanna, PalaandSechi, 2014; Wicki, Witzigmann, BalasubramanianandHuwyler, 2015). Nanomedicine can be defined as the medical application of nanotechnology. Furthermore, it has the ability

to allow early determination and prevention and, to compulsively improve diagnosis, treatment and following of many diseases. (De LazaroandMooney, 2021; Souri et al., 2022).

Recent advances in biotechnology and emerging drug technology have made significant progress in effective drug design and delivery systems in cancer treatment. The use of nano-sized structures for cancerous site, comes down to their ability to be readily modified and easily regulated. Also, developing therapeutics with novel functionalized nanoparticles improve the pharmaceutical ingredients effectiveness (Souri et al., 2022). Nano-sized drugs that are currently produced for the treatment of cancer are reported by several researchers (Sanna et al., 2014). DaunoXome-Daunorubicin, Myocet-Doxorubicin, Onco TCS-Vincristine, Depocyt-Cytarabine, Doxil/Caelyx-Doxorubicin, Thermodox-Doxorubicin, Genexol-PM-Paclitaxel, Opaxio-Paclitaxel, ProLindac-DACH-Pt, Abraxane-Paclitaxel, Paclical-Paclitaxel and Oncaspar-Asparagine specific enzyme are the examples that have the phase studies (Sanna et al., 2014). These products and their owner companies are listed in Table 2.1. It was seen that they were functionalized with liposomes and modified liposomes with polyethylenglycol, polyethylenglycol-poly(lacticacid), polyglutamicacid, hydroxypropylmethacrylamide, micellar retinoid derived and polyethylenglycol L-asparaginase (Sanna et al., 2014). However, their ability in controlled release for the target cell is questionable. The important point should be targeting the cancerous cells, not the healthy cells. Only the nano-sized production is not enough for treatment. It is important to design targeted drug delivery systems that are selective towards the target. However, several companies are currently running phase studies for targeting drug delivery systems. They are aimed to increase bioavailability, controlled drug delivery, specification of the target and reducing toxicity. Polymer-based and liposome-based carriers in preclinical trials for targeting the cancerous tissues are listed in Table 2.2 (Wicki et al., 2015).

Generally, nano-drug delivery systems are designed and developed by encapsulating, conjugating or entrapping active drugs into a nanoparticle-based system. In this way, it is aimed to reach the targeted area in a controlled manner and release the drug effectively. Due to their chemical structure, these drugs are not metabolized and are not released in the healthy cells. The drug reaches the target area effectively and does not cause toxic side effects in the body due to the release

mechanisms. In addition, multi drug resistance can be prevented by the controlled release (GilletandGottesman, 2010; Kumari et al., 2016; Souri et al., 2022).

Table 2.1. The nano-drugs that have phase studies in the therapy of cancer (Sanna et al., 2014)

Product	**Active Ingredient**	**Company**
DaunoXome	Daunorubicin	Galen US
Myocet	Doxorubicin	Sopherion Therapeutics
Onco TCS	Vincristine	Inex Pharmaceuticals
Depocyt	Cytarabine	Pacira Pharmaceuticals
Doxil/Caelyx	Doxorubicin	Janssen Biotech Inc
Thermodox	Doxorubicin	Celsion Corporation
Genexol-PM	Paclitaxel	Samyang Biopharmaceuticals
Opaxio	Paclitaxel	Cell Therapeutics
ProLindac	DACH-Pt	Access Pharmaceuticals
Abraxane	Paclitaxel	Celgene Corporation
Paclical	Paclitaxel	Oasmia Pharmaceutical
Oncaspar	Asparagine specific enzyme	Enzon Pharmaceuticals

Table 2.2. The active targeted drugs with ligands that have phase studies in the treatment of cancer (Wicki et al., 2015)

Product	**Target**	**Active Ingredient**	**Company**
PK2-FCE28069	Lectin	Doxorubicin	Pfizer
2B3-101	Glutathione	Doxorubicin	To-BBB
MBP-426	Transferrin	Oxaliplatin	Mebiopharm
MCC-465	Fragment GAH	Doxorubicin	Mitsubishi Pharma
MM-302	Antibody	Doxorubicin	Merrimack
SGT-53	Transferrin	Plasmid-DNA	SynerGeneTherapeutics
BIND-014	Aptamer	Docetaxel	Bind Therapeutics
SP1049C	P-Glycoprotein	Doxorubicin	Supratek Pharma

Therefore, the controlled release of the drug in the target area has been broadly researched in the last years. Drug delivery systems which are sensitive to external factors (light, temperature, ultrasound, electrochemical triggers) or sensitive to tumour microenvironment (pH, enzyme activity, redox properties) are being investigated to overcome their release problems (Felber, DufresneandLeroux, 2012; Fleige, QuadirandHaag, 2012; Y. Liu, Wang, Yang, ZhouandSun, 2013; Rapoport, 2007; TavanoandMuzzalupo, 2016; Thornton, McConnellandUlijn, 2005).

Hassanpour et al., (2021) synthesized salicylic acid/ionotropic gelation of

chitosan nanoparticles with the average size about 170–180 nm. Salicylic acid release was found to be 68 % in pH 5.5 and 31 % in pH 7.4. Finally, the cytotoxic effects of salicylic acid and nanoparticle based-salicylic acid were studied *in vitro* for breast cancer cell lines (MDA-MB-231). Results showed that salicylic acid loaded nanoparticle system was more cytotoxic for cancer cells than free salicylic acid (Hassanpour et al., 2021). Also, Zhai et al., (2018) studied on lipid-based nanoparticles as paclitaxel carriers. System was functionalised with antiEGFR aptamer for active targeting which were able to enhance its antitumor influence against ovarian cancer cell lines *in vitro*. Paclitaxel loaded nanoparticles had significantly higher cytotoxicity than a free paclitaxel against the ovarian cancer cell lines (Zhai et al., 2018). Ghosh et al., (2022) synthesized nanosized 3-carboxy-phenyl boronic acid conjugated and polyacrylic acid gated mesoporous silica against the breast cancer cell line. Targeted drug delivery system was tested *in vitro* and *in vivo*. It caused the apoptosis in cells also, *in vivo* intravenous injection effectively reduce growth of 4T1 induced mammary pad tumour in female BALB-c mice via augmented accumulation of cuminaldehyde (Ghosh et al., 2022). Besides, Ghalehkhondabi et al., (2022) were synthesized folic acid conjugated poly(methacrylic acid) nanospheres as a pH-sensitive drug delivery system. The cumulative DOX releases were 22 % in pH 7.4 and 32 % pH 5.5. The IC50 of free doxorubicin, poly(methacrylic acid), and folic acid conjugated poly(methacrylic acid were 12.8, 11.0, and 2.7 mg/mL, respectively (Ghalehkhondabi, FazlaliandSoleymani, 2022). Further, Mo et al., (2021) were prepared doxorubicin loaded hyaluronic acid modified halloysite complexes. In vitro cytotoxicity tests carried out. Results showed better uptake of nano-drug delivery system in CD44 receptor positive cells than in CD44 receptor negative cells (Mo, Wu, LiandCai, 2021).

As it seen from the researches, the effectiveness of cancer treatment is increased with the development of controlled release and also, increased with targeting mechanisms which are selective to target.

2.2. Targeted Drug Delivery and Controlled Release

Cells and tissues can be targeted by physical, active and passive pathway. Thus, active ingredients can be transferred to the individual targets for directly with controlled drug delivery system. So, side effects which might be seen in many organs can be prevented. One of the breakthroughs in nanoscience is nano-sized targeted drug delivery systems with high drug loading capacity, excellent tumour accumulation with low toxic metabolism pathways. The basic aim in the development of them are; certain drug targeting and delivery, greater safety and biocompatibility, increasing innovation of new nanosystems in confidence and developed pharmacokinetic behaviour (Kumari et al., 2016; Souri et al., 2022; Wicki et al., 2015). In this part, design and synthesis of targeting mechanisms were summarized.

2.2.1. Physical Targeting

In the physical targeting, cancer drugs can be navigated to a specific region with external sources such as light, ultrasound, electric field and magnetic field. Effectiveness of the physical targeting mechanism is mainly depending on energy sources, physiological properties of targeted area and biochemical features of the carrier systems (Sun, Dasgupta, Zhao, NurunnabiandMitragotri, 2020; Yu et al., 2016). Generally sonophoresis, sonopermeation, microbubbles, acoustic cluster therapy, nanobubbles, nanodroplets, hyperthermia, photosensitizer mediated drug delivery, upconversion, photodynamic, photothermal, photoacoustic, iontophoresis, electroporation and electrically responsive drug carriers are used for physical targeting to cancer cells (Sun et al., 2020).

Especially, nanostructures which are sensitive to external sources are remarkable for the psychically targeting. For example, Lyon et al., (2018) used thermosensitive liposomes loaded doxorubicin for liver tumours. Drug delivery system was triggered by mild hyperthermia, induced non-invasively by focused ultrasound. Results showed that an average increase of 3.7 times in intra-tumoral biopsy doxorubicin concentrations, from an estimate of 2.34 μg/g immediately after doxorubicin infusion to 8.56 μg/g after targeted treatment. Also, no death was observed for patients (Paul C. Lyon et al., 2018). Also, same research group was investigated cancer drug concentration before and after exposure of focused ultrasound for liver cancer cells. Biopsies were evaluated for doxorubicin concentration by high performance liquid chromatography (P. C. Lyon et al., 2017). Further, Caldera et al., (2022) prepared

magnetic nanosponges for targeted drug delivery systems. Maltodextrin polymers crosslinked with 1,1′-carbonyldiimidazole were synthesised and, Fe_3O_4 was added to system. The release of DOX was found approximately 30 % after 48 hours (Caldera et al., 2022). Besides, Ahmed et al., (2022) prepared superparamagnetic iron oxide nanoparticles and targeted to hyperthermia therapy with magnetic field. 50 μL of superparamagnetic iron oxide nanoparticles solution at a concentration of 200 mg mL^{-1} injected into the PC3 cells for mice groups. Cancer cells were observed for 22 days. 85 % decrease in tumour volume was found in treated mice group (A. Ahmed, Kim, Jeon, KimandChoi, 2022). There are several publications about physically targeting. Especially, clinical trials are promising (Paul C. Lyon et al., 2018; P. C. Lyon et al., 2017).

2.2.2. Active Targeting

Active targeting mechanism generally related with the kind of cancer and therefore with a particular targeting ligand. These ligands are conjugated by chemically or physically on the nano-drug delivery systems and in this way specific receptors can be detected to cancerous area. Cellular uptake of the drug delivery system is performed via receptor mediated endocytosis and, active component releases in the target effectively. This phenomenon is called the active targeting (Dutta et al., 2021; Nandi et al., 2021; Prabhuraj et al., 2020).

Especially, EPR effect takes an important role for the drug delivery systems transport before the cellular uptake of it. Some physiological features of the most tumours such as vascular permeability, rapid growth of tumour vessels, and poor structural integrity are distinguished from those of normal tissues and organs. Thus, nanosystems reach the region through permeable tumour vessels and attach to the tumour bed due to the low lymphatic drainage. So, this process is called the “EPR” effect (Bilal, Qindeel, Raza, MehmoodandRahdar, 2021; Z. Liu et al., 2022). EPR effect primarily helps in effective transportation of nanosystems in the cancerous side. Then, ligand and receptor interaction perform.

Ligands can be classified as two sub divisions. Cell surface targeting ligands which are folate receptor (C. Chen et al., 2013), transferrin receptor (Jose et al., 2019), epidermal growth factor receptor (EGFR) (X. Zhou et al., 2020), human epidermal growth factor receptor (ErbB1, ErbB2, ErbB3 and ErbB4) (Ringhieri et al., 2017), cluster of differentiation (CD14, CD22, CD36, CD44, and CD133) (Dutta et al., 2021;

PiechuttaandBerghoff, 2019), estrogen receptor (estrone, estradiol and estriol) (Saha, Makar, Swetha, GuttiandSingh, 2019), αvβ3 (Steiger et al., 2021) and Aptamer (Carvalho et al., 2019) are the first group. Organelle targeting ligands which are mitochondrial (Battogtokh, Cho, Lee, LeeandKang, 2018), nuclei (P. Zhang et al., 2019), lysosome (M. Yang et al., 2021) and endoplasmic reticulum (Dutta et al., 2021) are the second group. Further, chemokine, luteinizing hormone-releasing hormone, biotin and interleukin are the ligands for active targeting mechanism (Dutta et al., 2021). These active targeting agents can be effective on certain cancer types.

Mariadoss et al., (2022) synthesised p-Coumaric acid-loaded aptamer conjugated starch nanoparticles for triple negative breast cancer. Results showed that aptamer consist drug delivery system was inhibited the cancer cells by apoptosis (Mariadoss, Saravanakumar, Sathiyaseelan, KarthikkumarandWang, 2022). Also, Rompicharla et al., (2019) were loaded the paclitaxel to the PAMAMG4 complex. After functionalizing PAMAM with PEG, biotin was added to the system as an active targeting agent. System was tested in the human lung cell line (A549). As a result, the nano-system was inhibited the tumor significantly (Rompicharla, Kumari, Bhatt, GhoshandBiswas, 2019). Prabhuraj et al., (2020) reported that curcumin, loaded PLGA nanoparticles coated with PEG and then, conjugated with different targeting ligands (folic acid, or hyaluronic acid, or transferrin). PLGA nanoparticles with the hyaluronic acid and folic acid ligands showed better targeting properties to the aggressive and metastatic MDA-MB-231 breast cancer cell line (Prabhuraj et al., 2020). Besides, Nandi et al., (2021) reported that stealth liposomes were linked with transferrin-(Tf) for sirolimus-(SRM). BT-474 cancer cell line showed an antiproliferative effect of the SRM loaded Tf-DPPC-liposomes indicates high cell cytotoxicity compared to Tf-DSPC-liposomes. SRM loaded liposomes were showed anticancer effect for Tf-liposomes with tumor growth inhibition compared to the free-drug and nonconjugated nanoparticles (Nandi et al., 2021).

2.2.3. Passive Targeting

Vascular permeability and lymphatic drainage of the most solid tumours have remarkably differences of normal tissues. So, one of the advantages of the nano-sized drug delivery systems is that they cannot pass through the tight junction between the healthy vascular linings. However, these systems can easily reach to target via leak vascular permeability of the tumour tissues. Thus, active ingredients are accumulated

largely into the target due to the damaged lymphatic drainage (EPR effect). Therefore, the EPR effect is the primary driver for the passive targeting mechanism. Besides, the pore cutoff-sizes of growing solid tumour vascular permeability is in the range of 200 nm to 1.2 μm (Fan Yuan, 1995b; Susan K. Hobbs, 1998; Z. Wang et al., 2018). Also, this physiological difference of cancer cells is provided the large amount of nutrients and oxygen for rapid growth. On the other hand, the average sizes of the drug-loaded nanoparticle systems are varying between 60-500 nm (Huang et al., 2021; TavanoandMuzzalupo, 2016; Z. Wang et al., 2018). Therefore, the targeted systems are small enough to pass through these pores.

After reaching to the target lesion, unloading of the drug cargo is achieved via external or internal factors of the tumour microenvironment. Controlled release of the drug in the target region is ensured through intracellular properties such as redox potential, pH and enzymatic factors or external factors such as light, magnetic field, temperature, electric field and ultrasound applications (Cao et al., 2019; Kalyane et al., 2019; Theek et al., 2014; Tsujimoto et al., 2021; Y. Wang et al., 2014; Yu et al., 2016).

In the recent years, pH responsive drug delivery systems are getting more attraction for passive targeting mechanisms. As it is known, tumour tissue contains an acidic environment compared to normal tissues (J. Haveman and H. S. Reinhold J. L. Wike-Hooley, 1984; Warburg, 1956b) because cancer cells mainly provide their energy by glycolysis and lactic acid occurred as a metabolite (Fadaka et al., 2017). They over-perform this pathway for their energy needs, in the presence or absence of oxygen. So, gaining energy is 2 ATP at the end of every cycle. As a result, lactic acid accumulates in the environment as a metabolite and the pH of the cell cytosol is remarkably decreased. However, in the case of oxygen lacking, healthy cells produce 2 ATP. But, 38 ATP are produced with glycolysis in the presence of oxygen and the pH of the healthy cell cytosol is in the range of pH 7.0 – 7.4 (Fadaka et al., 2017).

Therefore, the release of the drugs at low pH is easily accomplished in the low pH ranges. In the literature, Long et al., (2020) modified the drug delivery system consisting of MoS_2 (Molybdenum disulfide) nanoparticles with hydrazine groups that can form bonds with PEG and doxorubicin hydrochloride (DOX). Drug releases were tested at pH 5.4 and pH 7.2 for 72 hours. It has been reported that the slow release of DOX into the nucleus killed the cancer cells (Long et al., 2020). Also, Li et al., (2020) reported that multiporous silica nanoparticles (MSN-NH_2) were loaded with 5-

fluorouracil (5-FU). For 5-FU encapsulation, the system was coated with pullulan using the schiff base reaction. Since the bond between MSN and pullulan tends to hydrolyze under acidic conditions, the encapsulated 5-FU is easily released from the structure in acidic conditions. Drug releases were achieved at pH 5.5, pH 6.8 and pH 7.4 (37°C). Cytotoxicity study was evaluated by LO2 and HepG2 cell lines by conventional CCK-8 test (S. Li et al., 2020). Saravanakumar et al., (2021) reported TM2 metabolite for prostate cancer. Different concentrations of TM2 loaded into chitosan. Its cytotoxicity in PC3 cells were evaluated. The drug release was higher than 50 % at the pH 5.8 and less than 10 % in pH 7.4 (Saravanakumar et al., 2021). Besides, Xie et al., (2019) synthesised acid labile methotrexate prodrug self-assembling nanoparticles loaded with curcumin for cancer therapy. At pH 5.0, only 20 % of the methotrexate was released from methotrexate-imine-micellar-curcumin. But the release amount increased to 60 % at pH 5.0 under the same conditions (Xie et al., 2018).

2.3. Nanostructures Used in Drug Delivery Systems

Over the next couple of years for the drug delivery would possess a strategic tool for medical sciences (Miranda et al., 2022). Especially, nanoparticle-based systems are favourable for drug delivery because of their prolonged time in the blood stream and good carrier properties. Size and surface properties are important to prevent nanostructures from RES clearance. Especially, modification and functionalization with a preferred polymer can protect them from immune system clearance (Miranda et al., 2022).

Nanoparticles and polymeric materials are commonly used for drug delivery. Their advantages, disadvantages and synthesis methods are explained in this following section.

2.3.1. Nanoparticles

Nanoparticles are technically described as the manipulation of matter with at least one dimension sized from 1 to 100 nanometres. They can be classified as the combination of atoms and molecules with the creation of 0-dimensional, 1-dimensional, 2-dimentional or 3-dimentional functional structures (Gavas, QuaziandKarpinski, 2021).

Their individual features like stability, high drug carrying and loading capacity,

sensitive to controlled release, transportation of both hydrophilic and hydrophobic ingredients that make them hopeful candidates for a lot of targeted drug delivery applications. Due to their surface area, they can be functionalized by variety of ligands and therapeutics. Furthermore, their surfaces are large enough to encapsulate lots of active compounds. This phenomenon enables combination of diagnostic, drug delivery and treatment. So, decreasing the drug dosage and yet have the same advantage of the treatment is highly possible (Gavas et al., 2021; Miranda et al., 2022; J. Wang, LiandNie, 2021).

Mainly, synthesis methods are important to obtain them with dedicated features. Thus, nanoparticles with various shapes, sizes and structures can be synthesised by bottom-up and top-down approach. Nanoparticles and their synthesising methods are listed in Figure 2.1 (Behzad et al., 2021).

Bottom up approach is described as synthesising a structure from atoms to clusters to nanoparticles, also known as constructive method. Top Down Approach is defined as the reduces bulk material or substance to obtain smaller units like nanoparticles (Behzad et al., 2021; Gavas et al., 2021). But, toxic chemicals that in used production of nanoparticles can cause side effects on human health. Therefore, in the recent years, non-toxic, environmentally friendly and more economical green pathway is preferable for nanoparticle synthesis (Nair, SajiniandMathew, 2022).

In this method, microorganisms, fungi and plants can be used in the synthesis of nanoparticles. But, plant-based green synthesis is easier and more economical and advantageous than the use of bacteria and fungi (ParmarandSanyal, 2022). In particular, metallic nanoparticles have been effectively synthesized by green chemistry method, Figure 2.1 (Behzad et al., 2021).

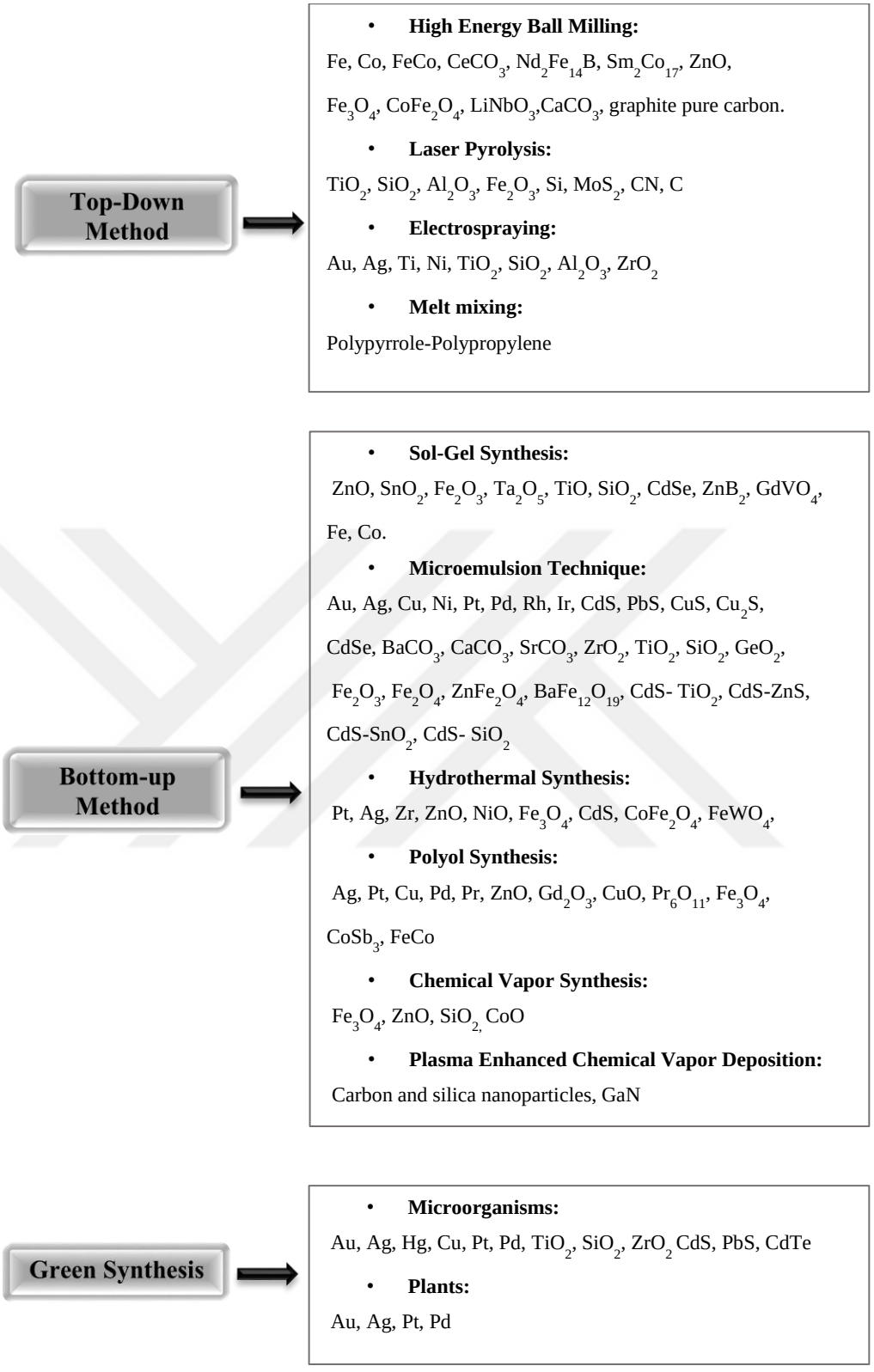

Figure 2.1**.** Summary of the methods for the synthesis of various nanoparticles (Behzad et al., 2021)

Especially silver nanoparticles which have antitumoral, antibacterial, antifungal and antiviral properties, are easily synthesized via green chemistry method. It is also possible to eliminate the toxic effects which occurred by chemical methods. Besides, the loss of energy and time in physical methods can be prevented (Alkhalaf, HusseinandHamza, 2020; Hekmati et al., 2020; TamilarasiandMeena, 2020).

In green synthesis, shells, fruits or leaves of the plant can be used and extracts are prepared at a certain temperature and time, and contain reducing agents such as flavonoids, alkaloids and antioxidants. Also, properties of plant extracts, reaction time, temperature, pH and concentration of metal salts are effected the size, morphology and quality of the produced nanoparticles (DeivanathanandPrakash, 2022; Hidayat et al., 2022; S. Tian et al., 2022).

Most recently, silver nanoparticles have gained a special interest in drug delivery systems because of their antitumoral features in tumours (Swanner et al., 2019). Sriram et al., (2010) produced silver nanoparticles by *Bacillus licheniformis* as an anticancer agent using Dalton's lymphoma ascites (DLA) cell lines both *in vitro* and *in vivo*. Results showed that the volume of tumour in mice decreased by 65 % (Sriram, Kanth, KalishwaralalandGurunathan, 2010). Also, Naggar et al., (2017) synthesised of silver nanoparticles using a phycocyanin extract via green chemistry approach. IC50 results showed 27.79 ± 2.3 μg/mL inhibitory concentration against to MCF-7. Silver nanoparticles inhibited the growth of tumour in Ehrlich ascites carcinoma bearing mice (El-Naggar, HusseinandEl-Sawah, 2017). Further, Hekmat et al., (2012) reported that the synergic effects of silver nanoparticles and cancer drugs has been extensively investigated. AgNPs and DOX appeared to interact more strongly with T47D and MCF7 cell DNA compared to AgNPs and DOX alone (Hekmat et al., 2012). AgNPs are highly promising structures for design of novel drug delivery systems for cancer.

2.3.2. Polymers and Polymeric Materials

Polymeric structures take a significant role in targeted drug delivery systems. Active drugs can be physically entrapped, conjugated or chemically bounded with these structures. In the case of drug conjugates, the increase of the molar mass leads to decreased kidney excretion of the system. Besides, interactions with the blood ingredients is reduced by functionalization or modifications of nanocarriers. So, fast recognition by the immune system clearance is prevented and, the therapeutics circulation time in the body is extended with these applications (Knop et al., 2010).

For example, various natural polymers like chitosan and heparin have been studied for different biomedical applications. Chen et al., (2022) synthesised pH sensitive chitosan/doxorubicin nanoparticles effect on MDR tumour in human breast cancer (MCF-7/ADR) (Q. Chen et al., 2022). Also, She et al. (2013) reported that pH sensitive dendronized heparin/doxorubicin drug delivery system for 4T1 breast tumour model (She et al., 2013).

Mostly, hydrophilic polymers which reduce aggregation, enhance the water solubility and have a stealth effect is usually preferable for drug delivery applications. PEG is widely used for functionalization of the nanocarriers (Figure 2.2). The molar mass and polydispersity of the polymer are important for biocompatibility and stealth behaviour. So, the molecular weight of PEG is changing from 400 Da to about 50 kDa in various pharmaceutical studies. (Knop et al., 2010).

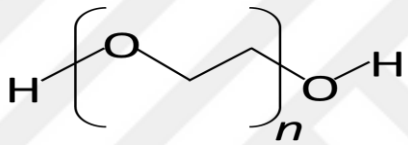

Figure 2.2. Chemical structure of Poly(ethyleneglycol)

Rhein/PEG6000/nanohydroxyapatite system for DOX and Phosphorus-32 was reported for simultaneous chemo/radiotherapy. The inhibition of bone metastases of breast cancer was observed (X. Yang et al., 2020). Also, zein nanoparticles/PEG35000 were investigated for mucus permeability during oral drug uptake. Functionalized nanoparticles get mucus permeating features with reaching the gut epithelium (Reboredo, Gonzalez-Navarro, Martinez-Oharriz, Martinez-LopezandIrache, 2021). Khutale and Casey, (2017) reported HS-PEG5K-NH_2-5000Da with gold-doxorubicin drug delivery system for human lung adenocarcinoma (A549) (KhutaleandCasey, 2017). With PEGylation, drug delivery systems size and their surface properties are getting importance to avoid from RES. This approach can protect them from phagocytic system and kidney clearance. Thus, their circulation time is extended in the blood stream.

Synthetic and biodegradable polymers like poly(amino acid)s are also used for nanocarriers. Such as, poly(glutamic acid), poly(hydroxyethyl-l-asparagine) and poly(hydroxyethyl-l-glutamine) have been studied for drug delivery systems (Knop et al., 2010).

Further, non-biodegradable polymers have been studied as alternatives to PEG for drug delivery systems. Poly(glycerol), poly(2-oxazoline)s, poly(acrylamide), poly(vinylpyrrolidone) and poly(N-(2-hydroxypropyl)methacrylamide) can be listed as PEGs alternatives (Knop et al., 2010).

However, drug release from the polymeric structure should be in controlled conditions. Therefore, polymeric structures which are responsive to internal stimulus (pH, enzyme, redox potential) of tumour microenvironment or sensitive to external sources (magnetic field, sonication, heat, light) have been investigated (Alsehli, 2020). Polymeric structures, like liposomes and dendrimers, which have pH, temperature, redox potential, enzyme, light and dual sensitive properties, are usually used for controlled release studies. A pH responsive liposome, which contains peptidomimetic doxorubicin conjugate was reported. Results showed that doxorubicin release at pH 6.5 was more efficient than psychological pH. Also, system suppressed the NSCLC tumour in mice (Sonju et al., 2022). Because of their aqueous core inside and surrounded by the hydrophobic layer, they can carry both water-soluble and lipophilic molecules owing to their hydrophilic and hydrophobic regions. Phosphatidylcholine, phosphatidylglycerol, phosphatidylethanolamine and phosphatidylserine have been used as phospholipids to create the liposomes (Ochekpe N. A., 2009). Also, dendrimers are highly branched three-dimensional architecture-based structures which are synthesized by mono dispersed of macro molecules. These unique molecules have great functions owing to their great molecular structure. They can be used wide range of biomedical applications and generally they are smaller than 100 nm. Further, there are three regions in these macro molecules which are polyfunctional core, interior dendrons and surface functional groups (Kannan, Nance, KannanandTomalia, 2014).

Commonly studied and commercially available dendrimers are listed as the Denkewalter/type PLL, Tomalia/type PAMAM, Hult/type poly (ester) (bis-MPA), Majoral-Caminadetype phosphorous based and Vögtle-Meijer-Multhaupt/type poly(propyleneimine) (PPI) dendrimers (Kannan et al., 2014). Especially, PAMAM dendrimers are one of the promising and preferable nano structures for drug delivery. Their core, generation, cavities, and surface functional groups can be modified for the targeted drug delivery systems and also, controlled release can be modulated by the bonding between drug and dendrimer surface groups. Therefore, dendrimers are a good choice in the field of efficient delivery system, especially the controlled release

studies (Kannan et al., 2014).

Release mechanism is triggered by the internal or external stimulus. One of the most widely studied mechanism is pH responsive release of active cancer drugs. Therefore, different structures of pH responsive dendrimers as drug carriers have distinct fundamentals and routes of drug release. Dendrimers with ionizable surface groups can accept or donate protons in response to tumours low pH and, this causes releasing of the active drug. On the other hand, hydrolysis of acid labile bonds between cancer drug and dendrimer at low pH can be led to drug release (Z. Wang et al., 2018).

Biotin coupled PAMAM PG4.5 dendrimer was reported and nanosystem was synthesised to enhance the HeLa cell targeted drug delivery. *In vitro* drug release was carried out 48 hours at the acidic pH 6.5 and pH 5.0 (Hanurry et al., 2020). Also, it has been reported that carboxyl terminated PAMAMG3.5 dendrimer was grafted with PEG(methylether) as a drug delivery system and loaded with carboplatin. Nano-system was tested on HeLa cell line, MCF-7 cells, and, healthy mouse fibroblast cells L929 (Vu et al., 2019). Further, Zhang et al., (2018) was synthesised folic acid-conjugated PAMAMG5 dendrimers for a pH sensitive cis-aconityl linkage with doxorubicin. System was tested in vitro at pH 5.0 pH 6.0 for 48 hours (M. Zhang et al., 2018). PAMAMG4-camptothecin drug delivery system on HCT-116 (human colorectal carcinoma cells) (Thiagarajan G., 2010).

3. MATERIALS AND METHOD

3.1. Materials and Chemicals

L. officinalis leaves were collected between July and August, 2021 from Northern Turkiye: Samsun (41°22'16.1"n 36°12'33.0"e) and identified by Prof. Dr. Hasan Korkmaz, Department of Biology, Ondokuz Mayıs University, Samsun-Turkiye. Plant specimens were identified and listed according to the "Flora of Turkiye and the East Aegean Islands-Volume 4" (Davis, 1972). The collected plant specimens were recorded in the Herbarium of the Ondokuz Mayıs University, Department of Biology (OMUB). The herbarium number of the plant material is 8844., Figure 3.1.

Silver nitrate ($AgNO_3$), 1-ethyl-3-(3-dimethylaminopropyl) carbodimide (EDC.HCl, MW:191,70) citric acid, n-hydroxysulfosuccinimide (NHS, MW: 217.13), o-(benzotriazol-1-yl)-n,n,n,n-tetramethyluronium exafluorophosphate (HBTU, MW: 379.24), sodium hydroxide (NaOH), sodium chloride (NaCl), n,n-diisopropyl ethylamine (DIPEA, MW: 129.4), doxorubicin hydrochloride (DOX, MW: 579.98), phosphate buffered saline (PBS) tablets (pH 7.4), poli(amidoamine) succinamic acid dendrimer 1-4 diaminobutane core generation 4 (10 wt. % in H_2O, MW: 20646.87), thiol-PEG-amine (HS-PEG5K-NH_2) (MW: 5kDa), dialysis membrane (MWCO: 30 kDa) and dialysis kit (MWCO: 25 kDa) were purchased from Sigma Aldrich, USA and UK. Human cervix adenocarcinoma cell line (HeLa), Eagle's minimum essential medium (EMEM, with l-glutamine), and fetal bovine serum (FBS) were purchased from ATCC, USA. Non-essential amino acids (NEAA) and sodium pyruvate were purchased from biological industries, Israel. Phosphate buffered saline (pH 7.2, sterile-filtered), trypan blue, and 2-(2-methoxy-4-nitrophenyl)-3-(4-nitrophenyl)-5-(2,4-disulfophenyl)-2h tetrazolium mono-sodium salt (WST-8) were purchased from Sigma-Aldrich gmbh, USA and UK.

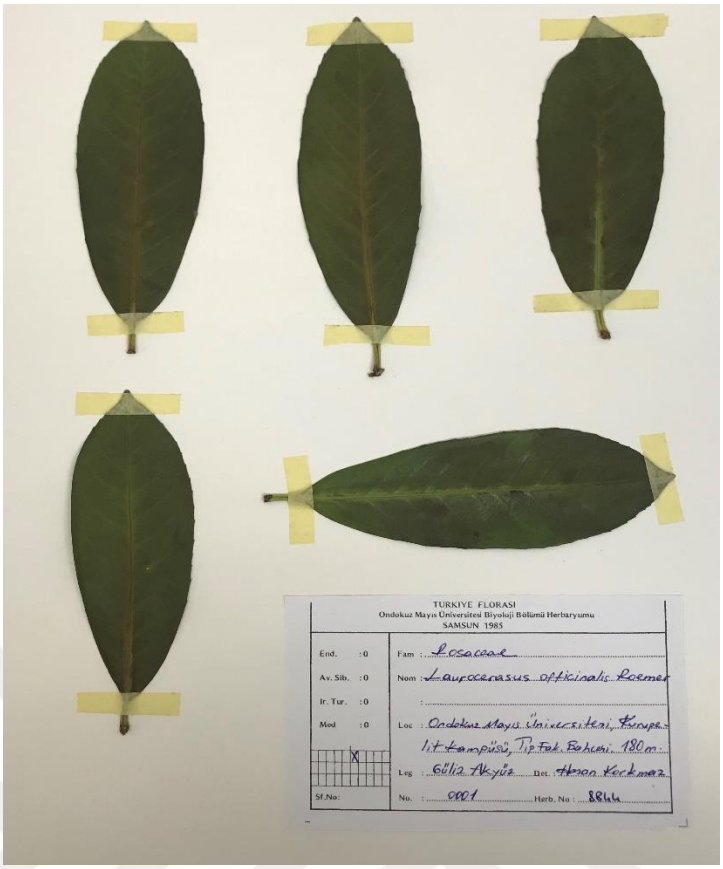

Figure 3.1. Samples of preserved biological material from OMUB Herbarium

3.2. Stock and Test Solutions Preparation

- Stock solution of 10 mM silver nitrate was prepared by dissolving 0.425 mg of silver nitrate to make 250 mL of solution. $AgNO_3$ working standard (1 mM) was made from Ag stock standard solution.
- Extract was prepared from 2 grams of *L. officinalis* leaves in 5 mL of deionized water.
- HS-PEG5K-NH_2 stock solution was prepared by dissolving 1 mg ($2x10^{-7}$ mole) of HS-PEG5K-NH_2 in 5 mL of deionized water.
- NHS stock solution was prepared by dissolving 1 mg ($4.61x10^{-6}$ mole) of NHS in 5 mL of deionized water.
- EDC.HCl stock solution was prepared by dissolving 1 mg ($5.216x10^{-6}$ mole) EDC.HCl in 5 mL of deionized water.
- PAMAMG4 stock solution was prepared by dissolving 100 µL of PAMAMG4 (0.1020 g, $4.94x10^{-7}$ mole) in 5 mL of deionized water.

- HBTU stock solution was prepared by dissolving 5 mg ($2.637x10^{-6}$ mole) in 5 mL of deionized water.
- DIPEA stock solution was prepared by dissolving 1 mL (d:0.742 g/mL), (0.0057 mole) in 10 mL of deionized water.
- DOX stock solution was prepared by dissolving 5 mg ($8.62\ x10^{-6}$ mole) in 5 mL of deionized water.
- The phosphate buffer solution (pH 7.4) was prepared by dissolving one phosphate buffered saline tablet in 100 mL of deionized water (KhutaleandCasey, 2017). NaCl (1 M) stock solution was prepared by dissolving 0.5844 g NaCl in 10 mL of deionized water.

3.3. Synthesis and Optimization of AgNPs

The biochemical compositions of plant extracts change according to the preparation technique. The extraction process effects the reducing agent content such as antioxidants, flavonoids and polyphenols in the aqueous media (Alghoraibi et al., 2020; Karabegović, Stojičević, Veličković, NikolićandLazić, 2013; Karabegović et al., 2014). The reducing agents play an important role for the synthesising of AgNPs.

In this thesis, for the preparation of plant extract, fresh *L. officinalis* leaves were collected and divided into three groups which were contained young, mature and mixed (young and mature) leaves. The leaves were collected daily and cleaned with deionized water. The leaves were dried before the extraction procedure. The ratio of the silver nitrate, and the ratio of the extracts were prepared according to previous studies, but ratios were modified (DuttandUpadhyay, 2018; Krishnaraj et al., 2012; Rolim et al., 2019; Yousaf et al., 2020). Reactions were carried out under fluorescent tube, FCL 22W. To monitor the AgNP formation, UV-Vis spectrums of the solutions were taken at specific intervals (0 to 40 by 2 minutes intervals, 45 to 60 by 5 minutes, 75 to 225 by 15 minutes). The formations of AgNPs were observed by the colour change of the solution from light yellow to reddish brown. The correlation between extraction temperatures and reducing agent content were investigated. The extractions are coded as EXMT. E is the extract. X is the volume of the water used for extraction. M is the maturity of the *L. officinalis* leaves. Y for young, Ma for mature and Mi for mixed leaves. T is the extraction temperature.

Table 3.1. Extract and $AgNO_3$ optimization for AgNPs

E2M65(mL)	1 mM $AgNO_3$ (mL)
1	1
1	2
1	4
1	6
1	8
E5M65 (mL)	1 mM $AgNO_3$ (mL)
1	1
1	2
1	4
1	6
1	8
E8M65 (mL)	1 mM $AgNO_3$ (mL)
1	1
1	2
1	4
1	6
1	8
E10M65 (mL)	1 mM $AgNO_3$ (mL)
1	1
1	2
1	4
1	6
1	8

Extract and $AgNO_3$ volume ratios were optimized to obtain high amount of AgNPs. Formation of AgNPs were investigated by UV–Vis analysis. The water content of the extraction was optimized at 65 °C by using mixed *L. officinalis* leaves. The extracts, E2Mi65, E5Mi65, E8Mi65 and E10Mi65 were obtained by adding 1 g of mixed *L. officinalis* into 2, 5, 8 and 10 mL deionised water, respectively, at 65 °C for 1 hour. The amount of $AgNO_3$ was optimized by adding 1 to 8 mL of 1mM $AgNO_3$ into the 1 mL of E2Mi65, E5Mi65, E8Mi65 and E10Mi65, and mixed by shaking. However, the effect of temperature on the extractions and AgNPs formation were tested at temperatures of 45 °C, 65 °C and 85 °C using young mature and mixed *L. officinalis* leaves. The optimised water content X=5 (E5Y45, E5Y65, E5Y85, E5Ma45, E5Ma65, E5Ma85, E5Mi45, E5Mi65 and E5Mi85) and the amount of $AgNO_3$, 6mL, were used for temperature optimizations. The extracts prepared by 1 g of young *L. officinalis* leaves in 5 mL of deionize water, E5Y45, E5Y65 and E5Y85, and subsequently synthesised AgNPs are seen in Figure 3.2. Then, the extract suspensions were filtered by Whatman filter paper and cooled at room temperature. The fresh filtrates used for the synthesis of silver nanoparticles. The samples prepared for the optimisations are summarised in Table 3.1

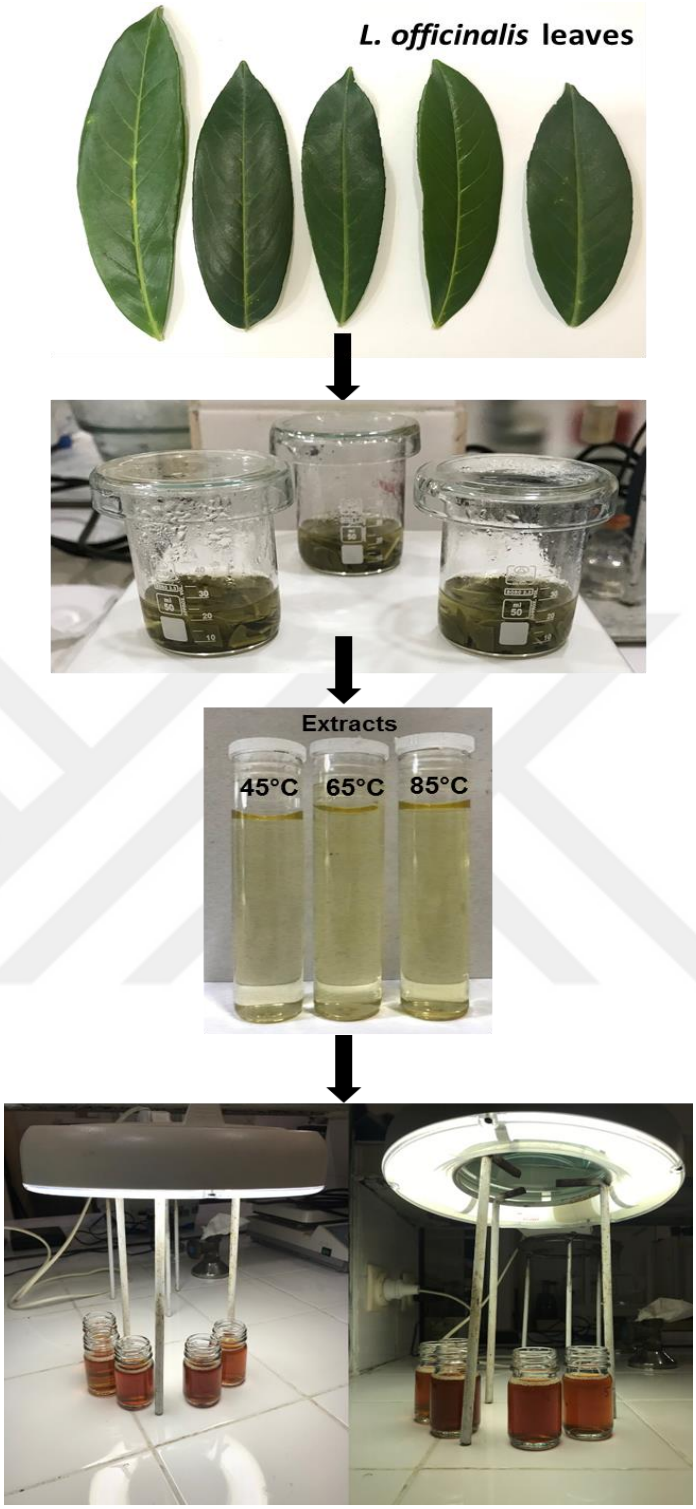

Figure 3.2. The Synthesising of silver nanoparticles under the day light florescence lamp by the *L. officinalis* leaves extracts (45 °C, 65 °C and 85 °C). Formation of silver nanoparticles was observed with a reddish-brown colour

3.4. Functionalization of AgNPs with HS-PEG5K-NH_2

PEG is flexible, hydrophilic and neutral polymer that can act as a dispersant because of its ability to bind water. It reduces the toxicity and increases the lifetime of the drug delivery system in the blood circulation. Also, it enhances the nanoparticle penetration into the mucus layer. So, the pharmacokinetic behaviour of the drug delivery system can be improved by the functionalization (Bastos et al., 2016; Díaz-Cruz et al., 2016; He et al., 2014; HuckabyandLai, 2018; Knop et al., 2010; Mishra et al., 2016; Rolim et al., 2019).

In this thesis, HS-PEG5K-NH_2 ($HS(CH_2CH_2O)nCH_2CH_2NH_2HCl$) was used for the functionalization of AgNPs. The functionalization process was carried out based on the previous studies but slightly modified (Gao, Huang, Liu, ZanandRen, 2012; KhutaleandCasey, 2017; Rolim et al., 2019). Firstly, different concentrations of HS-PEG5K-NH_2 aqueous solutions (100 to 1300 by 100 µL intervals) were added into the green synthesised AgNP solution. In this manner, it was aimed to observe the shifts at the UV-Vis spectrum peaks as a function of the HS-PEG5K-NH_2 concentrations.

Finally, 100 µL of HS-PEG5K-NH_2 was added into the AgNP solution dropwise under magnetic stirring for the functionalization. The final solution was stirred for a further 15 min at room temperature. Then the mixture was kept at 4 °C overnight to react. Schematic illustration of the functionalization of AgNPs with HS-PEG5K-NH_2 shown in Figure 3.3.

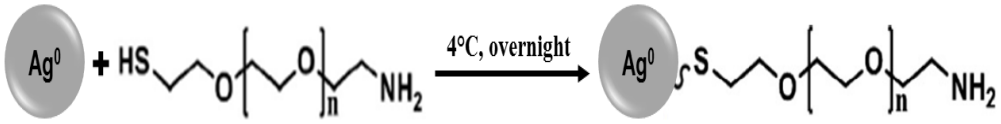

Figure 3.3. Schematic illustration of the functionalization of AgNPs with HS-PEG5K-NH_2

3.5. Modification of AgNP/HS-PEG5K-NH_2 with PAMAMG4

The surface of the nano-system modified with a carboxylated PAMAMG4 dendrimer through amide linkage with the amine group of HS-PEG5K-NH_2 via an EDC coupling reaction. Coupling procedure has two steps. First one is, activating the free carboxyl group on the PAMAM with EDC and sulfo-NHS. The second step is, covalently conjugating PAMAM to the PEG through displacement of sulfo-NHS groups (Ciolkowski et al., 2012; Hughes, 2015; KhutaleandCasey, 2017; ThermoScientific, 2011; W.-L. Zhang et al., 2010).

EDC (*n*-(3-dimethylaminopropyl)-*n′*-ethylcarbodiimide), reacts with the carboxyl group to form an amine reactive intermediate (o-acylisourea). The produced o-acylisourea can be easily displaced by nucleophilic attack from primary amino groups in the reaction medium. But this intermediate is not stable and hydrolysed in aqueous solutions. In order to prevent the intermediate hydrolysis, sulfo-NHS is added to EDC to produce a remarkably more stable and more soluble active ingredient (Hughes, 2015; ThermoScientific, 2011). The activation of the carboxylic group of PAMAMG4, a solution of PAMAM-COOH (0.98 $x10^{-4}$ M, 1 mL) was mixed with EDC.HCl (1.04 $x10^{-3}$ M, 1 mL) and NHS (0.92 $x10^{-3}$ M, 1mL) and then the solution was stirred for 30 min at room temperature. To modify the AgNP-HS-PEG5K-NH_2, different concentrations of activated PAMAMG4 (100 to 1000 by 100 µL intervals) were added into the synthesised 7.1 ml of AgNP/HS-PEG5K-NH_2 solution. Illustration of obtained nanostructure is given in Figure 3.4. Colloidal stability test was conducted with 100 µL of activated PAMAMG4 solution. Active PAMAMG4 solution was added into the AgNP/HS-PEG5K-NH_2 solution and it was stirred for 15 min. Then, the mixture was stored at 4 °C for 48 hours to react (Ciolkowski et al., 2012; KhutaleandCasey, 2017; W.-L. Zhang et al., 2010).

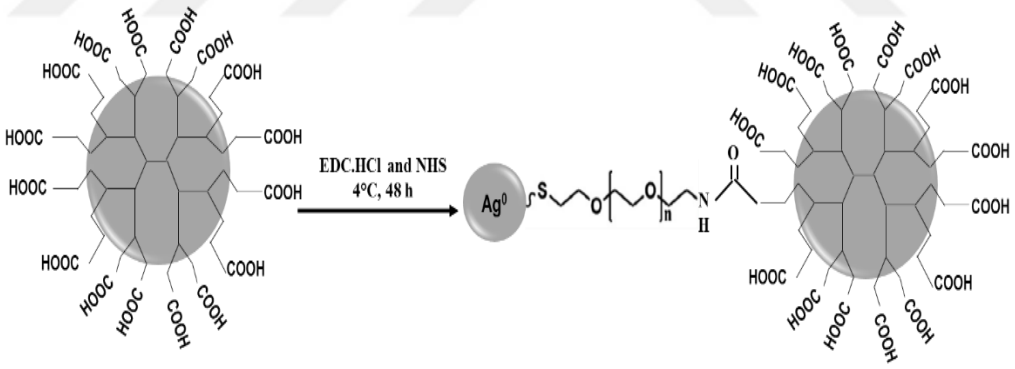

Figure 3.4. Schematic illustration of the modification of AgNPs/HS-PEG5K-NH_2 with PAMAMG4

3.6. Conjugation of DOX with AgNPs/HS-PEG5K-NH_2/PAMAMG4

The prepared AgNPs/HS-PEG5K-NH_2/PAMAMG4 (7.2 mL) were stirred at 0 °C for 5 minute, then HBTU (2.637 $x10^{-3}$ M, 1mL) and then DIPEA (100 µL, 0.57 M, 100µL) were added and stirred for 10 minute at 0 °C, Figure 3.5 (Mallick et al., 2015). A solution containing doxorubicin (1.724 $x10^{-3}$ M, 2 mL) was added to previously prepared mixture and stirred for 48 hours at room temperature, Figure 3.5. It was protected from the surrounding light during the reaction (KhutaleandCasey, 2017;

Mallick et al., 2015). The final solution was then dialyzed (5500 rpm, 15 minute) using a dialysis membrane (MWCO 30 kDa) to remove the free doxorubicin. The dialysed solution was stored at 4 °C, Figure 3.5 (KhutaleandCasey, 2017). Reaction chart of the AgNP/HS-PEG5K-NH_2/PAMAMG4/DOX was given in Figure 3.6.

Figure 3.5. Drug loading at 0 °C and then removing the free doxorubicin using a dialysis membrane

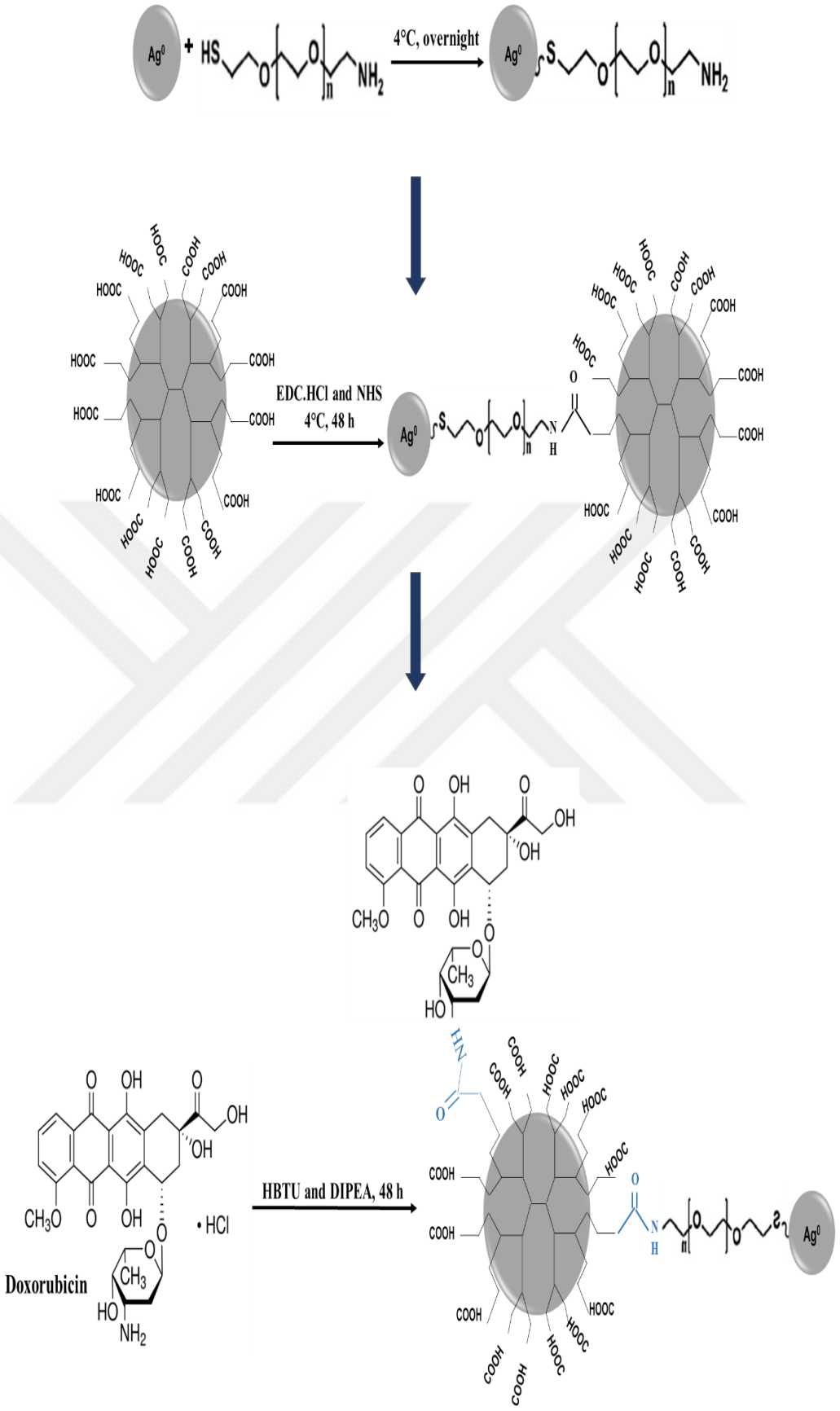

Figure 3.6. Reaction chart of AgNP/HS-PEG5K-NH_2/PAMAMG4-DOX for pH responsive drug delivery system

3.6.1. Drug Conjugation Efficiency and pH Dependent *In Vitro* Drug Release Studies

The efficiency of drug conjugation was calculated by a direct method using the absorption of the DOX at 480 nm. Briefly, the unknown DOX concentration of the nano-system was determined using a calibration curve based on series of known DOX concentrations. The DOX loading efficiency was then calculated using following Equation (3.1) (Dong et al., 2017; KhutaleandCasey, 2017; Z.-H. Zhou et al., 2020),

$$\text{Drug loading efficiency (\%)} = \frac{(\text{weight of loaded drug})}{(\text{weight of feeding drug})} x\ 100\ \% \qquad \textbf{(3.1)}$$

The pH dependent drug release of DOX from the AgNP/HS-PEG5K-NH_2/PAMAMG4 nano-system was verified using phosphate buffer solutions at pH 4.0, pH 6.6 and a pH 7.4 and the DOX release was monitored as a function of time (0.3 h, 0.5 h, 0.8 h, 1.0 h, 1.3 h, 1.5 h, 1.8, 2.0 h, 2.3 h, 2.5 h, 2.8 h, 3.0 h, 3.3 h, 3.5 h, 3.8 h, 4.0 h, 4.4 h, 4.9 h, 24 h, 48 h, 72 h, 96 h, 120 h, 144 h, 168 h, 192 h, 216 h and 240 h).The AgNP/HS-PEG5K-NH_2/PAMAMG4/DOX aqueous solution (400 µL) was added into a mini dialysis kit (MWCO 25 kDa). Then the mini dialysis kit was placed in 4 mL of corresponding buffer solution and incubated at 37 °C, Figure 3.7. 500 µL of solution from buffer was harvested overtime with subsequent replacement of equal volume of fresh buffer at the different time interval. The release of the DOX was then quantified by measuring its absorbance using absorption spectroscopy at 480 nm. Then, the concentration of the released DOX calculated with the aid of a standard curve.

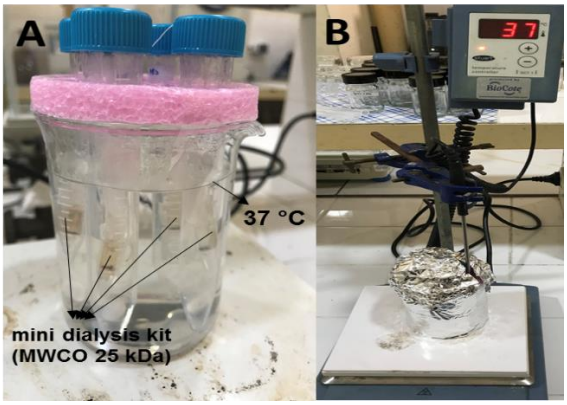

Figure 3.7. The pH dependent drug release of DOX from the AgNP/HS-PEG5K-NH_2/PAMAMG4 nano-system (A). Release environment was protected from the surrounding light (B)

3.6.2. Colloidal Stability of AgNP/HS-PEG5K-NH_2/PAMAMG4/DOX Based on pH and Salt Test

UV-Vis absorption spectroscopy was used to study the effect of pH and NaCl concentration on the colloidal stability of AgNP, AgNP/HS-PEG5K/NH_2, AgNP/ HS-PEG5K-NH_2/PAMAMG4 and AgNP/HS-PEG5K-NH_2/PAMAMG4/DOX in aqueous environment (Gao et al., 2012; KhutaleandCasey, 2017). A series of pH solutions (7.4, 6.6 and 4.0) were prepared by adding NaOH (1 M) or citric acid (1 M) to the phosphate buffer solution (pH 7.4).

3.7. Characterization Techniques

UV-Vis spectroscopy, atomic absorption spectroscopy (AAS), X-ray powder diffraction (XRD), FTIR spectroscopy, electron microscopy (SEM/STEM) and energy dispersive spectroscopy (EDS) were used for characterization of the targeted drug delivery system.

3.7.1. UV–visible Spectrometer

Thermo Scientific™ GENESYS™ 10S UV-Vis spectrometer was used for UV-Vis data collection by Thermo Scientific, Vision lite version 5.3, USA The formation of the AgNP, AgNP/HS-PEG5K/NH_2, AgNP/HS-PEG5K-NH_2/PAMAMG4 and AgNP/HS-PEG5K-NH_2/PAMAMG4/DOX were confirmed by the detection of the surface plasmon resonance (SPR) absorption bands at between 400 nm and 600 nm in the UV-Vis region. The baseline was corrected using deionised water.

3.7.2. Atomic Absorption Spectrometer

The concentrations of AgNPs in the solutions were determined using the AAS (Perkin Elmer PinAAcle 900f) with a silver hollow cathode lamp. $AgNO_3$ standards of 0.10 ppm, 0.25 ppm, 0.50 ppm, 0.75 ppm and 1.00 ppm were prepared and used for the calibration curve. The samples were centrifuged and supernatants were collected and, all samples were diluted 100 times with deionized water before the aspiration. The concentrations of silver ions in the supernatants were calculated by the calibration curve. The concentrations of AgNPs in the solutions were calculated by subtracting the initial concentration of silver ions from the concentration of silver ions in the supernatants.

3.7.3. X-ray Powder Diffraction Analyses

XRD analyses were performed for identification of the silver nanoparticles. The samples were dried under vacuum environment in the desiccator before the XRD analyses. The crystal structure of the AgNPs was investigated by XRD on a Rigaku Smartlab (Japan) with CuKα radiation operating at 40 kV, 30 mA and in the range of 20-80° 2θ at a scanning rate of 1°/min.

3.7.4. Fourier Transform Infrared Spectroscopy

The extract powder, AgNPs, AgNP/HS-PEG5K/NH_2, AgNP/ HS-PEG5K-NH_2/PAMAMG4 and AgNP/HS-PEG5K-NH_2/PAMAMG4/DOX were analysed using a FTIR (Perkin Elmer Spectrum Two FTIR) spectrometer. FTIR analysis was performed to detect the presence of various functional groups, interactions and bindings in the synthesised system. The FTIR spectra were recorded from 400 to 4000 cm^{-1}. The samples were dried under vacuum environment in the desiccator before the FTIR analyses.

3.7.5. Scanning Electron Microscopy, Transmission Electron Microscopy and Energy Dispersive Spectroscopy Analyses

The synthesised system was examined by SEM, TEM and EDS. The morphology of the products was analysed using SEM (JEOL-JSM-7001F). To prepare SEM samples, solutions placed onto SEM stubs and dried at room temperature. The samples were analysed without coating. The EDS analysis demonstrates the presence of the elemental composition of the samples. Carbon coated 300 mesh copper grids were used, for the preparation of TEM sample. The sample solutions were dropped to the cupper grid and dried at room temperature. TEM images were obtained on a JEOL-JSM 7001F using a STEM detector with an accelerating voltage of 30 kV. The particle sizes were calculated using the ImageJ software.

3.8. Cell Viability Tests

3.8.1. Cell Culture

Cells were cultured in EMEM supplemented with 10 % FBS, 1 % NEAA, and 1 mM sodium pyruvate. Frozen HeLa cells were thawed in a 37 °C water bath and immediately centrifuged at 700 g (NF-800R, Nuve, Turkey) for 5 minutes. Then the cells were transferred into 25 cm^2 flasks containing 5 mL medium and incubated in a

humidified incubator (EC-160, Nuve, Turkey) at 37 °C with 5 % CO_2. Cells were passaged at 70 - 80 % confluence and counted with a Thoma slide by trypan blue staining. All cell culture procedures were carried out in a sterile laminar flow cabinet (MN 120, Nuve, Turkey).

3.8.2. Cytotoxicity Test

Cytotoxicity tests (WST-8 test) were performed at 24 and 48-hour exposure periods. Stock solutions of AgNP/HS-PEG5K-NH_2/PAMAMG4/DOX and DOX were prepared in ultra-pure water (Simplicity 185, millipore, France) at 500 μm and diluted with medium (without FBS) to final concentrations of 50, 25, 10, 5, 2.5, 1, 0.75, 0.5, 0.25 μM. Cells ($2x10^4$) were transferred into 96-well sterile plates. After 24 hours of incubation, mediums were removed, and the test mediums (100 μL) containing different concentrations of AgNP/HS-PEG5K-NH_2/PAMAMG4/DOX and DOX were added. Then the cells were exposed to AgNP/HS-PEG5K-NH_2/PAMAMG4/DOX and DOX for either 24 or 48 hours. At the end of the exposure period, mediums were removed, and wells were washed with PBS. Fresh medium was added, and cells were incubated for half an hour. Then, WST-8 solution (10 μL) was added to each well, and the cells were incubated 2 - 3 hours to allow colour development, and absorbance was measured at 450 nm wavelength (RT-6000, Rayto, China). Untreated cells were used as control (100 % viability), and blank wells containing only medium were used for subtracting background absorbance. All tests (24 hours and 48 hours) were repeated three times, and percent viability was calculated according to Equation (3.2). Inhibitor concentrations of nano-drug and DOX were calculated by probit-regression analysis.

$$\text{Viability} = \frac{(\text{Treated cell absorbance} - \text{Blank absorbance})}{(\text{Untreated cell absorbance} - \text{Blank absorbance})} x\ 100 \qquad \textbf{(3.2)}$$

3.8.3. Statistical Analysis of Cell Culture Experiments

The experiments were conducted in triplicates. The normality of the data was evaluated with the Shapiro-Wilk Test. Inhibitor Concentrations (IC) of the compounds were calculated by the Probit-Regression analysis used SPSS software. Dose-response data of the compounds were compared with the One-Way Analysis of Variance (ANOVA) followed by the Tukey's and Duncan tests. Differences were considered statistically significant when P values were less than 0.05.

4. RESULTS AND DISCUSSION

4.1. AgNPs

Green synthesis method of AgNPs has attracted considerable attention due to its advantages like eco-friendly and absence of toxic chemicals. In this part, synthesis, optimization and characterization of AgNPs were detailed discussed. In this manner, Uv-Vis, FTIR, XRD, SEM, TEM and EDS results were discussed extensively.

4.1.1. UV-Vis Spectroscopy Results of AgNP

The optimization of water contents for the extraction were carried out using 2-, 5-, 8- and 10-mL water. The extracts, E2Mi65, E5Mi65, E8Mi65 and E10Mi65 and AgNPs formation can be seen in Figure 4.1. The maximum intensity of the absorption peak was observed in 1 mL E5Mi65 and 6 mL 1 mM $AgNO_3$ mixture, Figure 4.2. The extractions were performed in 5 mL water for further studies.

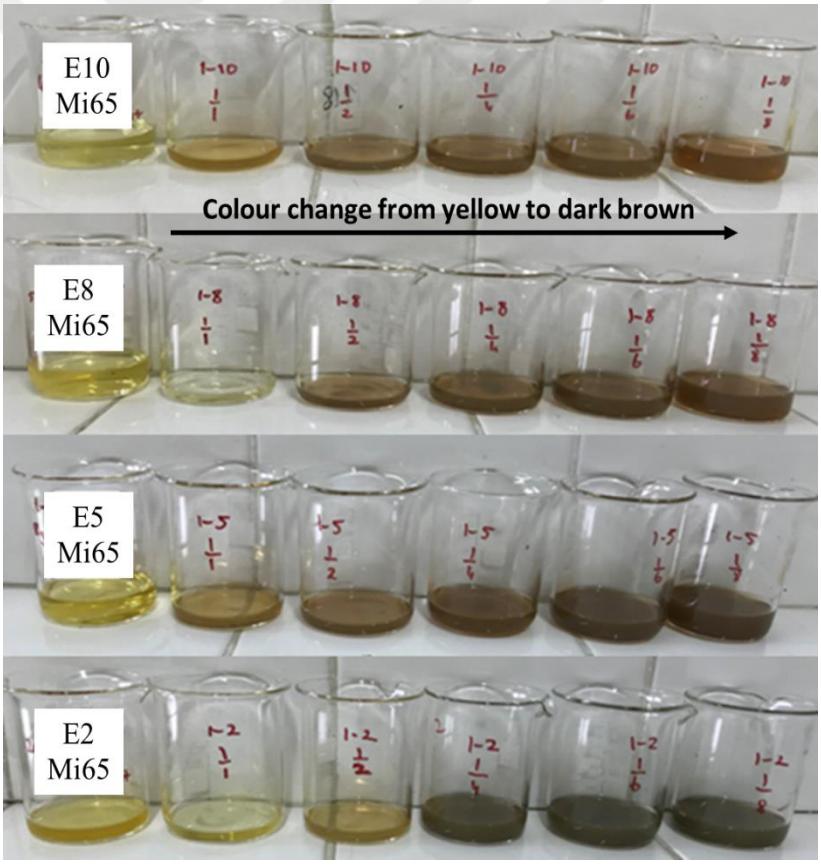

Figure 4.1. Formation of AgNPs with different amount of $AgNO_3$ and extracts (E2Mi65, E5Mi65, E8Mi65 and E10Mi65)

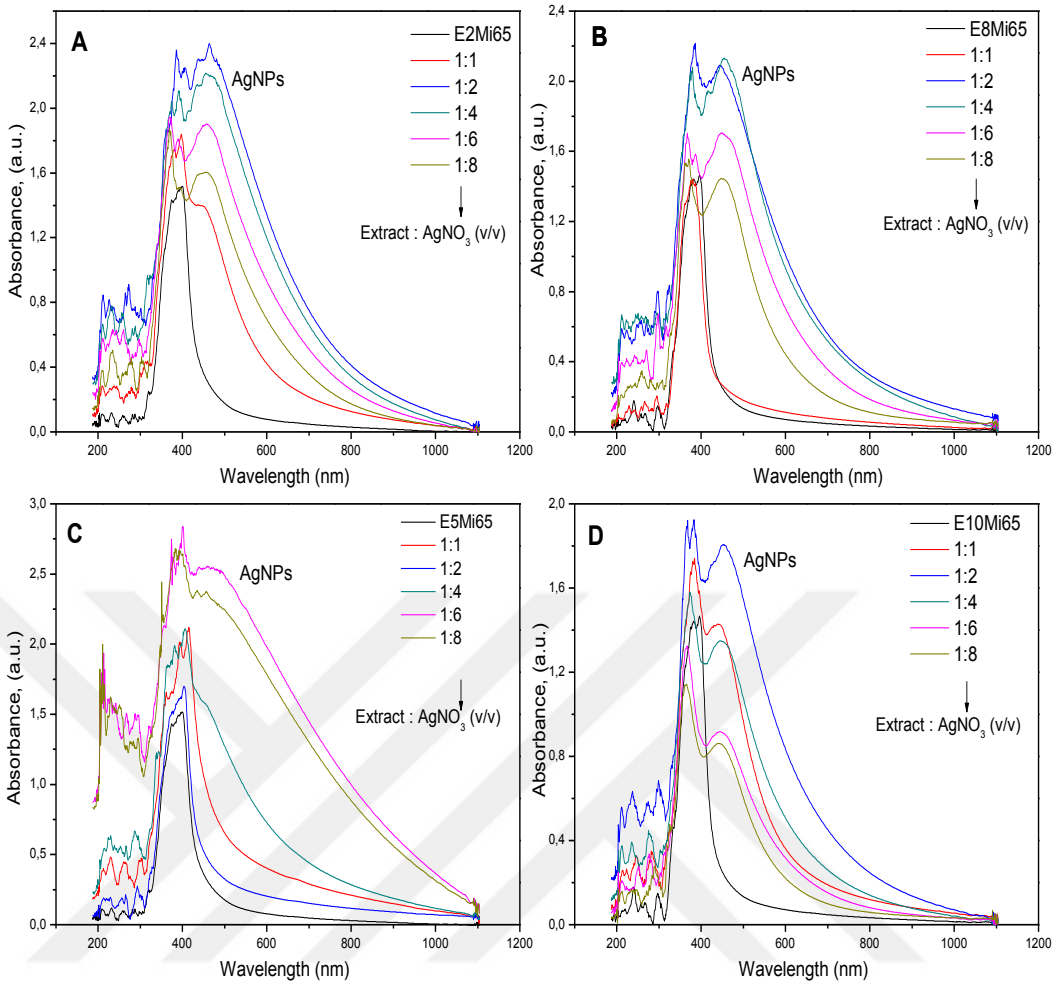

Figure 4.2. The SPR bands of synthesized AgNPs with different volume ratios (A, B, C and D)

Then, the reducing effect of young, mature and mixed leaves extract was investigated at different temperatures. Extractions were carried out using 1 g of *L. officinalis* leaves in 5 ml of deionised water at temperatures of 45 °C, 65 °C and 85 °C (E5Y45, E5Y65, E5Y85, E5Ma45, E5Ma65, E5Ma85, E5Mi45, E5Mi65 and E5Mi85) for 60 minutes then cooled down to room temperature and finally filtrated. Filtrates were used for synthesis of AgNPs.

$AgNO_3$ (6mL, 1mM) solution was added into 1 mL of E5Y45, E5Y65, E5Y85, E5Ma45, E5Ma65, E5Ma85, E5Mi45, E5Mi65 and E5Mi85 solution slowly and the reaction was carried out under the day light florescence lamp.

The reduction of Ag^+ to Ag^0 was observed by a colour change. The colour of the samples was changed from light yellow to reddish-brown (Dare et al., 2012; Elemike, Onwudiwe, ArijehandNwankwo, 2017; Ghassan H. Matar, 2022).

The formation of the AgNPs was confirmed by the detection of the SPR absorption band at between 400 nm and 600 nm at the UV–Vis region and, monitored up to 4 hours. Samples of the solutions were taken at specific intervals (0 to 40 by 2 minutes intervals, 45 to 60 by 5 minutes, 75 to 225 by 15 minutes) and studied by UV-Vis spectrometer. Figure 4.3 shows the UV-Vis absorption spectra (430 nm) of AgNPs obtained from the young, mature and mixed leaves extract at different temperatures. The Figure 4.3 shows the gradual increase of absorptions by the time due to the AgNPs concentration increase. It was observed that the amount of AgNPs obtained were associated with the extraction temperature and the type of leaves. Different amount of AgNPs were obtained from young, mature and mixed leaves extracts. AgNPs which were obtained by young leaves extract at 45 °C, 65 °C and 85 °C (E5Y45, E5Y65, E5Y85) showed maximum absorptions, Figure 4.4. It can be deducted from absorptions that young leaves possessed high level of reducing and/or caping agents. Mature leave extracts were resulted low amount of AgNPs comparing with young leaves, Figure 4.3. It was seen that mature leaves lacked in terms of the reducing agents. The absorption depends on the reducing agent content, chemical surroundings, particle size and dielectric medium. AgNPs which were obtained by the mixed leaves extracts were showed moderate results for all kind of extract temperature. Overall, the maximum SPR bands were observed for AgNPs obtained from young leaves extracts at 85 °C, E5Y85, Figure 4.4.

The absorption peaks of AgNPs obtained from young leaves extract at 85 °C was shown gradual increase up to 150 minutes, Figure 4.5. The increased peak is the characteristic SPR absorption peak of AgNPs (CorciovaandIvanescu, 2018; Rolim et al., 2019). However, SPR bands were overlapping after 150 minutes and this indicates that the reaction was completed. The particle size relevance can also be seen in Figure 4.5. Red shift in the SPR bands were observed with increase in size of the nanoparticles. Furthermore, enhancement the nanoparticle size and also aggregation of nanoparticles cause a sensible broadening of the plasmonic band towards larger wavelengths (A. Taleb, C. PetitandPileni, 1998; Desai, Mankad, GuptaandJha, 2012; Sujit Kumar GhoshandPal, 2007). AgNPs obtained from E5Y85 was used for further characterization studies. 1 mL E5Y85 and 6 mL 1 mM $AgNO_3$ are the optimized parameters and used for subsequent AgNPs synthesis. Optimization parameters of silver nanoparticles are given in Table 4.1.

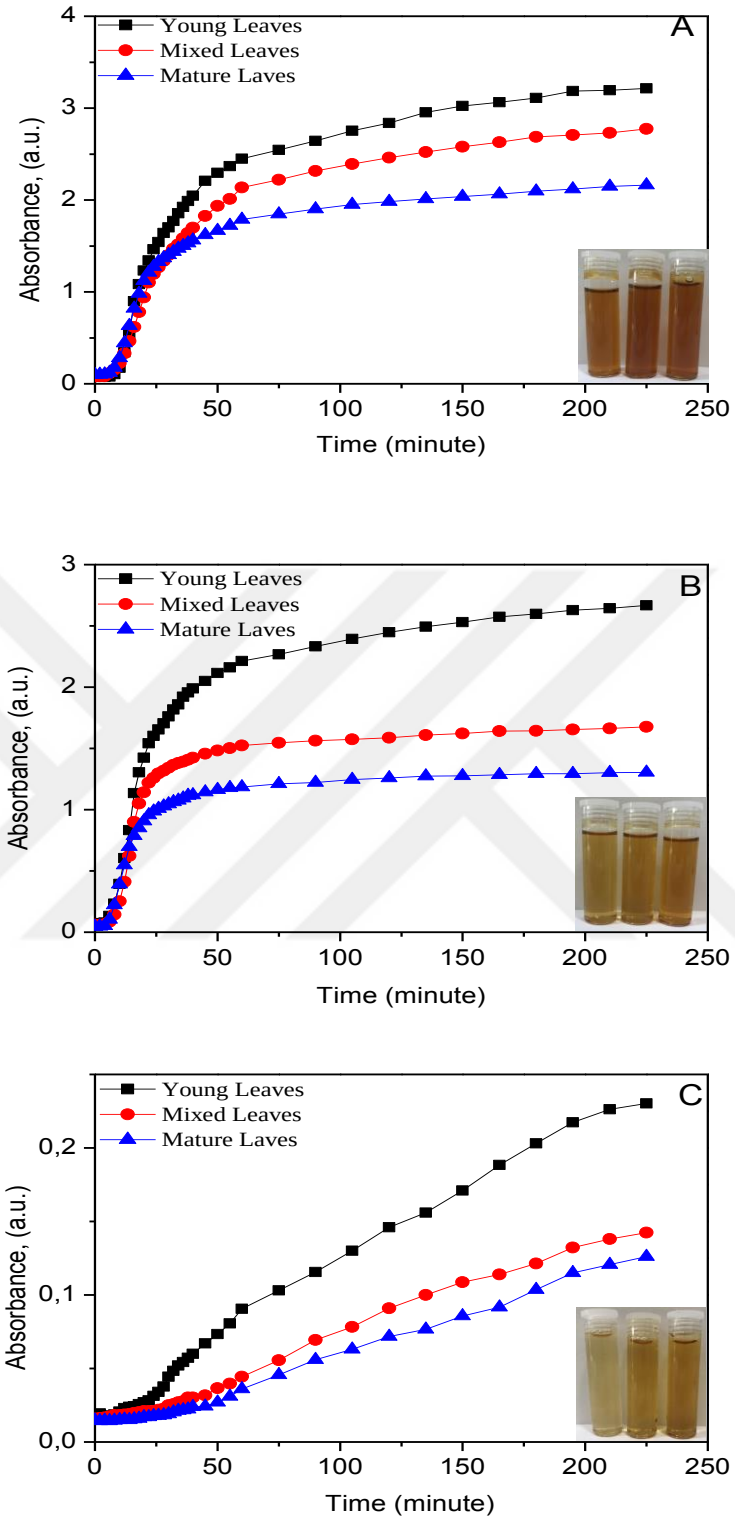

Figure 4.3. Obtained AgNPs from E5Y85, E5Mi85, E5Ma85 (A), E5Y65, E5Mi65, E5Ma65 (B) and E5Y45, E5Mi45, E5Ma45 (C) at 225 minutes

Table 4.1. Optimization parameters of silver nanoparticles

The leaf extract, (w/v)	1 g *L. officinalis* leaves + 5 ml distilled water
Extract temperature	85 ± 2 °C
Concentration of $AgNO_3$	1 mM
Volume ratio of leaf extract and $AgNO_3$, (v/v)	1 mL – 6 mL
Reaction time	3 hours
Reaction pH	6.5
Temperature	Room temperature, 24 ±2 °C

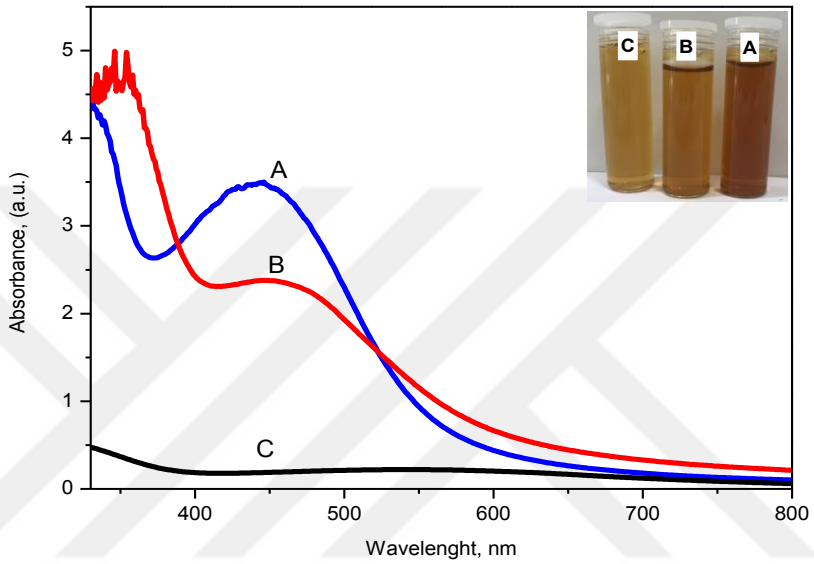

Figure 4.4. Comparation of the E5Y85 (A), E5Y65 (B) and E5Y45 (C) for obtaining AgNPs at 225 minutes

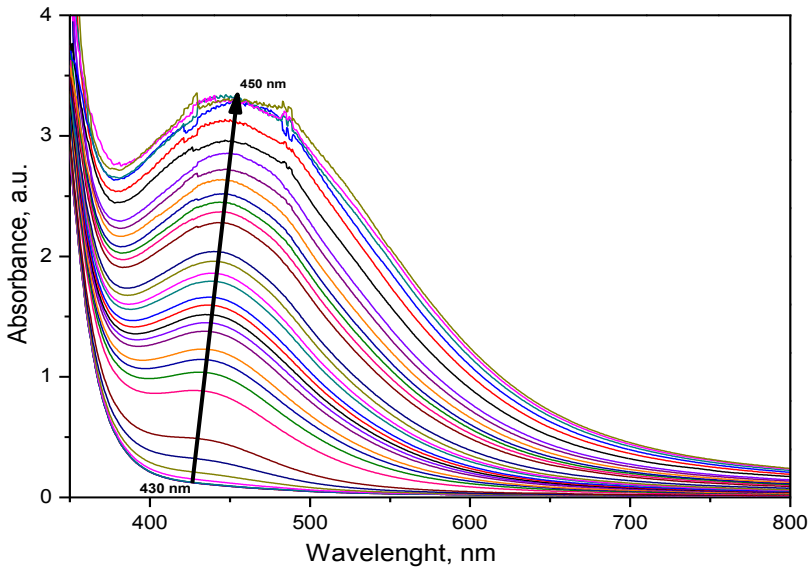

Figure 4.5. Synthesised AgNPs by E5Y85 at 225 minutes

4.1.2. FTIR Results of AgNPs

FTIR spectrum of E5Y85 extract and AgNPs obtained from it are seen in Figure 4.6. The FTIR spectra of AgNP revealed the wide peak at 3256 cm^{-1} and, it can be attributed to -O-H stretching of phenols and alcohols. The band at 1233 cm^{-1} in leaf extract was due to the presence of -C-N stretching aromatic amines. The band at 1597 cm^{-1} belongs to aromatic ring stretching of flavonoids (Gaffney J. S.andD.E., 2012) The peak at 1379 cm^{-1} belongs to $-CH_3$ symmetric deformation in leaf extract and, was shifted to lower frequency (1361 cm^{-1}) in AgNPs. The peak at 1240 cm^{-1} indicates the -C-N stretching aromatic amines and was shifted to lower frequency in AgNPs because of the proteins that possibly bind to AgNPs through the amine groups. The peak at 1046 cm^{-1} belongs to -C-O stretching of alcohols and this band was shifted to lower frequency in AgNPs. Besides, the peak at 600 cm^{-1} indicates the -S-C stretching of sulfides and thiocyanates (Jeffrey S. GaffneyandJones, 2012).

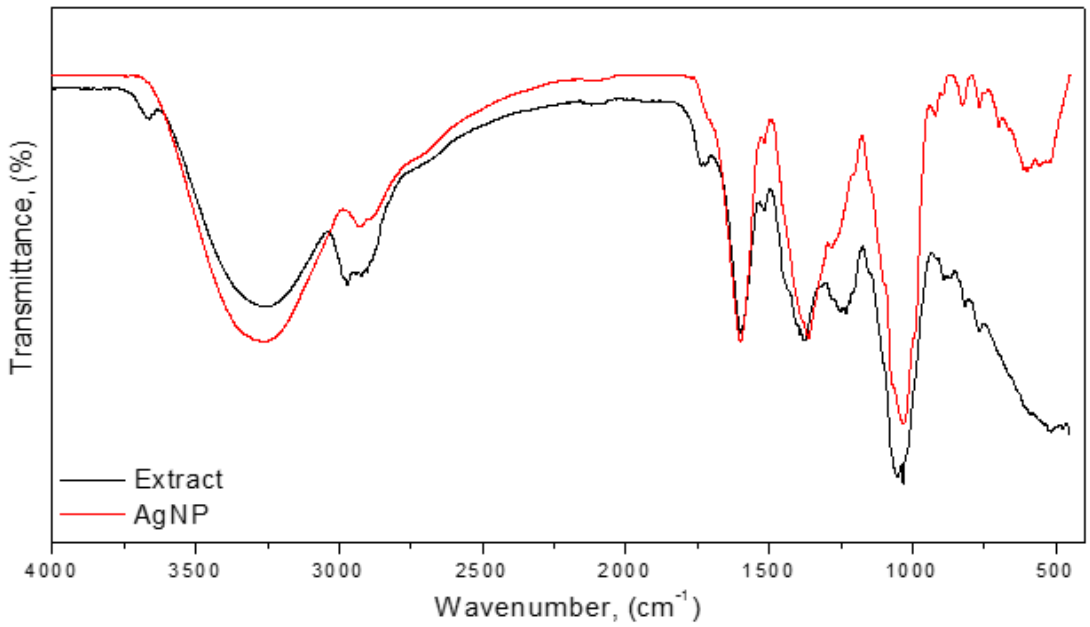

Figure 4.6. FTIR spectra of green synthesised AgNPs

Also, Heredia-Guerrero et al., (2014) reported similar FTIR signals of *L. officinalis* extract (Heredia-Guerrero et al., 2014). Common characteristic group frequencies of some organic functional groups are shown in Table 4.2.

Table 4.2. Common characteristic group frequencies of some organic functional groups (Gaffney J. S. & D.E., 2012)

*Range (cm^{-1})	Vibration	Species
3700–3600 s	-OH str	Alcohols, phenols
3420–3250 s	-OH str	Alcohols, phenols
2990–2850 ms	-CH asym/sym str	Aliphatics
3100–2400 v br	H-bonded OH str	Carboxylic acids
2990–2850 ms	-CH asym/sym str	Aliphatics
1750–1730 s	-C-O str	Lactones
1740–1720 s	-C=O str	Aldehydes
1765–1725 vs	-C=O sym str	Anhydrides Part of a doublet
1650–1580 m–s	$-NH_2$ dfm	Prim amines
1615–1590 m	Arom ring str	Aromatics
1615–1565 s	Arom ring str	Pyridines
1610–1580 s, br	$-NH_2$ dfm	Amino acids
1610–1560 vs	-COO- asym str	Carboxylic acid salts
1550–1490 s	$-NO_2$ asym str	Aromatic nitro
1560–1510 s	Arom ring str	Triazine Sharp peak
1565–1475 vs	-NH dfm	Sec amides
1465–1440 vs	$-CH_3$ asym dfm	Aliphatics
1475–1450 vs	$-CH_2$ scissor	Aliphatics
1360–1335 vs	$-SO_2$ asym str	Sulfonamides
1360–1320 vs	$-NO_2$ sym str	Aromatic nitro
1350–1280 m–s	-N=N-O sym str	Azoxy
1375–1350 s	$-NO_2$ sym str	Aliphatic nitro
1380–1370 s	$-CH_3$ sym def	Aliphatics
1380–1360 m	$-CH_3$ def	Isopropyl 2 Bands
1240–1070 s-vs	-C-O-C str	Ethers, esters
1245–1155 vs	-S=O str	Sulfonic acids
1280–1180 s	-C-N str	Aromatic amines
1280–1180 s	-C-N str	Aromatic amines
1200–1015 vs	-C-O str	Alcohols
1120–1030 s	-C-N str	Prim aliphatic amines
1100–1000 vs	-Si-O-Si asym str	Siloxanes
1080–1040 s	$-SO_3$ sym str	Sulfonic acids
1065–1015 s	-C-O str	Cyclic alcohols
1060–1025 vs	-C-O str	Prim alcohols
980–960 vs	=CH oop def	Trans disubst alkenes
900–865 vs	$-CH_2$ oop wag	Vinylidenes
820–800 s	-CH oop def	Triazines
860–760 vs, br	NH_2 wag	Prim amines
830–810 vs	-CH oop def	Para–Subst benzenes
800–690 vs	-CH oop def	Meta–Subst benzenes 2 Bands
785–680 vs	-CH oop def	1,2,3–Subst benzenes 2 Bands
770–690 vs	-CH oop def	Monosubst benzenes 2 Bands
710–570 m	-C-S str	Sulfides
565–440 w–m	-C-C- def	Alkyl
2600–2540 w	-S-H str	Alkyl thiols
775–650 m	-C-S str	Sulfonyl chlorides
710–570 m	-C-S str	Sulfides
650–600 s	-S-C str	Thiocyanates

* s: strong, m: medium, w: weak, br: broad, v: very.

4.1.3. AAS Results of AgNPs

The concentrations of AgNPs in the samples were determined using the AAS with silver hollow cathode lamp. Silver standards of 0.10 ppm, 0.25 ppm, 0.50 ppm, 0.75 ppm and 1.00 ppm have been used to obtain a calibration curve with R^2 =0 .9841.

Five different AgNPs were synthesised from E5Y85. *L. officinalis* leaves were collected in five consecutive days from different branches of the same tree. After synthesising AgNPs, the samples were centrifuged. Then, supernatants were analysed by AAS. All samples were diluted 100 times with deionized water before the aspiration. The concentrations of silver ions in the supernatants were calculated using the calibration curve shown in Figure 4.7. The concentrations of silver nanoparticles in the solutions were calculated by subtracting the initial concentration of silver ions from the concentration of silver ions in the supernatants. AAS results of the samples are given in Table 4.3. The conversion of the silver ions to AgNPs were increased with the increase of concentration of silver ions in the biomass. The mean concentration of the solutions was found to be 0.2446 mg/L.

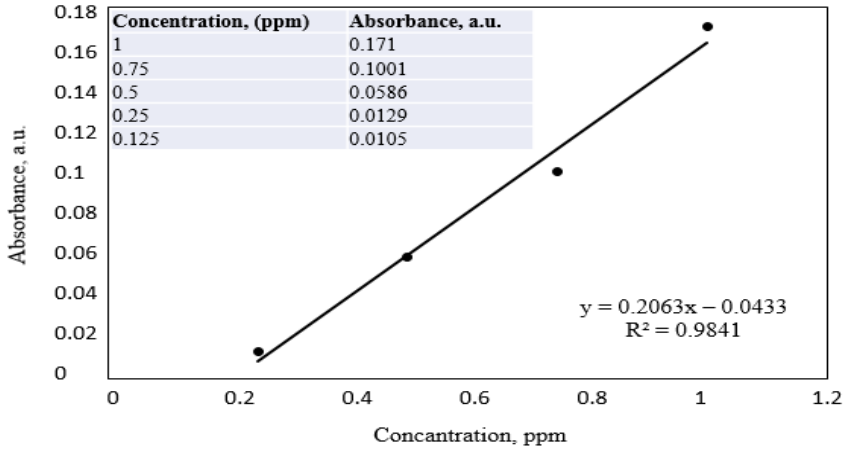

Figure 4.7. The calibration curve of the $AgNO_3$ solution standards

Table 4.3. AAS results of the green synthesised AgNPs

Time (Day)	Absorbance	Concentration	Initial	AgNP (mg/L)
1	0.030	0.353	0.605	0.252
2	0.054	0.469	0.605	0.136
3	0.050	0.452	0.648	0.196
4	0.028	0.343	0.648	0.305
5	0.021	0.314	0.648	0.334

4.1.4. XRD Results of AgNPs

The AgNP solution was placed on glass sample holder and dried under vacuum desiccator before the analysis. The 2θ values of the green synthesised AgNPs are shown in Figure 4.8. XRD measurement conditions of AgNPs are given in Table 4.4..

The AgNPs showed four diffraction peaks at 2θ values of 37.98°, 43,72°, 64.73° and 77.71°, which correspond to the reflection of (111), (200), (220), and (311) planes of the AgNPs (Zarei et al., 2020). The four characteristic band patterns are the indication of pure AgNPs. Thus, successful synthesising of AgNPs and crystalline structure were proved by the XRD results. In the literature, synthesising of AgNPs by the different plant extracts have similar 2θ values with ours (Banala et al., 2015; Kambale et al., 2020; Mehta et al., 2017; Rajkumar et al., 2021; Tailor et al., 2020).

However, the additional peaks 26.9° and 27.24° were observed in the XRD patterns. These peaks are defined to the crystalline and amorphous organic phases (Kambale et al., 2020; Rajkumar et al., 2021; Tailor et al., 2020). The capping and reducing agents of the *L. officinalis* leaves extract showed the 2θ values of 26.9° and 27.24°. Besides, these values relevant with the other characterization (FTIR and EDS) results of the AgNPs.

Table 4.4. XRD measurement conditions of AgNPs

X-Ray	40 kV, 30 mA	Scan speed	2.0000 deg/min
Goniometer	SmartLab	Step width	0.0100 deg
Attachment	Standard	Scan axis	Theta/2-Theta
Filter	Cu_K-beta	Scan range	10.0000-90.0000 deg
CBO selection slit	BB	Incident slit	1/2deg
Diffrectedbeammono	None	Lengthlimitingslit	10.0mm
Detector	SC-70	Receiving slit #1	1/2deg
Scan mode	Contınuous	Receiving slit #2	0.300mm

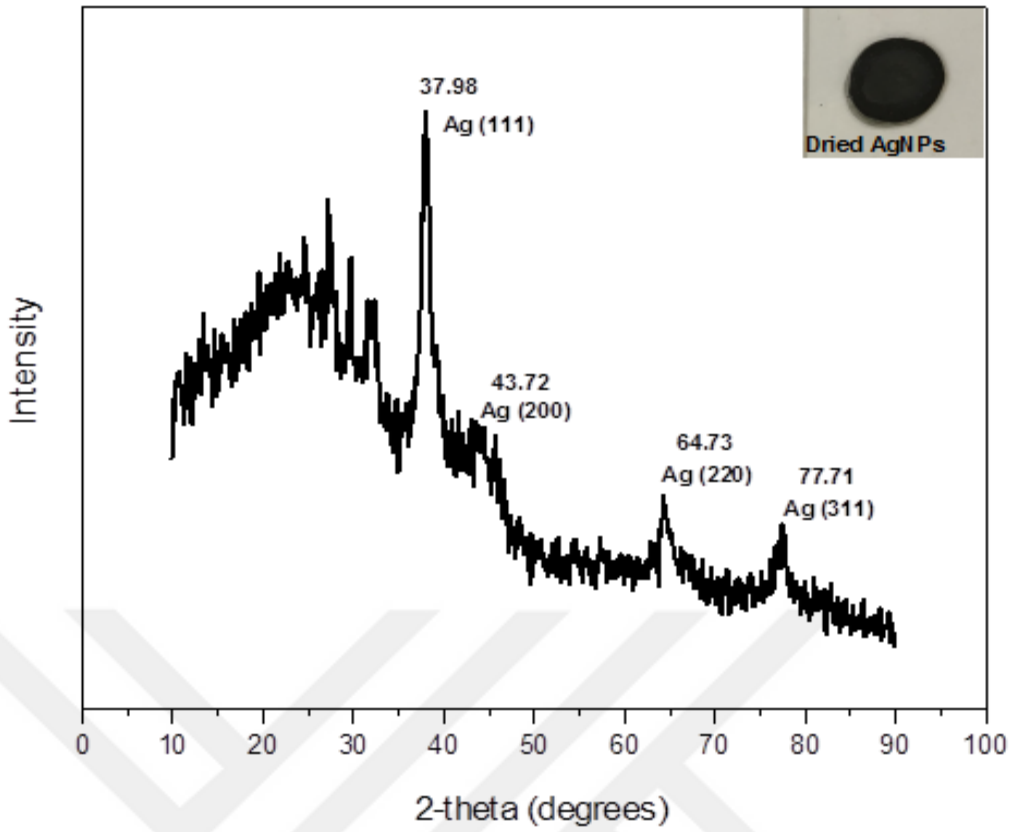

Figure 4.8. The XRD pattern of AgNP

4.1.5. SEM, EDS and TEM Results of AgNPs

AgNP solution was placed onto SEM stubs with carbon tapes. Sample was dried under room temperature without coating.

Figure 4.9 shows a well dispersed spherical AgNPs. TEM images were obtained using a STEM detector with an accelerating voltage of 30 kV and the particle sizes were calculated by the ImageJ software. The STEM images show the presence of spherically shaped AgNPs and comparable with the UV–Vis spectral study. The STEM image reveals an average mean diameter of 13.40 nm after 3 hours reaction time. Figure 4.10 shows the histogram of AgNPs with the average size distribution. EDS results showed the major sharp peak at 3 keV, which occurs of the green synthesised AgNPs. The appearance of other elemental signals Cl, O and, Cu along with silver indicates the occurrence of capping and reducing agent composition of the *L. officinalis* leaves extract. Overall, the results are correlated well with the XRD analysis.

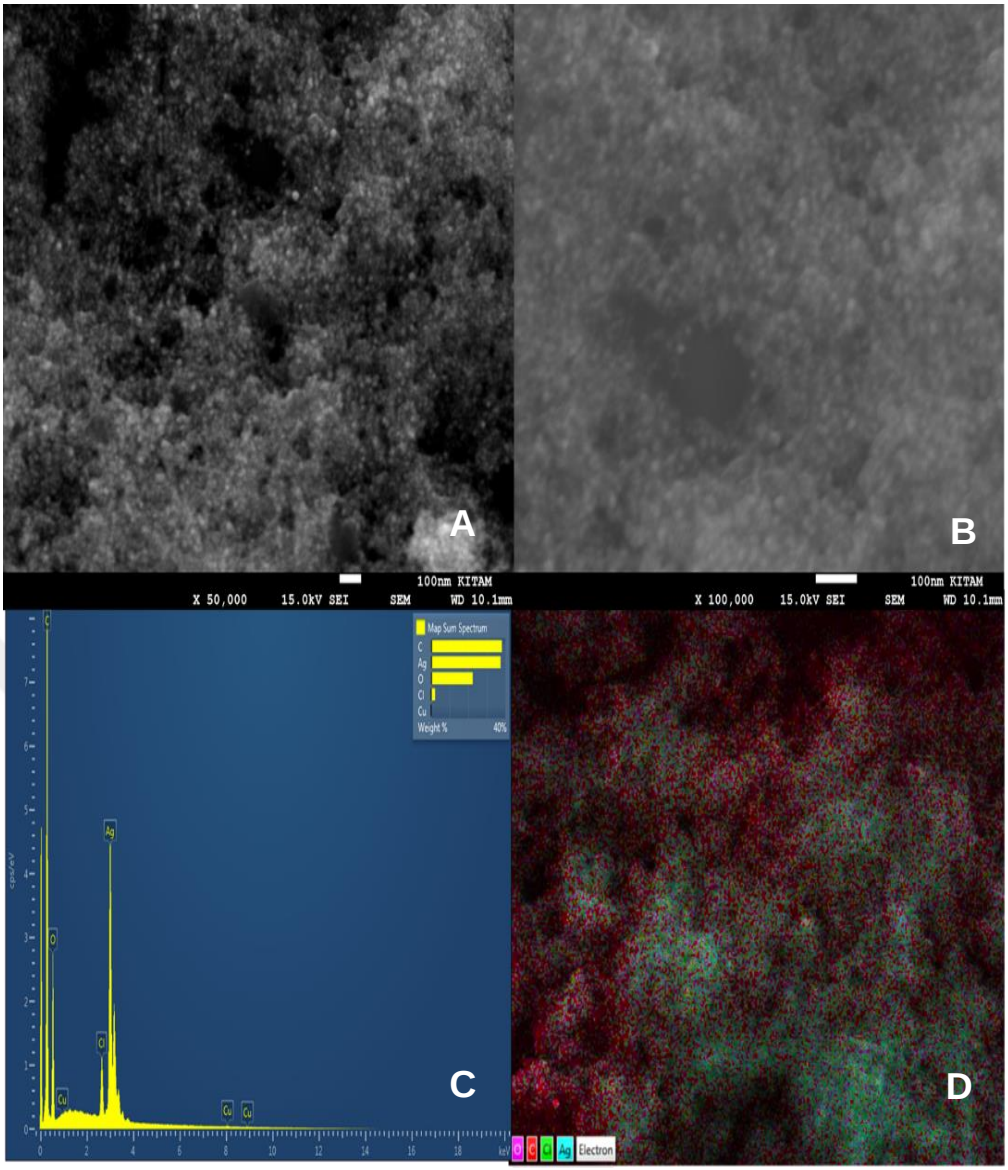

Figure 4.9. SEM (A, B) and EDS (C, D) images of silver nanoparticles

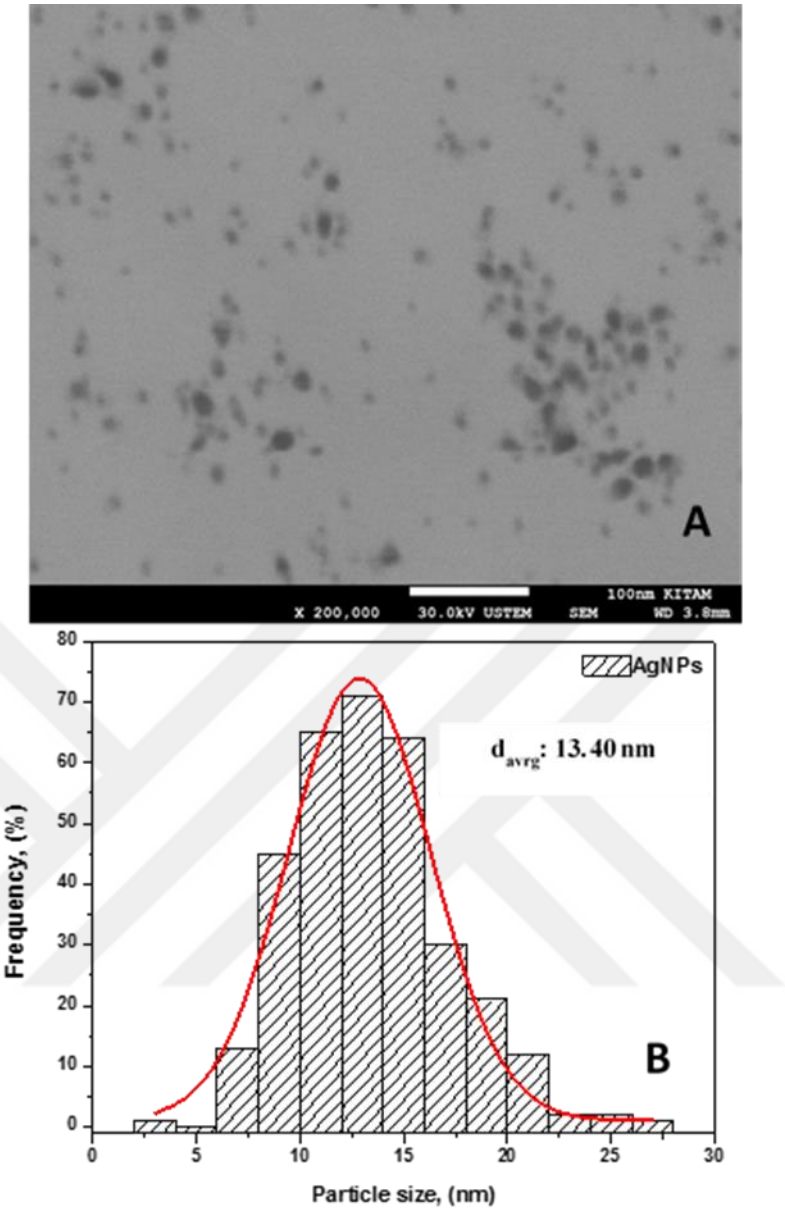

Figure 4.10. STEM image (A) and particle size distribution (B) of AgNPs

4.2. AgNPs/HS-PEG5K-NH_2

The surface of the green synthesised AgNPs was functionalized with HS-PEG5K-NH_2 to increase their biocompatibility, circulation time and protection of immune system clearance. In this part, synthesis and characterization results of AgNPs/HS-PEG5K-NH_2 were discussed.

4.2.1. UV-Vis Spectroscopy Results of AgNPs/HS-PEG5K-NH_2

Firstly, different concentrations of HS-PEG5K-NH_2 aqueous solutions (100 to 1300 by 100 μL intervals) were added into the green synthesised AgNP (1.65×10^{-8} mole of 7 ml) solution. The UV-Vis spectroscopy results are given in Figure 4.11.

Absorption bands which are located between the 400 and 600 nm are indication of the characteristic surface plasmon resonance absorption of AgNPs. The UV-Vis absorption spectrum shows weak and broad absorption peaks at 400 to 456 nm after adding 200 μL of HS-PEG5K-NH_2 aqueous solution. It is clearly seen in Figure 4.11, when the concentration of HS-PEG5K-NH_2 was increased, the intensity of the bands were decreased. Besides, broader bands and red shifts were observed after the addition 200 μL of HS-PEG5K-NH_2 aqueous solution. Therefore, 100 μL of HS-PEG5K-NH_2 were used for testing the colloidal stability of AgNP/HS-PEG5K-NH_2. Firstly, maximum absorption was recorded with the 3.5 (a.u.) of the synthesised AgNPs at the 450 nm Figure 4.11. Then, 100 μL of HS-PEG5K-NH_2 aqueous solution was added dropwise into the AgNP solution, and stirred for a further 15 min at room temperature. The absorption was recorded and, after that it was decreased to almost 1.8 (a.u.), Figure 4.11. This indicates the successful functionalization of AgNPs with HS-PEG5K-NH_2. Then, final solution was kept at 4°C overnight to reaction to complate. Also, the stability of peglated AgNPs were observed for 96 hours by UV-Vis. It was observed that absorption of AgNP/HS-PEG5K-NH_2 was stable for 96 hours, Figure 4.11. Similar findings were reported in the literature. Pinzaru et al., (2018) reported toxicological profile of AgNPs and PEGlated AgNPs for *in vitro* studies for HaCat cells and for *in vivo* non-invasive tests. PEG400 was used for the functionalisation study. It was reported that absorption intensity of the SPR bands between 435 nm and 425 nm decreased after peglation (Pinzaru et al., 2018). Further, Rolim et al., (2019) reported *Camellia sinensis* extract to synthesise AgNPs. Then, the AgNPs functionalized with PEG200 increased dispersion and biocompatibility. Absorption intensities of AgNPs were recorded at almost 0.8 (a.u.) and, 0.5 (a.u.) after peglation

(Rolim et al., 2019). As a result, PEG supports the stability and also affects the size of AgNPs.

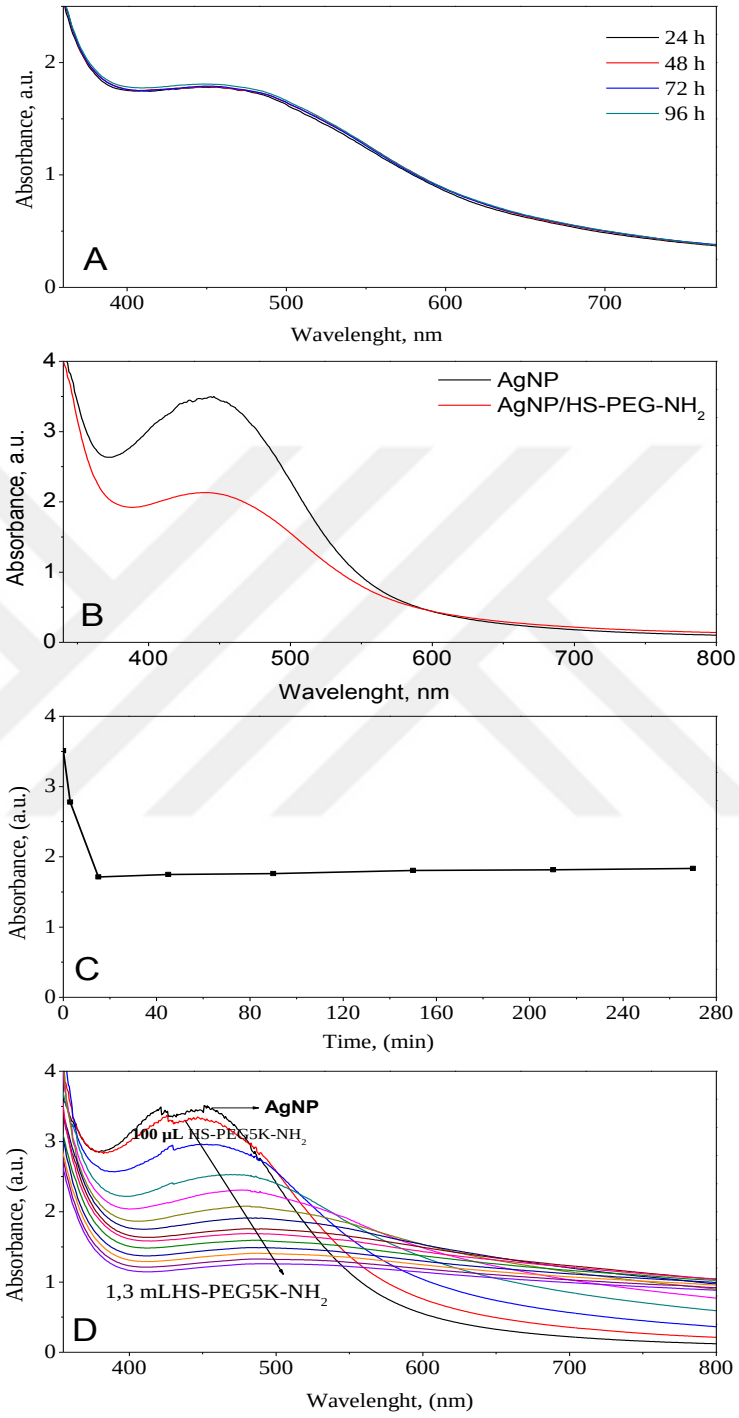

Figure 4.11. UV-Vis absorption spectra of the solutions with different concentrations of polyethylene glycol (A), stability tests of AgNP/HS-PEG5K-NH_2 (B), optimized AgNPs/HS-PEG5K-NH_2 after 24 hours (C) and stability tests for 96 hours of AgNP/HS-PEG5K-NH_2 (D)

4.2.2. Fourier Transform Infrared Spectroscopy Results of AgNPs/HS-PEG5K-NH_2

AgNPs have a strong affinity towards polymer functional groups such as CN, NH_2 and SH. FTIR spectrums of AgNPs and PEGlated AgNPs are seen in Figure 4.12. Both spectrums are similar except slight absorption intensities. The infrared peak of the -OH stretching vibration was located at 3268 cm^{-1} and -C-H stretching vibrations were located at 2927 cm^{-1}. The peak at 1603 cm^{-1} is associated to aromatic ring stretching (Jeffrey S. GaffneyandJones, 2012; Pinzaru et al., 2018; Rolim et al., 2019). The band at 1512 cm^{-1} is representing the -NH_2 deformation of amines. The band at 1366 cm^{-1} is associated to -NO_2 symmetric stretching of aliphatic nitro, and the band at 1025 cm^{-1} is associated with -C-O stretching vibration of alcohols. The band at 815 cm^{-1} is -CH out of plane deformation (Jeffrey S. GaffneyandJones, 2012), the band at 768 cm^{-1} shows the -CH stretching and -C-S stretching Also, the band at 570 cm^{-1} shows the -C-S stretching of bonding between Ag^0-$HS(CH_2CH_2O)nCH_2CH_2NH_2$ which was consistent with the previous reports for HS-PEG5K-NH_2 (Keles, HazerandComert, 2013). In conclusion, all the data demonstrated the successful functionalization of the HS-PEG5K-NH_2 on the surface of AgNP via the -C-S covalent bonding.

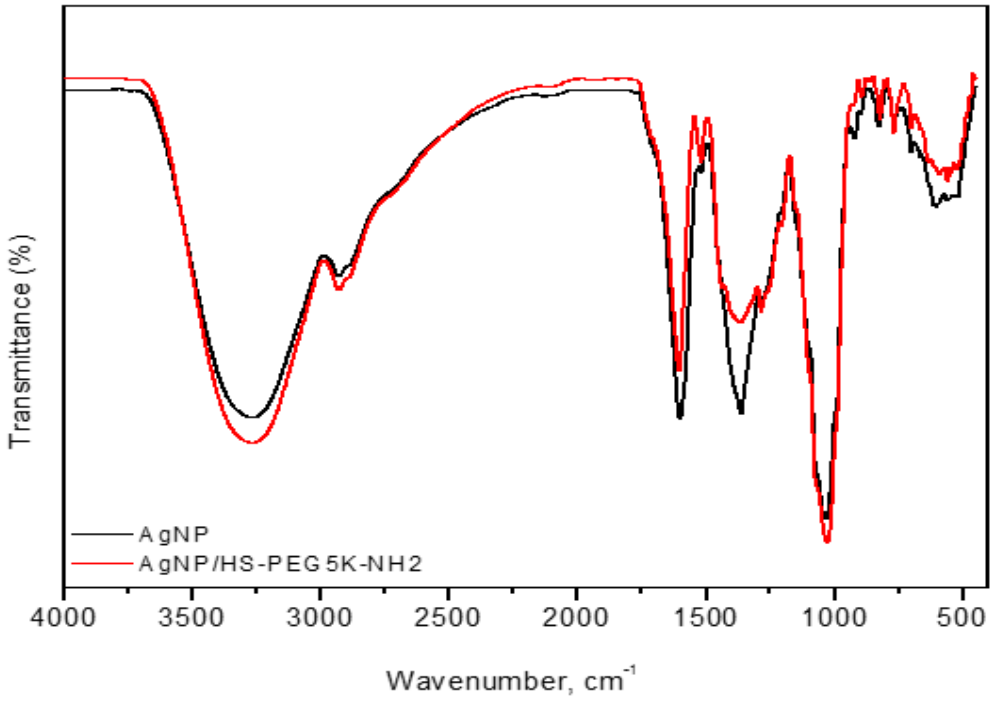

Figure 4.12. FTIR spectroscopy results of HS-PEG5K-NH_2 and AgNPs/HS-PEG5K-NH_2

4.2.3. SEM, TEM and EDS Results of AgNP/HS-PEG5K-NH_2

The size and surface morphology of AgNPs/HS-PEG5K-NH_2 was investigated by SEM and TEM. The TEM images were obtained with an accelerating voltage of 30 kV with STEM detector. The elemental signals of Ag, C, O, Cl and Cu were observed by EDS analysis. Organic ligands and their functional groups in the extract gives the elemental signals like Cl and Cu signals comes from sample holders. Extract ingredient conjugates to the AgNPs surface in addition to HS-PEG5K-NH_2. Spherical and well dispersed agglomerates were observed in SEM images (Figure 4.13). STEM images showed that AgNPs/HS-PEG5K-NH_2 were mainly spherical in shape with an average diameter of 21.86 nm (Figure 4.14).

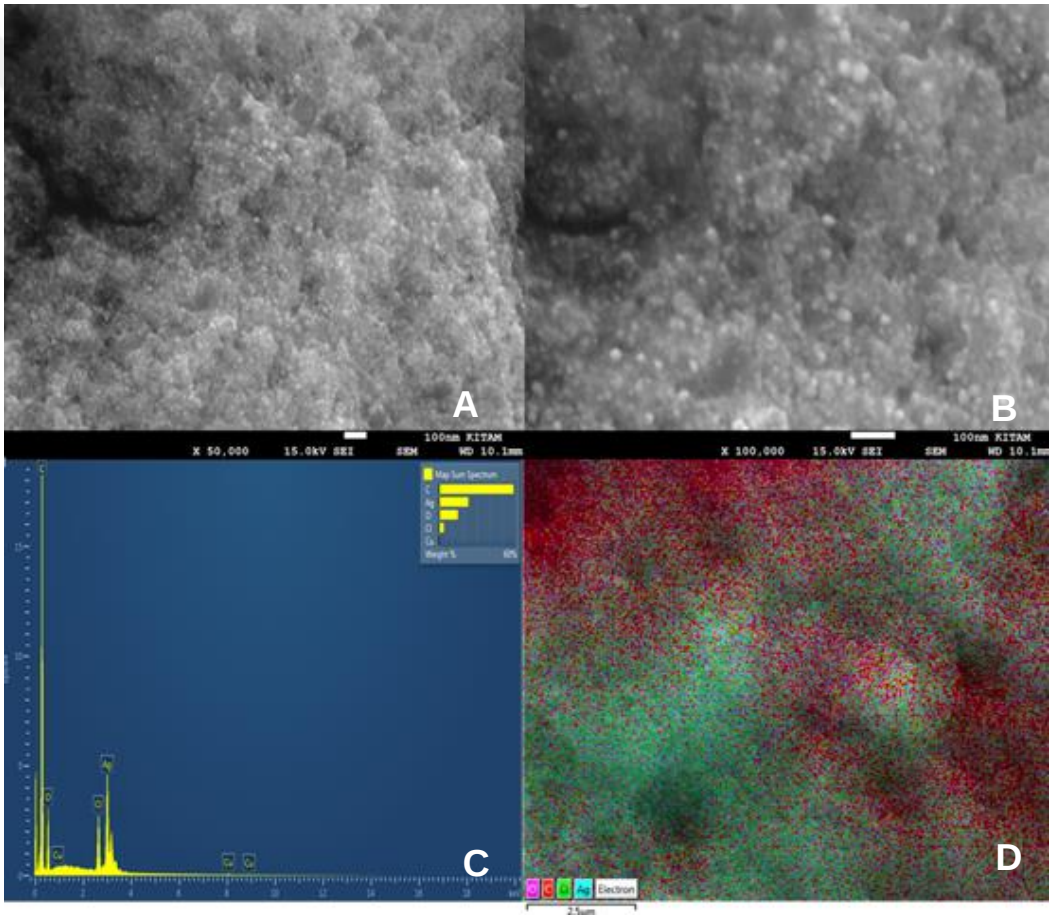

Figure 4.13. SEM (A, B) and EDS (C, D) images of AgNPs/HS-PEG5K-NH_2

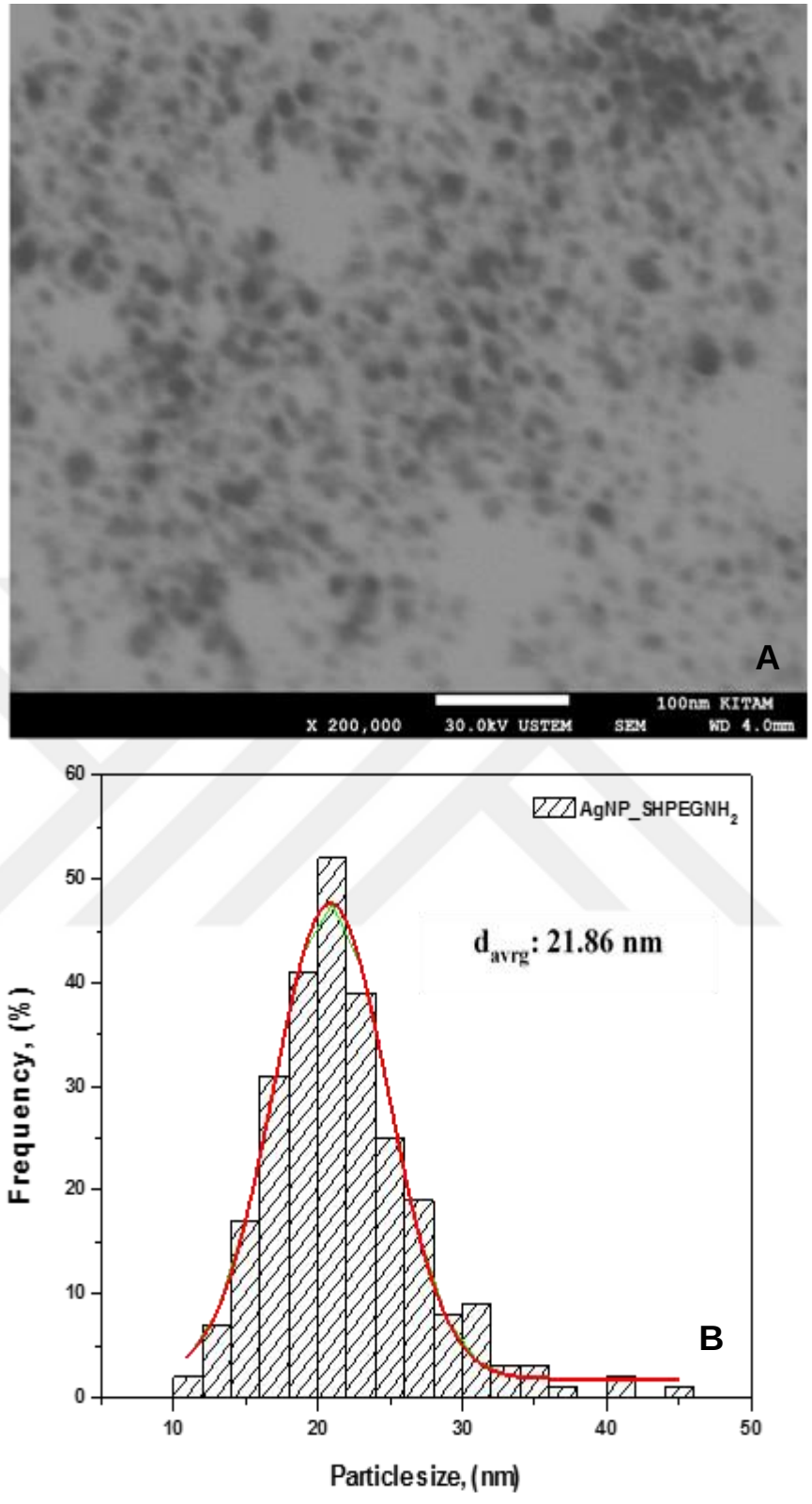

Figure 4.14. STEM image (A) and particle size distribution (B) of AgNPs/HS-PEG5K-NH_2

4.3. AgNPs/HS-PEG5K-NH_2/PAMAMG4

4.3.1. UV-Vis Spectroscopy Results of AgNPs/HS-PEG5K-H_2/PAMAMG4

The surface of AgNPs/HS-PEG5K-NH_2 modified with a carboxylated PAMAMG4 dendrimer through amide linkage with the amine group of AgNPs/HS-PEG5K-NH_2 via an EDC coupling reaction.

The nano-system was characterized by using Uv–Vis spectroscopy to confirm the successful conjugation of AgNPs/HS-PEG5K-NH_2 with PAMAMG4. The UV–Vis absorption spectra of AgNPs/HS-PEG5K-NH_2/PAMAMG4 is shown in Figure 4.15. As it seen in Figure 4.15 (A), different concentrations of activated PAMAMG4 was added into the synthesised AgNPs/HS-PEG5K-NH_2 solution. Firstly, concentrations are increased with the addition of (100 μL and 200 μL) activated PAMAMG4. Then, absorption band was showed broad absorption peaks at 400 to 456 nm with the addition of 300 μL of activated PAMAMG4.

To understand the such increased peaks, AgNP-NHS interaction and AgNP-EDC.HCl interaction was investigated, Figure 4.15 (B) and Figure 4.15 (C). Additions of NHS and EDC.HCl into the AgNP solution were showed the similar dilution effect with the addition of pure water into AgNP solution, Figure 4.15 (D). When EDC.HCl and NHS were added into AgNPs/HS-PEG5K-NH_2 solution, which is given in Figure 4.15 (E) and Figure 4.15 (F), similar concentration increased trend was observed with the Figure 4.15 (A).

The colloidal stability test was conducted with 100 μL, 0.98 $x10^{-8}$ mole of activated PAMAMG4 solution. After 48 hours of reaction, stable AgNPs/HS-PEG5K-NH_2/PAMAMG4 nano-structure was obtained, Figure 4.16.

As it shown in Figure 4.16, red shift of surface plasmon resonance band was detected after conjugation of the AgNP/HS-PEG5K-NH_2 with PAMAM G4. The shift, which were observed in the absorption spectrum of AgNPs/HS-PEG5K-NH_2/PAMAMG4 was considered an indication of the successful conjugation of PAMAMG4 with AgNPs/HS-PEG5K-NH_2. Li et al.(Li, He, LuandJia, 2017), Jiang et al. (Jiang et al., 2010) and Khutale and Casey (KhutaleandCasey, 2017) reported the similar UV-Vis results about conjugation of PEG with PAMAM dendrimer.

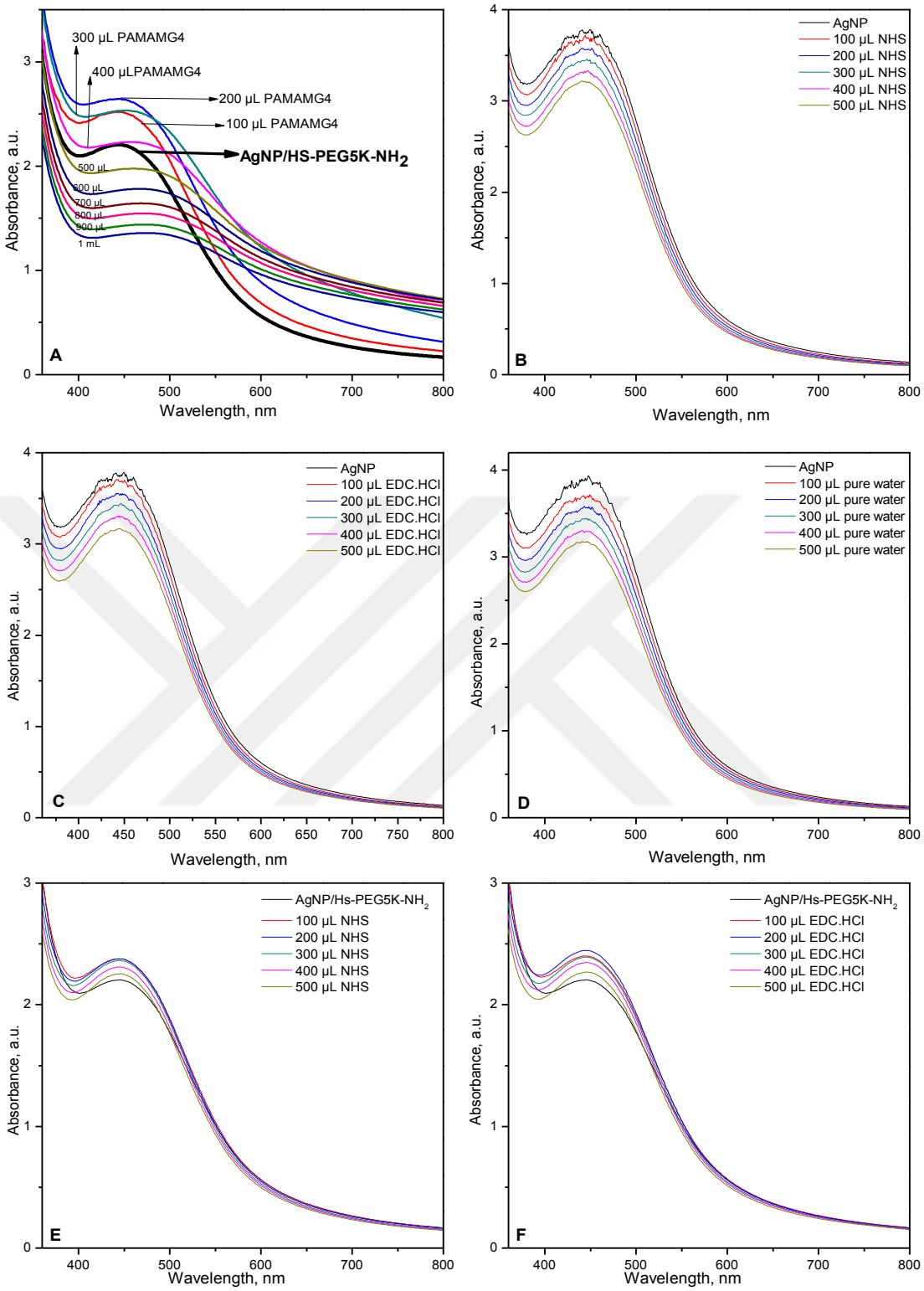

Figure 4.15. Functionalization of AgNP/HS-PEG5K-NH_2 with PAMAMG4 (A), interaction between AgNP and NHS (B), AgNP and EDC.HCl (C), addition of the pure water in the AgNP solution (D), interaction between AgNP/HS-PEG5K-NH_2 and NHS (E), interaction between AgNP/HS-PEG5K-NH_2 and EDC.HCl (F)

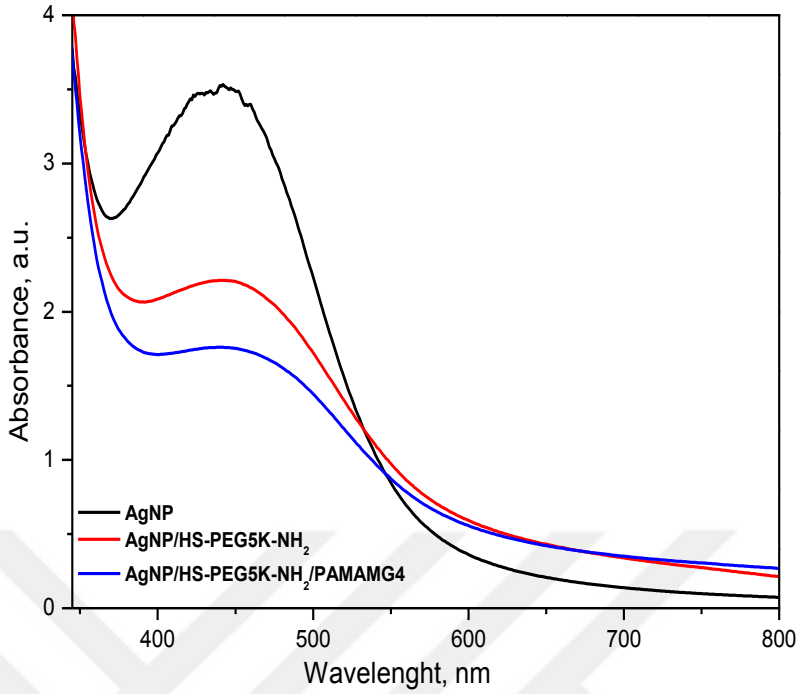

Figure 4.16. Conjugation of the HS-PEG5K-NH_2 with PAMAMG4

4.3.2. Fourier Transform Infrared Spectroscopy Results of AgNPs/HS-PEG5K-NH_2/PAMAMG4

FTIR spectroscopy was used in order to investigate the interaction of AgNP/HS-PEG5K-NH_2 and PAMAMG4. FTIR spectrum of AgNP/HS-PEG5K-NH_2/PAMAMG4 shown in Figure 4.17

AgNP/HS-PEG5K-NH_2/PAMAMG4 showed a broad peak at 3264 cm^{-1} which corresponds to -O–H stretching vibration (Jeffrey S. GaffneyandJones, 2012). Also, as seen from HS-PEG5K-NH_2 and AgNP interaction band, -C-H stretching vibrations were shift from 2927 cm^{-1} to 2910 cm^{-1} which corresponds to PAMAM G4 and HS-PEG5K-NH_2 interaction. Comparing the FTIR spectra of the AgNP/HS-PEG5K-NH_2 with AgNP/HS-PEG5K-NH_2/PAMAMG4 indicated the disappearance of the bands at 1516 cm^{-1} and 1281 cm^{-1} which were representing the -NH_2 deformation vibration of amines and -C-N stretching of aromatic amines which are obtained from HS-PEG5K-NH_2 (Jeffrey S. GaffneyandJones, 2012).

Furthermore, the peaks at 1595 cm^{-1} 1387 cm^{-1} and 1024 cm^{-1} were shifted to higher frequencies after covalently bonding. Also, the band at 815 cm^{-1} is -CH out of plane deformation vibration (Jeffrey S. GaffneyandJones, 2012) and the band at 768

cm^{-1} is the -CH stretching and -C-S stretching are showed lower frequencies. These findings suggested possible inter-molecular interaction between AgNP/HS-PEG5K-NH_2 and PAMAMG4. So, it can be concluded that PAMAMG4 successfully conjugated with HS-PEG5K-NH_2. In the literature, similar findings were reported about PAMAM and PEG conjugation (R. Ahmed et al., 2021; Elfiyani et al., 2018; Li et al., 2017).

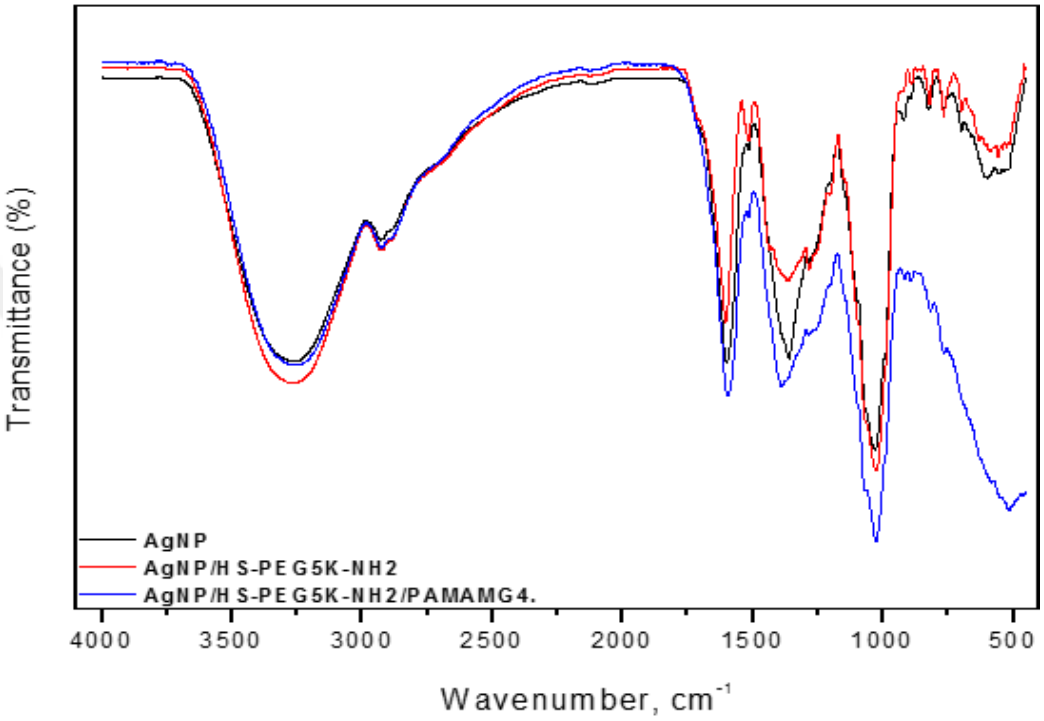

Figure 4.17. FTIR spectrum of AgNP/HS-PEG5K-NH_2/PAMAMG4

4.3.3. SEM, TEM and EDS Results of AgNP/HS-PEG5K-NH_2/PAMAMG4.

The images of the AgNP/HS-PEG5K-NH_2/PAMAMG4 were taken at a magnification of 200k at 30 kV for STEM, and 100k and 50k at 15kV for SEM. Figure 4.18 shows that most of the nanostructure were spherical and uniformly dispersed. Agglomerations were also observed, and in agreement with the SPR band in the UV–Vis spectrum. STEM micrograph demonstrates spherical agglomerates with size ranging between 20 and 50 nm. The average particle size of AgNP/HS-PEG5K-NH_2/PAMAMG4 was found to be 34.35 nm. The EDS profile shows the silver signal with relative compositions of elements such as C, O, N, Al and Cu.

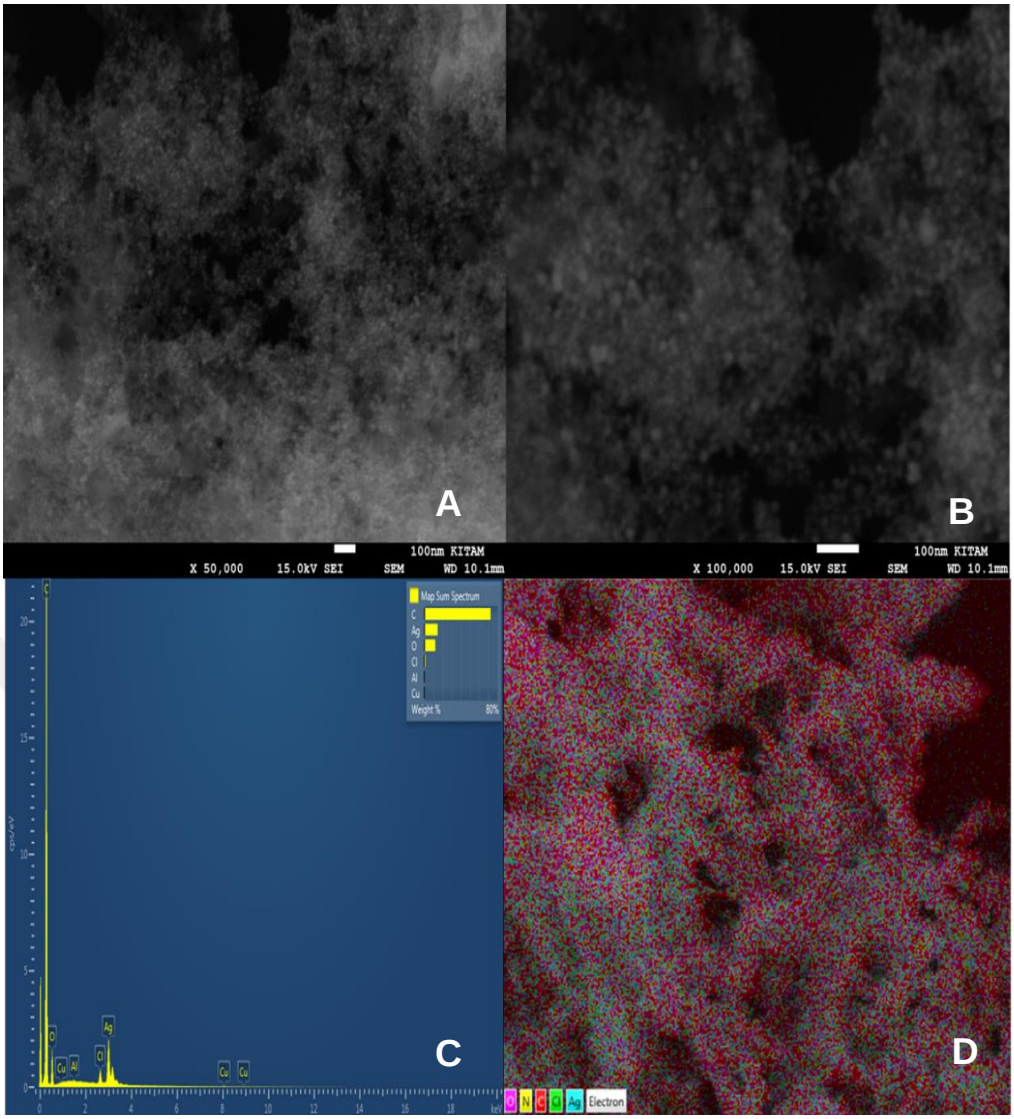

Figure 4.18. SEM (A, B) and EDS (C, D) images of AgNP/HS-PEG5K-NH_2/PAMAMG4

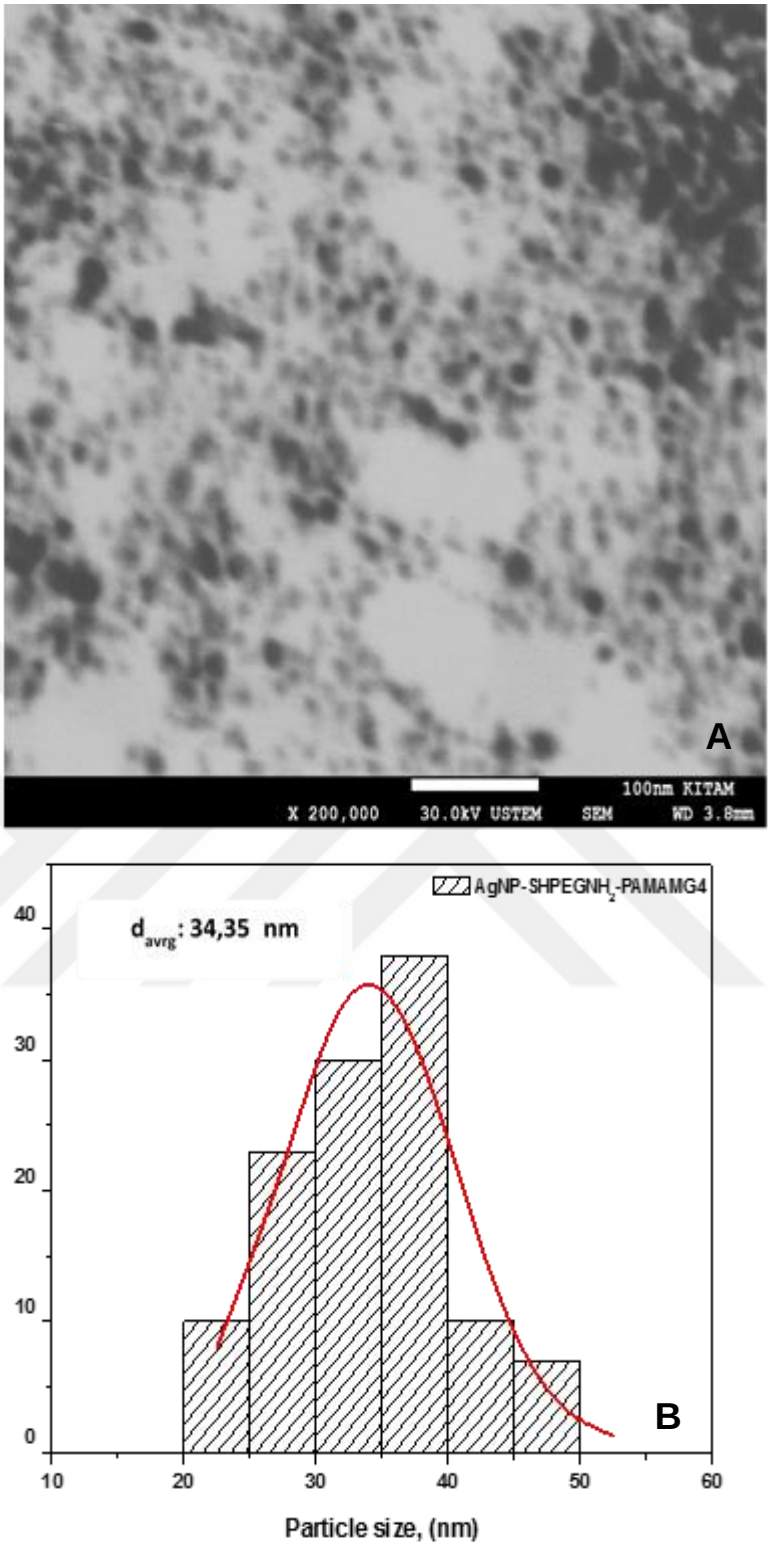

Figure 4.19. STEM micrograph (A) and particle size distribution (B) of AgNP/HS-PEG5K-NH_2/PAMAMG4

4.4. AgNPs/HS-PEG5K-NH_2/PAMAMG4/DOX

4.4.1. UV-Vis Spectroscopy Results of AgNPs/HS-PEG5K NH_2/PAMAMG4/DOX

The DOX was bounded to the carboxylic acid group of the PAMAMG4 through amide bonding by using DIPEA as a base and HBTU as a coupling agent to get the AgNP/HS-PEG5K-NH_2/PAMAMG4/DOX nano drug delivery system, Figure 4.20. The UV–Vis absorption spectra of the AgNP, AgNP/HS-PEG5K-NH_2, AgNP/HS-PEG5K-NH_2/PAMAMG4 and AgNP/HS-PEG5K-NH_2/PAMAMG4/DOX are given in Figure 4.21.

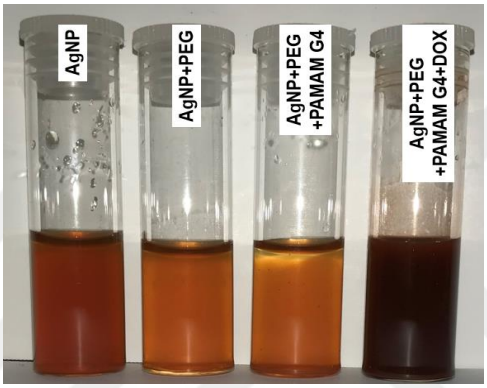

Figure 4.20. The synthesised AgNP, AgNP/HS-PEG5K-NH_2, AgNP/HS-PEG5K-NH_2/PAMAMG4 and AgNP/HS-PEG5K-NH_2/PAMAMG4/DOX

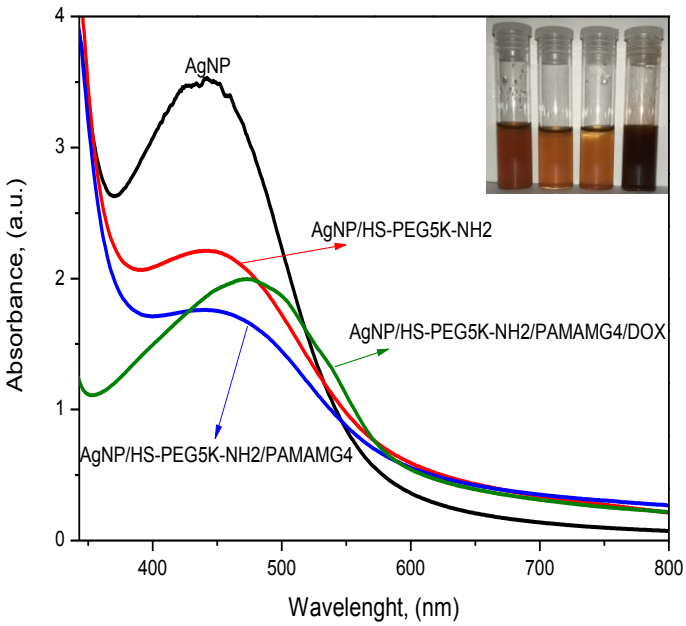

Figure 4.21. Conjugation of DOX with AgNP/HS-PEG5K-NH_2/PAMAMG4

As it seen in Figure 4.21, red shifts of the SPR bands were observed after each conjugation of HS-PEG5K-NH_2 on AgNPs, of PAMAMG4 on AgNPs/ HS-PEG5K-NH_2 and of DOX on AgNPs/ HS-PEG5K-NH_2/PAMAMG4. The shifts were indication of the successful conjugation of each molecule. Khutale and Casey (KhutaleandCasey, 2017) reported gold nanoparticle based nanocarrier system for doxorubicin and, similar shifts for the SPR bands of DOX were observed. Besides, Borker and Pokharkar (BorkerandPokharkar, 2018) synthesised pectin-capped gold nanoparticles for delivery of anticancer drug and doxorubicin was overexpressing asialoglycoprotein receptor. They reported similar red shift in the SPR band due to the DOX conjugation to the nanoparticle system. Mohamad (Mohamed, 2020) reported greenly synthesized, DOX loaded hybrid chitosan silver nanoparticles and, DOX loaded system showed broad SPR band which indicates the successful conjugation.

The release of the DOX was then quantified by measuring its absorbance using absorption band at 480 nm, Figure 4.22 and the concentration of the released DOX estimated with the aid of a standard curve, Figure 4.23. 2 mg/L DOX was loaded. Unloaded DOX was removed by dialysis membrane using centrifuge and its concentration was determined by UV-Vis spectroscopy. It was found that 1.6046 mg/L, in other words 80 % of DOX was loaded onto the AgNP/HS-PEG5K-NH_2/PAMAMG4 nano-system. Cumulative (%) DOX release from the drug delivery system are shown in Table 4.5, Table 4.7 and Table 4.9 for pH 7.4, pH 6.6 and pH 4.0, respectively. Cumulative (%) free DOX release are given in Table 4.6, Table 4.8 and Table 4.10 for pH 7.4, pH 6.6 and pH 4.0, respectively. Calibration curves for cumulative calculations are given in Figure 4.24, Figure 4.25 and Figure 4.26 for pH 7.4, pH 6.6 and pH 4.0, respectively.

The release of the loaded DOX was slow and prolonged, compared to free DOX. In vitro drug release studies showed that 33.28 %, 21.52 % and 7.75 % of the conjugated DOX were released from the drug delivery system for pH 4.0, pH 6.6 and pH 7.4, respectively, in ten days. Whereas, 100 % of free DOX was released in the 24 hours for pH 4.0 and pH 6.6. In the pH 7. 4, only 71.8 % of free-DOX was released at the end of the 10 days Figure 4.27. Bessone et al., (2020) reported glycol chitosan coated and uncoated albumin nanoparticles for releasing DOX. In vitro release kinetics were investigated. For release studies phosphate buffer saline pH 7.4 were used and continued up to 24 h. Semi-permeable cellulose membrane (cut off 14 kDa) was used

for the release. DOX release from DOX albumin nanoparticles and glycol chitosan DOX nanoparticles with free DOX solution as control. Almost 20 % of DOX cumulatively was released whereas free DOX was released almost 90 % in 24 hours (Bessone et al., 2020).

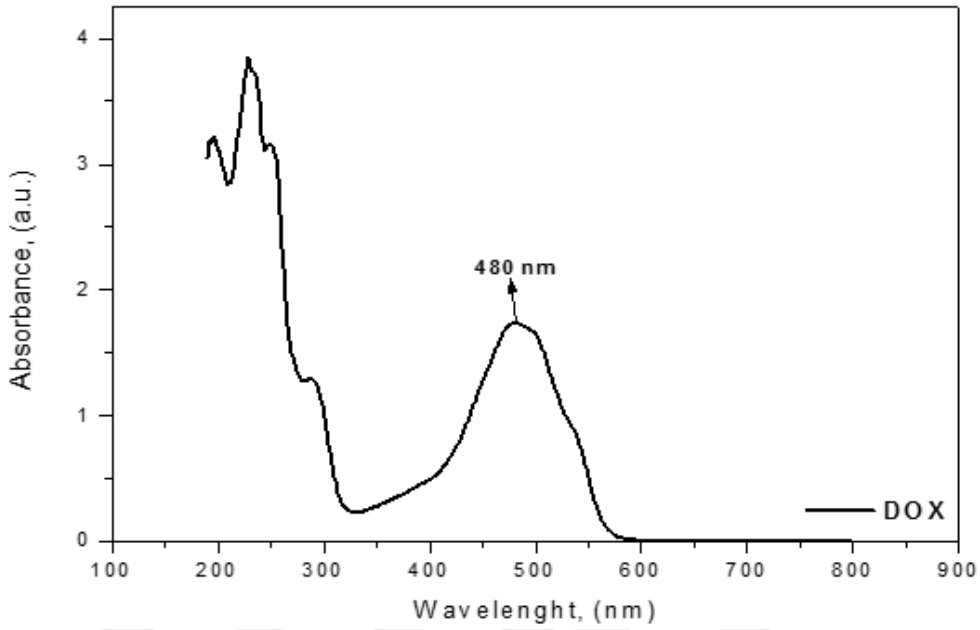

Figure 4.22. UV-Vis spectrum of DOX

Fuentes-Garcia et al., (2021) reported, sonochemical route for mesoporous silica coated magnetic nanoparticles towards pH triggered drug delivery system. The DOX release kinetics at pH 5.5, 6.6 and 7.4 were studied. Dialysis flask (MWCO 5 kDa) were used and, the total amount of DOX released at pH 7.4, 6.6 and pH 5.5 were 21.8 %, 18.4 % and 83 %, respectively (Fuentes-García et al., 2021).

Qiao et al., (2018) prepared, a pH sensitive poly(β-malic acid) conjugate for antitumor drug delivery for DOX. The release of DOX in the conjugate was pH dependent. The release experiments were performed at a pH of 5.6, 6.0, 6.8 and 7.4 in phosphate buffer solution. Dynamic dialysis method was used. Poly(β-malic acid)‑DOX system was investigated at different pH values at 37 °C. DOX releasing was markedly slower with 16.87 % and 9.93 % release rate at pH 6.8 and pH 7.4, respectively. The in vitro drug release experiments showed that the release of DOX was pH dependent (Youbei Qiao, 2018).

Scheeren et al., (2020) studied, transferrin (Tf) conjugated DOX loaded poly(lactic co-glycolic acid) (PLGA) nanoparticles with pH responsive behaviour. For

DOX release, pH adjusted to 7.4, 6.6 and 5.4. Closed dialysis bag (14,000 Da) was used for the release study. Process was performed at 37 °C, for 24 h under magnetic stirring. The release rate of DOX from Tf-DOX-PLGA-NPs was 17 % in the 24 hours (Scheeren et al., 2020).

Yang et al., (2018) studied, silver coated nanoparticles combined with doxorubicin for enhanced anticancer therapy. They silver nanoparticles were coated in the poly(aspartic acid) (PAsp) shell of polymer micelle via the in situ reduction of silver ions and DOX was encapsulated into the micellar poly(caprolactone) (PCL) core through hydrophobic interaction. A dialysis bag with a molecular weight cut off= 3500 Da was used. The cumulative release of DOX from Ag-NPs-DOX was more than 50 % for 50 h (L. Yang et al., 2018).

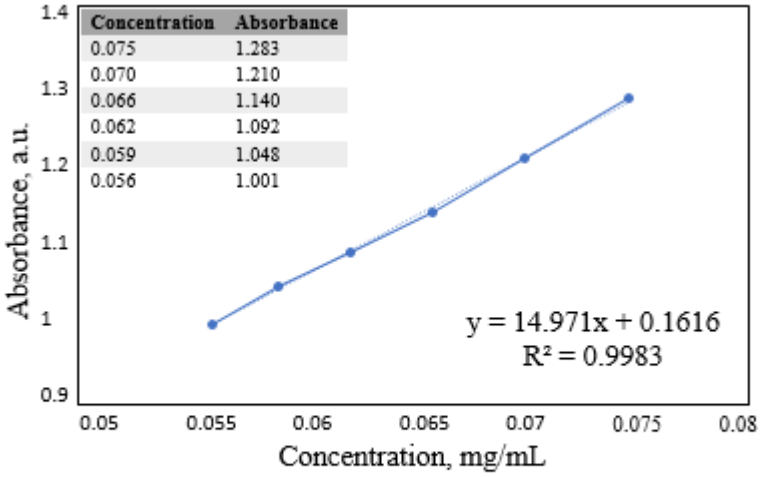

Absorbance	Concentration	100 µL	8 mL	Loaded drug (mg)	Loaded drug (%)
0.1690	0.0005	0.0049	0.3954	1.6046	80.2284

Figure 4.23. The calibration curve and calculation of the loaded DOX into the nano-structure

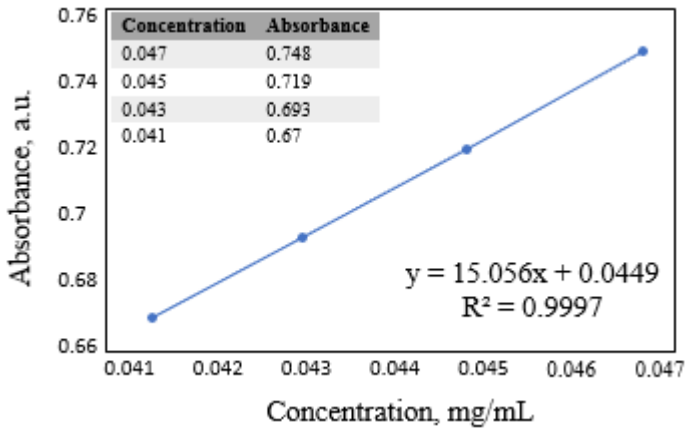

Figure 4.24. Calibration curve of AgNP/HS-PEG5K-NH_2/PAMAMG4/DOX for pH 7.4

Table 4.5. Cumulative release data of the DOX from the AgNP/HS-PEG5K-NH_2/PAMAMG4 in pH 7.4

Time (Hour)	Abs	Conc	400 µL	Df	Release	Cumulative release (mg)	Cumulative release (%)
0.3	0.04	0.0000	0.00001	0.0000	0.00001	0.00001	0.003
0.5	0.04	0.0000	0.00001	0.0000	0.00001	0.00002	0.006
0.8	0.04	0.0000	0.00009	0.0000	0.00009	0.00010	0.036
1.0	0.05	0.0004	0.00051	0.0000	0.00047	0.00058	0.206
1.3	0.05	0.0008	0.00109	0.0000	0.00102	0.00160	0.570
1.5	0.06	0.0013	0.00167	0.0001	0.00156	0.00316	1.129
1.8	0.06	0.0013	0.00167	0.0001	0.00156	0.00473	1.688
2.0	0.06	0.0014	0.00175	0.0001	0.00164	0.00637	2.274
2.3	0.06	0.0013	0.00167	0.0001	0.00156	0.00793	2.833
2.5	0.06	0.0012	0.00150	0.0000	0.00141	0.00934	3.336
2.8	0.06	0.0012	0.00150	0.0000	0.00141	0.01075	3.839
3.0	0.05	0.0009	0.00117	0.0000	0.00110	0.01185	4.231
3.3	0.05	0.0006	0.00076	0.0000	0.00071	0.01256	4.484
3.5	0.05	0.0005	0.00067	0.0000	0.00063	0.01319	4.709
3.8	0.05	0.0004	0.00059	0.0000	0.00055	0.01374	4.907
4.0	0.04	0.0002	0.00026	0.0000	0.00024	0.01398	4.993
4.4	0.04	0.0001	0.00017	0.0000	0.00016	0.01414	5.051
4.9	0.04	0.0001	0.00017	0.0000	0.00016	0.01431	5.109
24	0.05	0.0008	0.00109	0.0000	0.00102	0.01533	5.474
48	0.05	0.0008	0.00109	0.0000	0.00102	0.01635	5.838
72	0.06	0.0011	0.00142	0.0000	0.00133	0.01768	6.313
96	0.07	0.0016	0.00208	0.0001	0.00195	0.01963	7.011
120	0.06	0.0012	0.00159	0.0001	0.00149	0.02112	7.542
144	0.05	0.0003	0.00042	0.0000	0.00040	0.02151	7.684
168	0.04	0.0001	0.00017	0.0000	0.00016	0.02168	7.742
192	0.04	0.0000	0.00001	0.0000	0.00001	0.02169	7.745
216	0.04	0.0000	0.00001	0.0000	0.00001	0.02169	7.747
240	0.04	0.0000	0.00001	0.0000	0.00001	0.02170	7.750

Abs: Absorbance, Conc: Concentration, Df: Dilution factor

Table 4.6. Cumulative release data of the free-DOX in pH 7.4

Time (Hour)	Abs	Conc	400 µL	Df	Release	Cumulative release (mg)	Cumulative release (%)
0.3	0.074	0.0019	0.002	0.0024	0.0024	0.0024	0.9
0.5	0.074	0.0016	0.002	0.0001	0.0019	0.0043	1.5
0.8	0.108	0.0039	0.005	0.0003	0.0046	0.0089	3.2
1.0	0.118	0.0046	0.006	0.0004	0.0054	0.0143	5.1
1.3	0.136	0.0058	0.007	0.0005	0.0069	0.0212	7.6
1.5	0.135	0.0058	0.007	0.0005	0.0068	0.0279	10.0
1.8	0.151	0.0069	0.009	0.0005	0.0081	0.0360	12.9
2.0	0.157	0.0073	0.009	0.0006	0.0085	0.0445	15.9
2.3	0.163	0.0077	0.010	0.0006	0.0090	0.0536	19.1
2.5	0.168	0.0080	0.010	0.0006	0.0094	0.0630	22.5
2.8	0.171	0.0082	0.010	0.0006	0.0097	0.0726	25.9
3.0	0.173	0.0084	0.010	0.0007	0.0098	0.0825	29.5
3.3	0.179	0.0088	0.011	0.0007	0.0103	0.0928	33.1
3.5	0.185	0.0092	0.012	0.0007	0.0108	0.1036	37.0
3.8	0.176	0.0086	0.011	0.0007	0.0101	0.1136	40.6
4.0	0.183	0.0091	0.011	0.0007	0.0106	0.1243	44.4
4.4	0.175	0.0085	0.011	0.0007	0.0100	0.1343	47.9
4.9	0.183	0.0091	0.011	0.0007	0.0106	0.1449	51.7
24	0.222	0.0117	0.015	0.0009	0.0138	0.1587	56.7
48	0.211	0.0110	0.014	0.0009	0.0129	0.1715	61.3
72	0.14	0.0061	0.008	0.0005	0.0072	0.1787	63.8
96	0.127	0.0052	0.007	0.0004	0.0061	0.1848	66.0
120	0.112	0.0042	0.005	0.0003	0.0049	0.1898	67.8
144	0.106	0.0038	0.005	0.0003	0.0044	0.1942	69.4
168	0.086	0.0024	0.003	0.0002	0.0028	0.1970	70.4
192	0.078	0.0019	0.002	0.0001	0.0022	0.1992	71.2
216	0.062	0.0008	0.001	0.0001	0.0009	0.2001	71.5
240	0.061	0.0007	0.001	0.0001	0.0008	0.2010	71.8

Abs: Absorbance, Conc: Concentration, Df: Dilituon factor

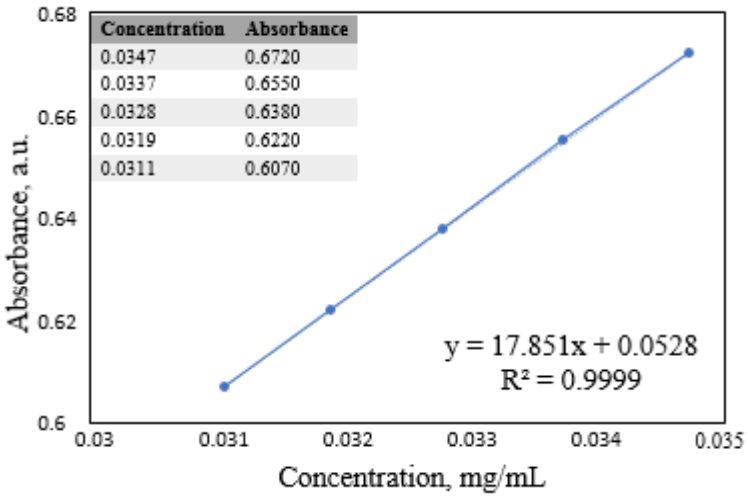

Figure 4.25. Calibration curve of AgNP/HS-PEG5K-NH_2/PAMAMG4/DOX for pH 6.6

Table 4.7. Cumulative release data of the DOX from the AgNP/HS-PEG5K-NH_2/PAMAMG4 at pH 6.6

Time (Hour)	Abs	Conc	400 µL	Df	Release	Cumulative release (mg)	Cumulative release (%)
0.3	0.053	0.00001	0.00001	0.00056	0.0006	0.0006	0.20
0.5	0.055	0.00012	0.00015	0.00001	0.0001	0.0007	0.25
0.8	0.062	0.00052	0.00064	0.00004	0.0006	0.0013	0.47
1.0	0.064	0.00063	0.00078	0.00005	0.0007	0.0020	0.73
1.3	0.067	0.00080	0.00099	0.00006	0.0009	0.0030	1.06
1.5	0.074	0.00119	0.00148	0.00009	0.0014	0.0044	1.56
1.8	0.077	0.00136	0.00169	0.00011	0.0016	0.0060	2.13
2.0	0.077	0.00136	0.00169	0.00011	0.0016	0.0075	2.69
2.3	0.079	0.00147	0.00183	0.00011	0.0017	0.0093	3.31
2.5	0.084	0.00175	0.00218	0.00014	0.0020	0.0113	4.04
2.8	0.088	0.00197	0.00246	0.00015	0.0023	0.0136	4.87
3.0	0.088	0.00197	0.00246	0.00015	0.0023	0.0159	5.69
3.3	0.085	0.00180	0.00225	0.00014	0.0021	0.0180	6.45
3.5	0.084	0.00175	0.00218	0.00014	0.0020	0.0201	7.18
3.8	0.084	0.00175	0.00218	0.00014	0.0020	0.0221	7.91
4.0	0.084	0.00175	0.00218	0.00014	0.0020	0.0242	8.64
4.4	0.090	0.00208	0.00260	0.00016	0.0024	0.0266	9.51
4.9	0.096	0.00242	0.00303	0.00019	0.0028	0.0295	10.53
24	0.141	0.00494	0.00618	0.00039	0.0058	0.0353	12.59
48	0.178	0.00701	0.00877	0.00055	0.0082	0.0435	15.53
72	0.137	0.00472	0.00590	0.00037	0.0055	0.0490	17.50
96	0.100	0.00264	0.00331	0.00021	0.0031	0.0521	18.61
120	0.089	0.00203	0.00253	0.00016	0.0024	0.0545	19.46
144	0.086	0.00186	0.00232	0.00015	0.0022	0.0567	20.24
168	0.076	0.00130	0.00162	0.00010	0.0015	0.0582	20.78
192	0.064	0.00063	0.00078	0.00005	0.0007	0.0589	21.04
216	0.063	0.00057	0.00071	0.00004	0.0007	0.0596	21.28
240	0.063	0.00057	0.00071	0.00004	0.0007	0.0603	21.52

Abs: Absorbance, Conc: Concentration, Df: Dilituon factor

Table 4.8. Cumulative release data of the free-DOX at pH 6.6

Time (Hour)	Abs	Conc	400 µL	Df	Release	Cumulative release (mg)	Cumulative release (%)
0.3	0.053	1.1E-05	0.00001	0.00001	0.00001	0.00001	0.005
0.5	0.109	3.1E-03	0.00394	0.00025	0.00369	0.00370	1.323
0.8	0.177	7.0E-03	0.00870	0.00054	0.00815	0.01186	4.235
1.0	0.201	8.3E-03	0.01038	0.00065	0.00973	0.02159	7.709
1.3	0.211	8.9E-03	0.01108	0.00069	0.01039	0.03197	11.418
1.5	0.220	9.4E-03	0.01171	0.00073	0.01098	0.04295	15.338
1.8	0.243	1.1E-02	0.01332	0.00083	0.01249	0.05543	19.798
2.0	0.241	1.1E-02	0.01318	0.00082	0.01235	0.06779	24.210
2.3	0.252	1.1E-02	0.01395	0.00087	0.01308	0.08087	28.881
2.5	0.270	1.2E-02	0.01521	0.00095	0.01426	0.09512	33.973
2.8	0.301	1.4E-02	0.01738	0.00109	0.01629	0.11142	39.792
3.0	0.306	1.4E-02	0.01773	0.00111	0.01662	0.12804	45.729
3.3	0.311	1.4E-02	0.01808	0.00113	0.01695	0.14499	51.782
3.5	0.315	1.5E-02	0.01836	0.00115	0.01721	0.16220	57.930
3.8	0.321	1.5E-02	0.01878	0.00117	0.01761	0.17981	64.218
4.0	0.321	1.5E-02	0.01878	0.00117	0.01761	0.19742	70.506
4.4	0.401	2.0E-02	0.02438	0.00152	0.02286	0.22027	78.670
4.9	0.416	2.0E-02	0.02543	0.00159	0.02384	0.24412	87.185
24	0.509	2.6E-02	0.03194	0.00200	0.02995	0.27407	97.881

Abs: Absorbance, Conc: Concentration, Df: Dilituon factor

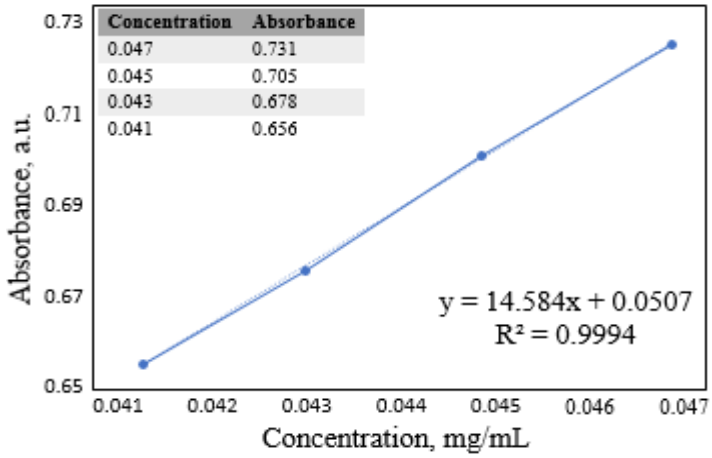

Figure 4.26. Calibration curve of AgNP/HS-PEG5K-NH_2/PAMAMG4/DOX for pH 4.0

Table 4.9. Cumulative release data of the DOX from AgNP/HS-PEG5K-NH_2/PAMAMG4 at pH 4.0

Time (Hour)	Abs	Conc	400 µL	Df	Release	Cumulative release (mg)	Cumulative release (%)
0.3	0.056	0.0004	0.0005	0.0005	0.0005	0.0005	0.16
0.5	0.057	0.0004	0.0005	0.0000	0.0005	0.0010	0.34
0.8	0.067	0.0011	0.0014	0.0001	0.0013	0.0023	0.81
1.0	0.072	0.0015	0.0018	0.0001	0.0017	0.0040	1.42
1.3	0.081	0.0021	0.0026	0.0002	0.0024	0.0064	2.29
1.5	0.098	0.0032	0.0041	0.0003	0.0038	0.0102	3.65
1.8	0.109	0.0040	0.0050	0.0003	0.0047	0.0149	5.32
2.0	0.117	0.0045	0.0057	0.0004	0.0053	0.0202	7.22
2.3	0.127	0.0052	0.0065	0.0004	0.0061	0.0264	9.41
2.5	0.125	0.0051	0.0064	0.0004	0.0060	0.0323	11.55
2.8	0.124	0.0050	0.0063	0.0004	0.0059	0.0382	13.65
3.0	0.119	0.0047	0.0059	0.0004	0.0055	0.0437	15.61
3.3	0.117	0.0045	0.0057	0.0004	0.0053	0.0490	17.51
3.5	0.117	0.0045	0.0057	0.0004	0.0053	0.0544	19.42
3.8	0.110	0.0041	0.0051	0.0003	0.0048	0.0591	21.12
4.0	0.105	0.0037	0.0047	0.0003	0.0044	0.0635	22.68
4.4	0.097	0.0032	0.0040	0.0002	0.0037	0.0672	24.00
4.9	0.100	0.0034	0.0042	0.0003	0.0040	0.0712	25.42
24	0.092	0.0028	0.0035	0.0002	0.0033	0.0745	26.60
48	0.087	0.0025	0.0031	0.0002	0.0029	0.0774	27.65
72	0.082	0.0021	0.0027	0.0002	0.0025	0.0799	28.54
96	0.075	0.0017	0.0021	0.0001	0.0020	0.0819	29.24
120	0.069	0.0013	0.0016	0.0001	0.0015	0.0833	29.77
144	0.078	0.0019	0.0023	0.0001	0.0022	0.0855	30.55
168	0.075	0.0017	0.0021	0.0001	0.0020	0.0875	31.25
192	0.075	0.0017	0.0021	0.0001	0.0020	0.0894	31.94
216	0.074	0.0016	0.0020	0.0001	0.0019	0.0913	32.61
240	0.074	0.0016	0.0020	0.0001	0.0019	0.0932	33.28

Abs: Absorbance, Conc: Concentration, Df: Dilution factor

Table 4.10. Cumulative release data of the free-DOX release in pH 4.0

Time (Hour)	Abs	Conc	400 µL	Df	Release	Cumulative release (mg)	Cumulative release (%)
0.25	0.090	0.003	0.003	0.003	0.003	0.003	1.2
0.50	0.090	0.003	0.003	0.000	0.003	0.007	2.3
0.75	0.122	0.005	0.006	0.000	0.006	0.012	4.4
1.00	0.137	0.006	0.007	0.000	0.007	0.019	6.9
1.25	0.159	0.007	0.009	0.001	0.009	0.028	10.0
1.50	0.178	0.009	0.011	0.001	0.010	0.038	13.6
1.75	0.196	0.010	0.012	0.001	0.012	0.050	17.8
2.00	0.220	0.012	0.015	0.001	0.014	0.063	22.6
2.25	0.236	0.013	0.016	0.001	0.015	0.078	28.0
2.50	0.243	0.013	0.016	0.001	0.015	0.094	33.5
2.75	0.254	0.014	0.017	0.001	0.016	0.110	39.3
3.00	0.266	0.015	0.018	0.001	0.017	0.127	45.5
3.25	0.274	0.015	0.019	0.001	0.018	0.145	51.9
3.50	0.281	0.016	0.020	0.001	0.019	0.164	58.5
3.75	0.281	0.016	0.020	0.001	0.019	0.182	65.1
4.00	0.291	0.016	0.021	0.001	0.019	0.202	72.0
4.42	0.290	0.016	0.021	0.001	0.019	0.221	78.9
4.92	0.294	0.017	0.021	0.001	0.020	0.240	85.9
24.00	0.571	0.036	0.045	0.003	0.042	0.282	100

Abs: Absorbance, Conc: Concentration, Df: Dilution factor

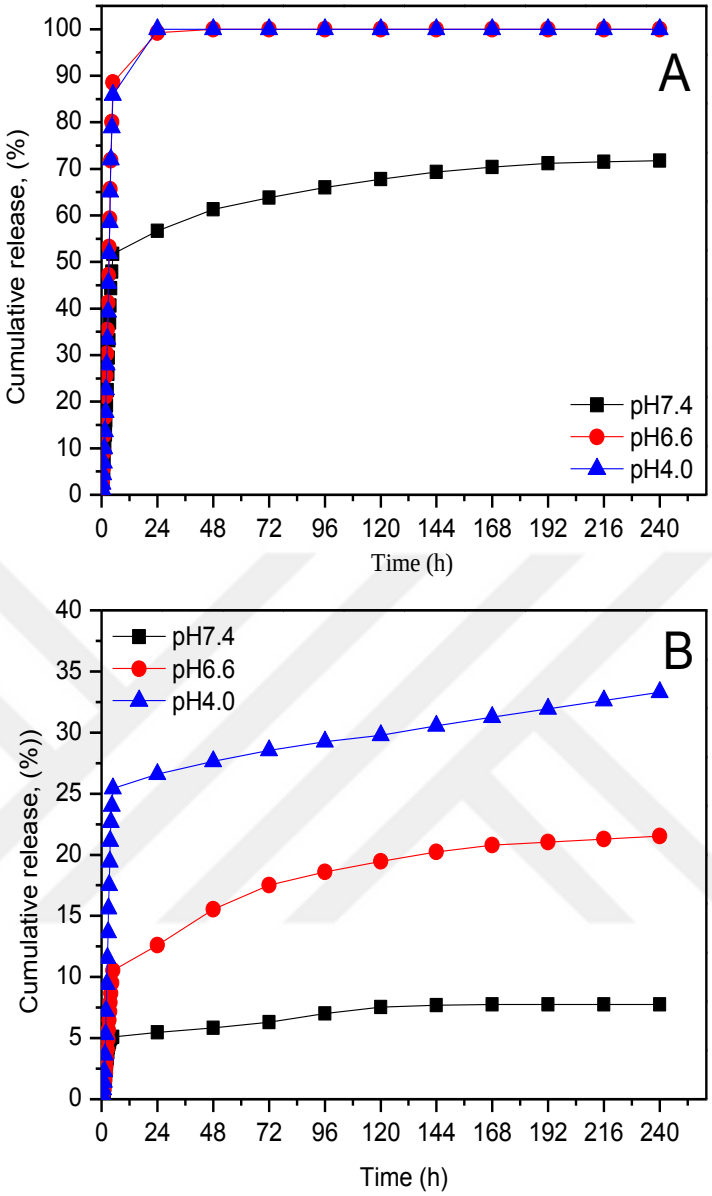

Figure 4.27. Cumulative release (%) of free-DOX in 10 days (A), cumulative release (%) DOX from drug delivery system in 10 days (B)

4.4.2. Fourier Transform Infrared Spectroscopy of AgNP/HS-PEG5K-NH_2/PAMAMG4/DOX

The DOX was conjugated with the carboxylic acid group of the PAMAMG4 through amide bonding. Figure 4.28 shows -NH stretching band of aromatic/primary amines in DOX molecule at 3527 cm^{-1} and it was disappeared after conjugation. The band which is located at 2922 cm^{-1} is representing -CH stretching of aliphatics. In the DOX molecule, -C=O symmetric stretching at the 1726 cm^{-1} was disappeared after PAMAMG4 conjugation. The band at the 1602 cm^{-1} shows the aromatic ring stretching of aromatics. 1396 cm^{-1} is $-COO^-$ symmetric stretching of carboxylic acid groups. Also, the frequency at the 1277 cm^{-1} get lower which represents the $-CH_3$ symmetric deformation vibration in the DOX molecule. The band at the 1206 cm^{-1} belongs to -C-O-C asymmetric stretching and the -C-N stretching of primary aliphatic amines is at the 1030 cm^{-1}. The NH_2 wagging of prim amines gives rise a band at the 844 cm^{-1}. The band at the 762 cm^{-1} belongs to the -C-S stretching and, the band at the 545 cm^{-1} is representing the -C-C=O bending of carboxylic acids, aldehydes and ketones (R. Ahmed et al., 2021; BorkerandPokharkar, 2018; Dong et al., 2017; Jeffrey S. GaffneyandJones, 2012). FTIR results are in agreement with the literature values.

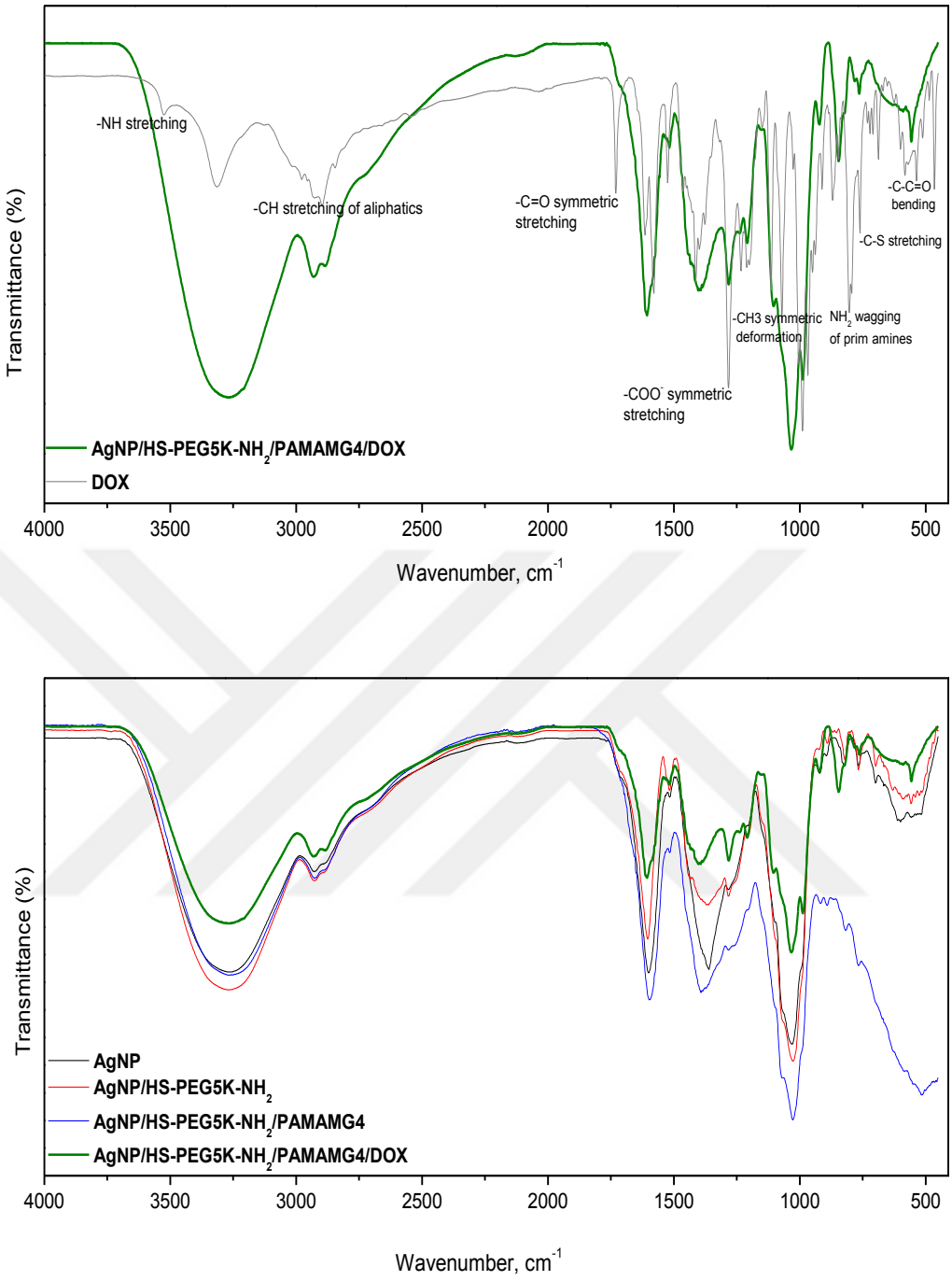

Figure 4.28. FTIR spectroscopy results of DOX and AgNP/HS-PEG5K-NH_2/PAMAMG4/DOX.

4.4.3. SEM, TEM and EDS Results of AgNP/HS-PEG5K-NH_2/PAMAMG4/DOX

The SEM images of AgNPs, DOX and drug delivery system size distribution diameter are illustrated in Figure 4.29 and Figure 4.30. The elemental signals of Ca, F, Mg, P, Ag, K, Ca, O and C were detected in the EDS spectrum. Also, AgNP/HS-PEG5K-NH_2/PAMAMG4/DOX system was observed in fine and well disperse form. The average diameter of AgNP/HS-PEG5K-NH_2/PAMAMG4/DOX was found to be 74.04 nm. The average diameter of the structure was increased with the loading of DOX into the drug delivery system. This behaviour indicates that the DOX were physically conjugated into the nano-system. The pore cutoff-sizes of growing solid tumour vascular permeability is in the range of 200 nm to 1.2 µm (Fan Yuan, 1995b; Susan K. Hobbs, 1998; Z. Wang et al., 2018). On the other hand, the average size of the synthesised drug delivery system is between 60 - 150 nm. Therefore, the synthesised drug delivery system is small enough to pass through these pores.

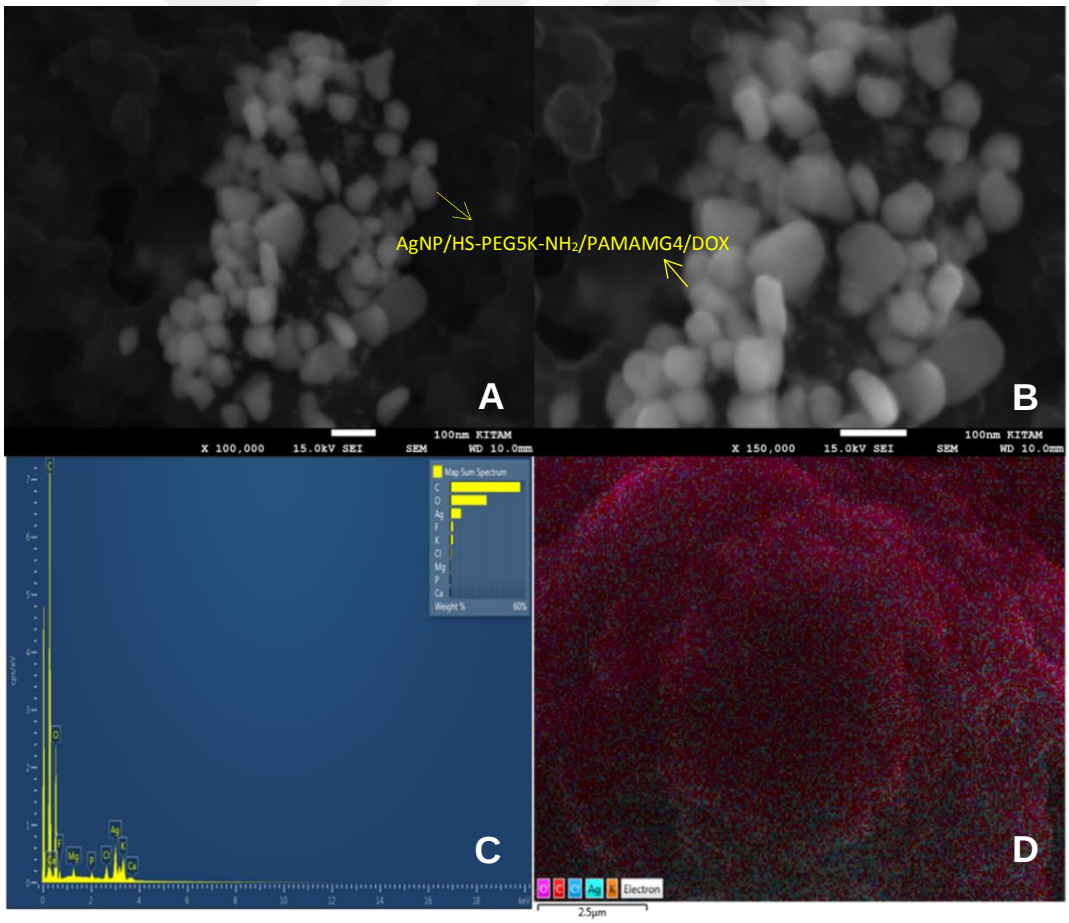

Figure 4.29. SEM (A, B) and EDS (C, D) images of AgNP/HS-PEG5K-NH_2/PAMAMG4/DOX

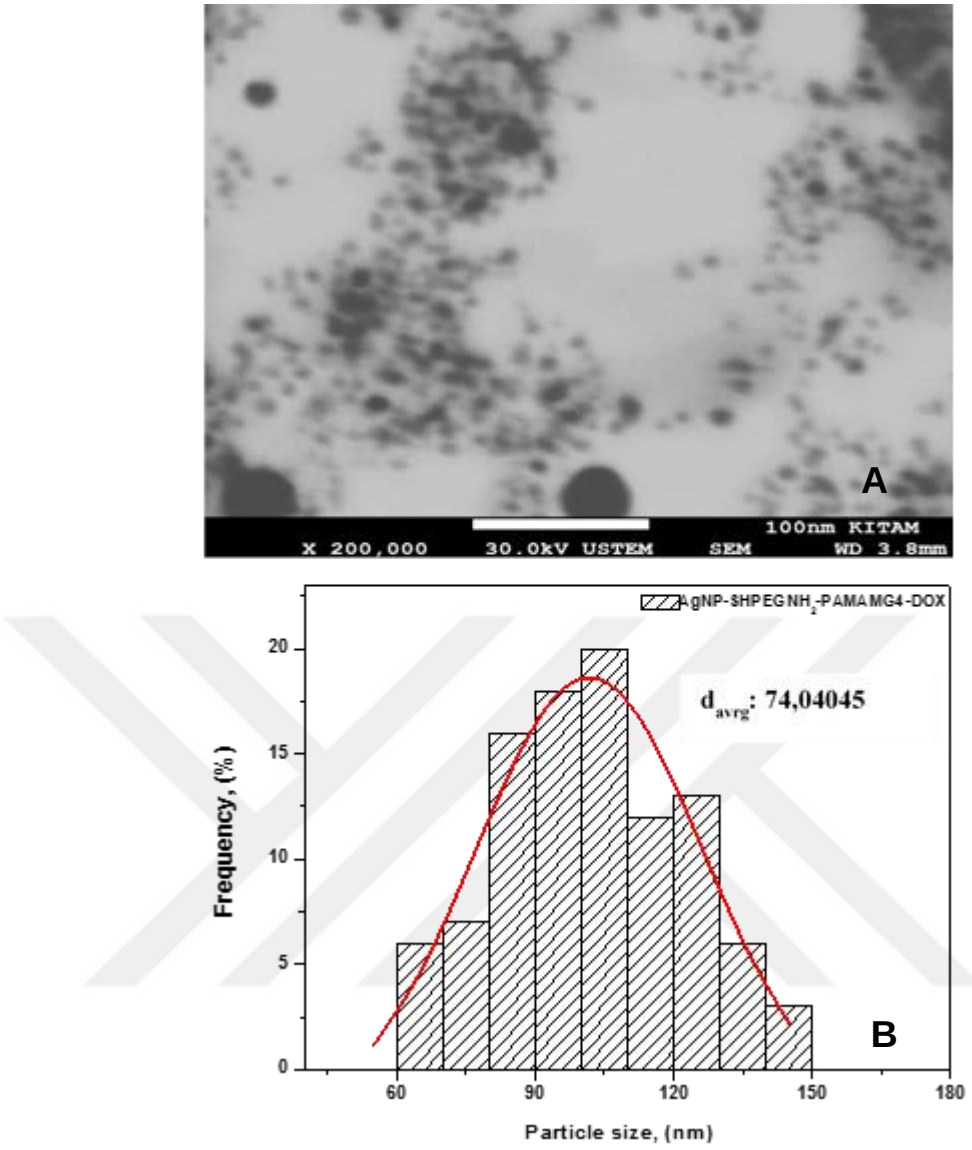

Figure 4.30. STEM image of DOX loaded nano stracture and drug delivery system size distribution histogram

4.4.4. Colloidal stability of AgNP/HS-PEG5K-NH2/PAMAMG4/DOX based on pH and salt test

The effects of pH and electrolyte changes on the colloidal stability of drug delivery system in aqueous solution was studied by UV-Vis absorption spectroscopy.

NaCl leads to aggregation of nanoparticle-based systems in terms of the the reduction in the electrostatic repulsion of nanoparticles (Gao et al., 2012). Normal saline solution, sometimes referred to as physiological or isotonic saline contains 0.9% NaCl (0,0154 M) (Reddi, 2013). Therefore, the samples were placed into the NaCl solution with the concentration range from 0.02 to 0.1 M (KhutaleandCasey, 2017). Also, the solutions with the pH 4.0, pH 6.6 and pH7.4 were prepared by citric acid (1

M) and NaOH (1 M) for pH test.

The addition of 0.02 M of NaCl solution lead a red shift in the UV-Vis absorption spectroscopy due to the particle aggregation caused by shortening of the bond between the AgNPs (Gao et al., 2012; KhutaleandCasey, 2017). But, the absorption spectra of AgNP/HS-PEG5K-NH_2, AgNP/HS-PEG5K-NH_2/PAMAMG4 and AgNP/HS-PEG5K-NH_2/PAMAMG4/DOX were not display any peak broadening or red shift in wavelength, Figure 4.31. This indicates an increased stability of the drug delivery system.

The stability of AgNP, AgNP/HS-PEG5K-NH_2, AgNP/HS-PEG5K-NH_2/PAMAMG4 and AgNP/HS-PEG5K-NH_2/PAMAMG4/DOX were studied at pH 4.0, pH 6.6 and pH 7.4. AgNP/HS-PEG5K-NH_2 and AgNP/HS-PEG5K-NH_2/PAMAMG4 were not exhibit any change in their absorption spectrum for the all tested pH values as shown in Figure 4.32. A higher stability of the samples in the acidic media and alkaline media was observed.

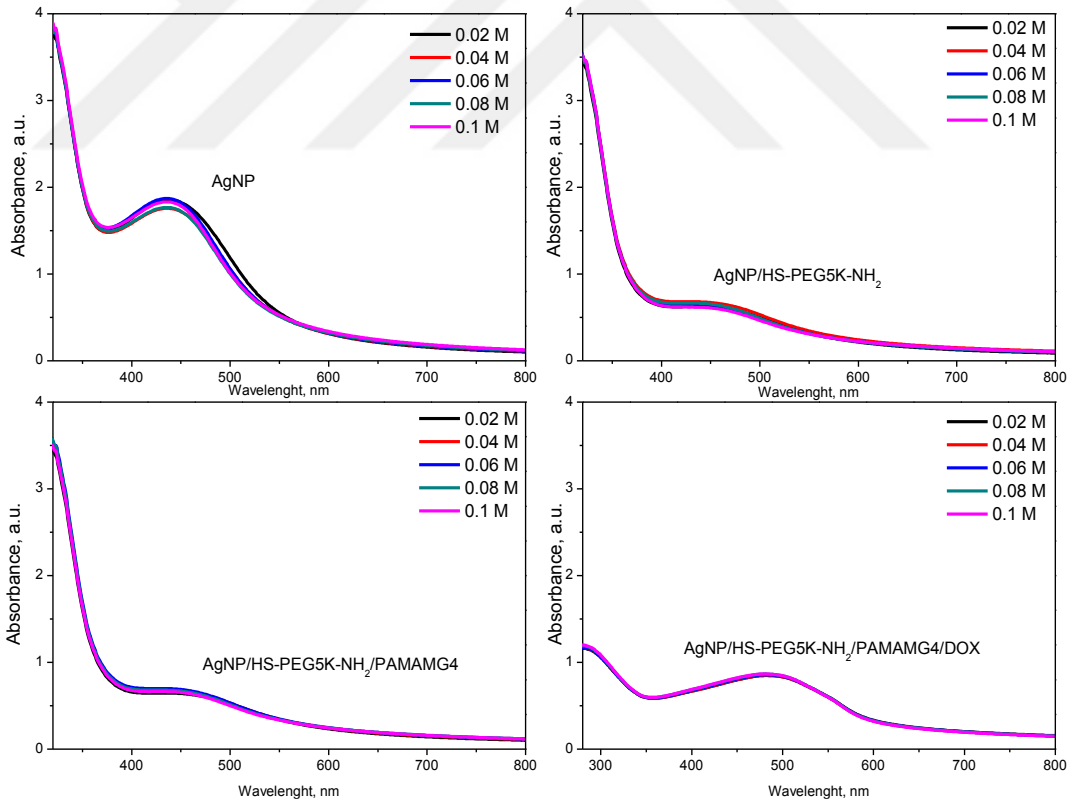

Figure 4.31. The effects of NaCl concentration on the colloidal stability of the drug delivery system in aqueous solution

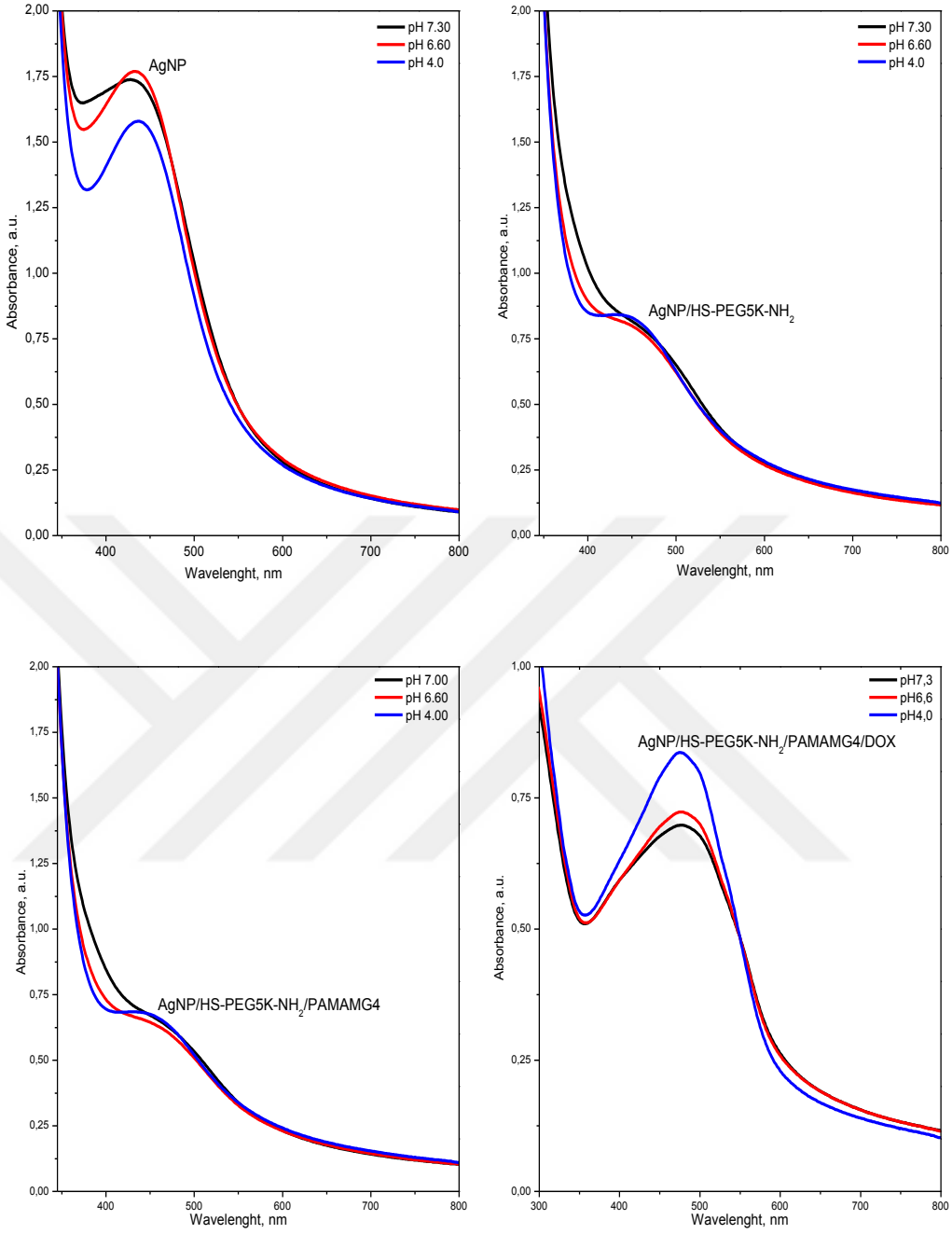

Figure 4.32. The effects of pH changes on the colloidal stability of the drug delivery system in aqueous solution

4.5. Cell viability tests

DOX and AgNP/HS-PEG5K-NH_2/PAMAMG4/DOX were tested at concentrations ranging from 0.1 μM to 50 μM, and the inhibitory concentrations (IC) for 24 and 48 h exposure periods are reported in Table 4.11. DOX and AgNP/HS-PEG5K-NH_2/PAMAMG4/DOX showed both a dose and time-dependent inhibitory effects on HeLa cells on 24 hours and 48 hours exposure periods, Figure 4.33, Figure 4.34, Figure 4.35 and Figure 4.36. Fluorescent and phase contrast images are given in Figure 4.37 and Figure 4.38.

After 24 h incubations with free DOX and AgNP/HS-PEG5KNH_2/PAMAMG4/DOX, the cell viabilities were 90 % and 30 % at the concentration of 2.5 μM and 50 % and 10 % at the concentration of 50 μM, respectively, Figure 4.33 and Figure 4.35. In the Figure 4.35, cellular viability of 0.05 % water group was numerically lower than the 0.1 μM DOX and AgNP/HS-PEG5KNH_2/PAMAMG4/DOX; however, the difference was not statistically significant. This might be due to the external factors such as unequal cell density or unequal medium volume, excess washing with PBS.

After 48 h incubations with free DOX and AgNP/HS-PEG5KNH_2/PAMAMG4/DOX, the cell viabilities were almost 45 % and 5 % at the concentration of 2.5 μM and almost 35 % and 7 % at the concentration of 50 μM, respectively, Figure 4.34 and Figure 4.36.

The IC_{50} of AgNP/HS-PEG5K-NH_2/PAMAMG4/DOX was indicated a higher inhibition than free DOX. This result is pointing that the final nano-system upgrades the efficacy of the DOX. Besides, The AgNP/HS-PEG5K-NH_2/PAMAMG4/DOX had a 24 hr IC_{50} of 1.66 μg/mL, significantly lower than that of the free DOX which had a 24 hr IC_{50} of 2.58 μg/mL. After 48 hours of exposure, the AgNP/HS-PEG5K-NH_2/PAMAMG4/DOX showed an IC_{50} of 1.04 μg/mL compared to 1.34 μg/mL for the free DOX, Table 4.11. Cell inhibition was more profound at 48 hours exposure periods, and AgNP/HS-PEG5K-NH_2/PAMAMG4/DOX was presented again lower IC50 than free DOX.

As it known cervical cancer cell, which leads major harm to the women health, is one of the most frequent malignant cancer. Also, HeLa cell line possesses resistance to cancer drugs (H. Wang et al., 2019). In the literature, Yang et. al., (2017) tested a

folate-PEG-immunoglobulinG-DOX antibody conjugated drug delivery system on HeLa cells. Free DOX had an IC50 value of 0.2 μg/mL whereas, folate-PEG-immunoglobulin G-DOX showed lower toxicity with an IC50 of 3.22 μg/mL (T. Yang et al., 2017). Yuan et. Al., (2011), synthesised DOX-Poly(acrylic acid)-mesoporous silica nanoparticles for pH-sensitive drug delivery system on HeLa cells. The IC50 value of DOX-Poly(acrylic acid)-mesoporous silica nanoparticles and free DOX was found 1.9 and 3.0 μg/mL respectively, after 24 h incubations (Yuan et al., 2011). Besides, Xing et. Al., (2003) reported the hollow iron oxide nanoparticles-DOX formulation for pH-dependent drug release behaviour. System was tested on multidrug resistant OVCAR8-ADR cells. Hollow iron oxide nanoparticles–DOX showed an IC50 = 7.2 μg/mL than to free DOX with and IC50 > 10 μg/mL (Xing et al., 2012).

Also, various targeted drug delivery systems which were tested on different cancerous cell lines, were reported. Khutela and Casey (2017) studied Gold-DOX nanoparticles for pH responsive drug delivery systems. System was tested on A549 cells (adenocarcinomic human alveolar basal epithelial cells). Gold-PEG-PAMAM-DOX showed an IC50 of 0.31 μg/mL whereas free DOX had an IC50 of 0.40 μg/mL. The nano drug delivery system was indicated significantly toxicity than free DOX by the differing IC50 values in the 24 h exposures (KhutaleandCasey, 2017). Li et. al, (2020) tested polycaprolactone/polyethyleneglycol copolymer-DOX nanomicelles on A549 cells. Toxicity results showed that, free DOX had an IC50 of 1.5×10^{-6} M and the nanosystem-DOX had an IC50 of 10×10^{-6} M. Nanostructure with DOX represented weaker toxicity and it was indicated that at the same toxicity level, more nano-drug was required to release equivalent DOX (H. Li et al., 2020). Chen et. Al., (2022) reported dual-pH sensitive chitosan nanoparticles-(DCCA/DOX-NPs) human breast cancer (MCF-7/ADR). Free DOX was exhibited IC50 of 2.77 μg/mL at pH 7.4 and, 2.48 μg/mL at pH 6.5. In contrast, DCCA/DOX-NPs were showed IC50 of 5.21 μg/mL at pH 7.4, and 1.81 μg/mL at pH 6.5 (Q. Chen et al., 2022).

Overall, in the study it was observed that, at most concentration tested AgNP/HS-PEG5K-NH_2/PAMAMG4/DOX caused more cell inhibition than free DOX. The targeted drug delivery system was significantly effective on the Hela cells as proof by the differing IC50 values in the 24 hours exposures. Obtained IC50 values for doxorubicin is within the acceptable criterias according to other studies.

Table 4.11. Inhibitor concentrations (IC) of the compounds for 24 hours and 48 hours exposure periods (µM±S.D.)

	DOX		AgNP/HS-PEG5KNH$_2$/PAMAMG4/DOX	
	24h	**48h**	**24h**	**48h**
IC$_{10}$	16.79±5.53	5.36±1.21	10.77±4.38	4.15±0.69
IC$_{50}$	2.58±0.85	1.34±0.3	1.66+0.67	1.04±0.17
IC$_{90}$	0.4±0.13	0.34±0.08	0.25±0.1	0.26±0.04

IC10: The concentration that will inhibit 10 % of the cells.
IC50: Half of the maximum inhibitory effect concentration.
IC90: The concentration that will inhibit 90 % of the cells.

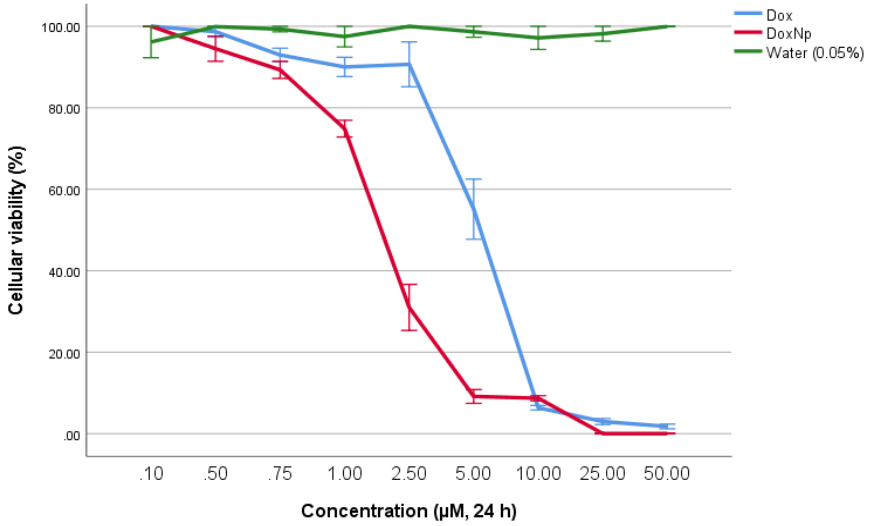

Figure 4.33. Cellular viability (%) of different concentrations of compounds for 24 hours (Mean ± S.E.M., WST-8 assay)

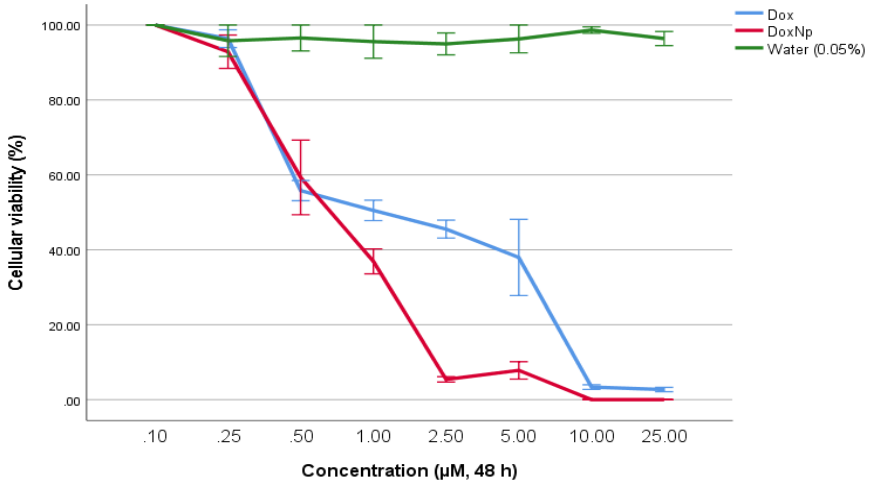

Figure 4.34. Cellular viability (%) of different concentrations of compounds for 48 hours (Mean ± S.E.M., WST-8 assay)

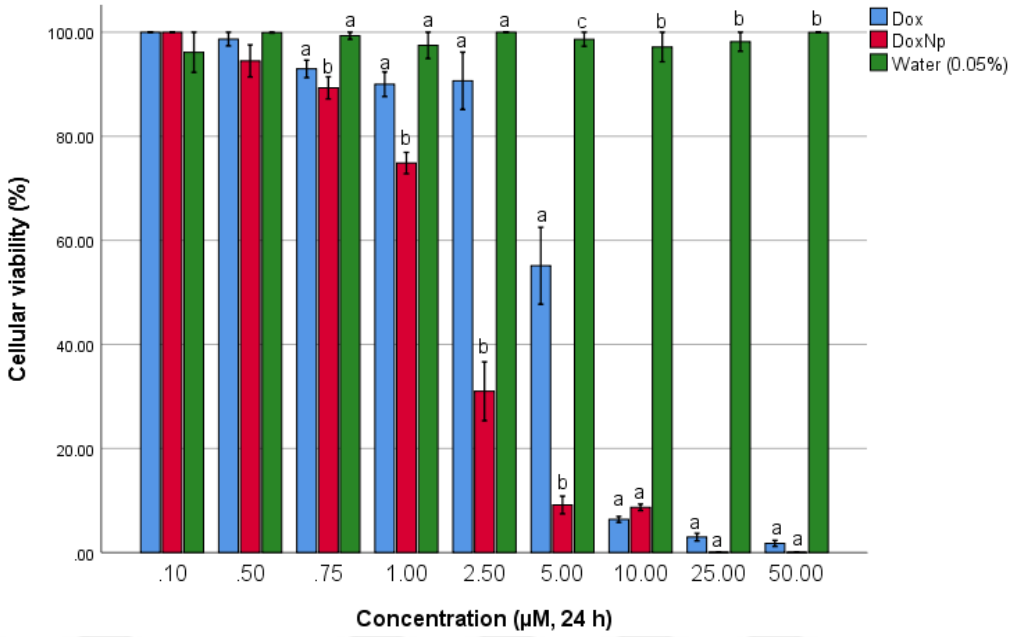

Figure 4.35. Statistical comparison of cellular viability (%) of different concentrations of compounds for 24 hours (WST-8 assay). [a,b,c] Different uppercase letters indicate a significant difference between groups (Mean ± S.E.M., $p<0.05$)

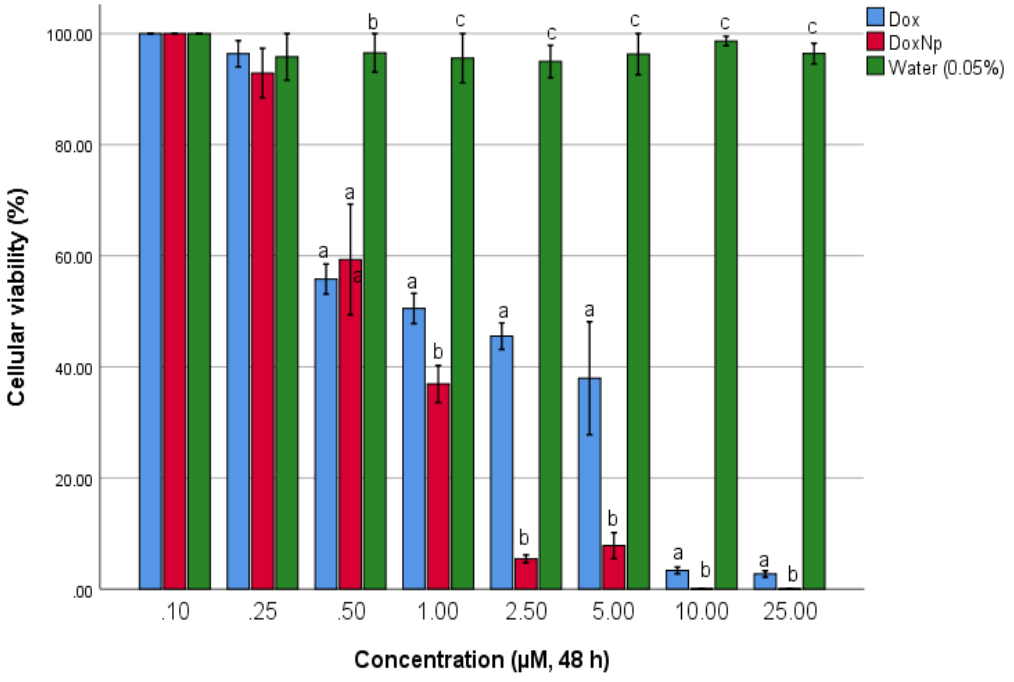

Figure 4.36. Statistical comparison of cellular viability (%) of different concentrations of compounds for 48 hours (WST-8 assay). [a,b,c] Different uppercase letters indicate a significant difference between groups (Mean ± S.E.M., $p<0.05$)

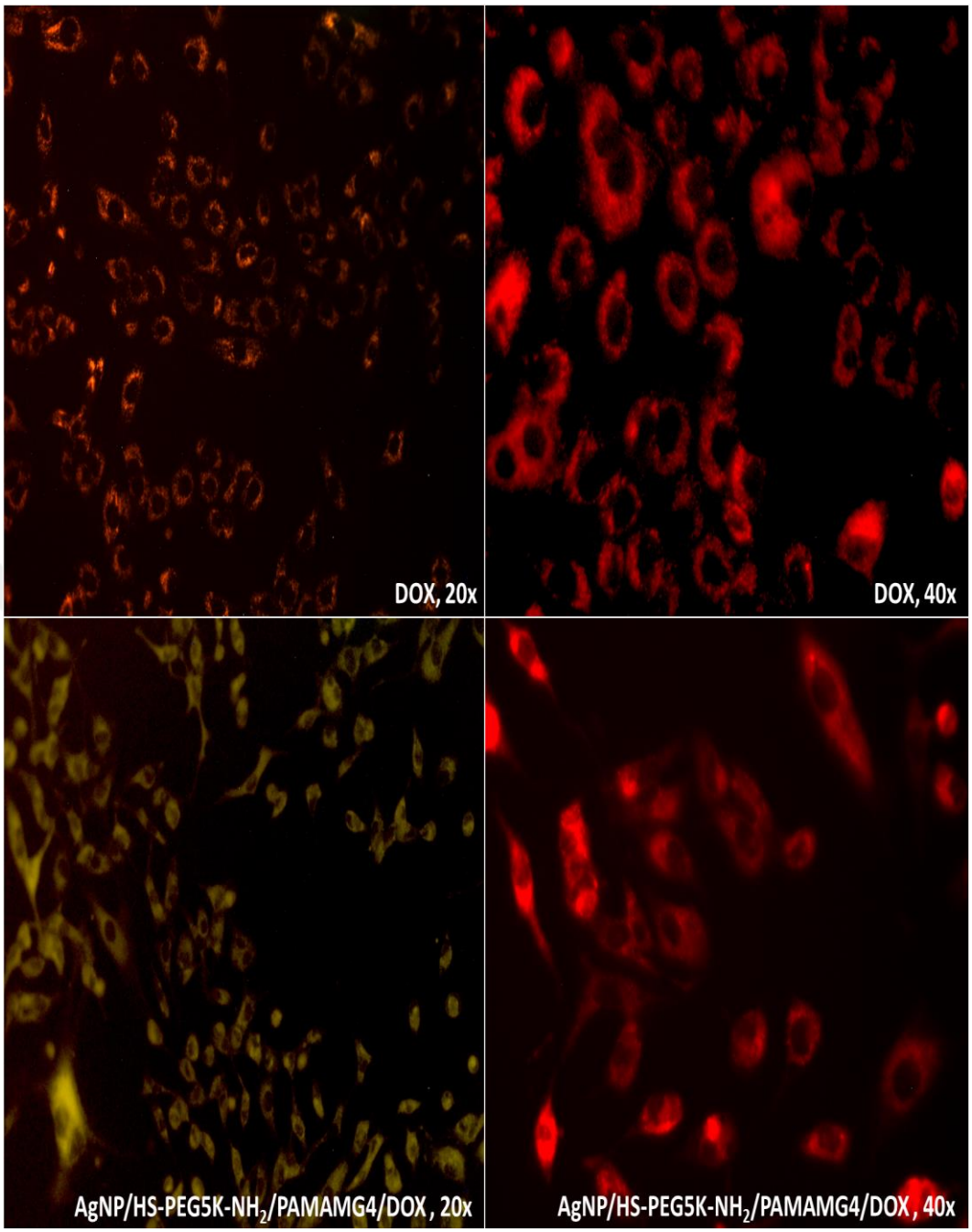

Figure 4.37. Fluorescent images of DOX and AgNP/HS-PEG5K-NH_2/PAMAMG4/DOX with the different magnitudes (20x and 40x)

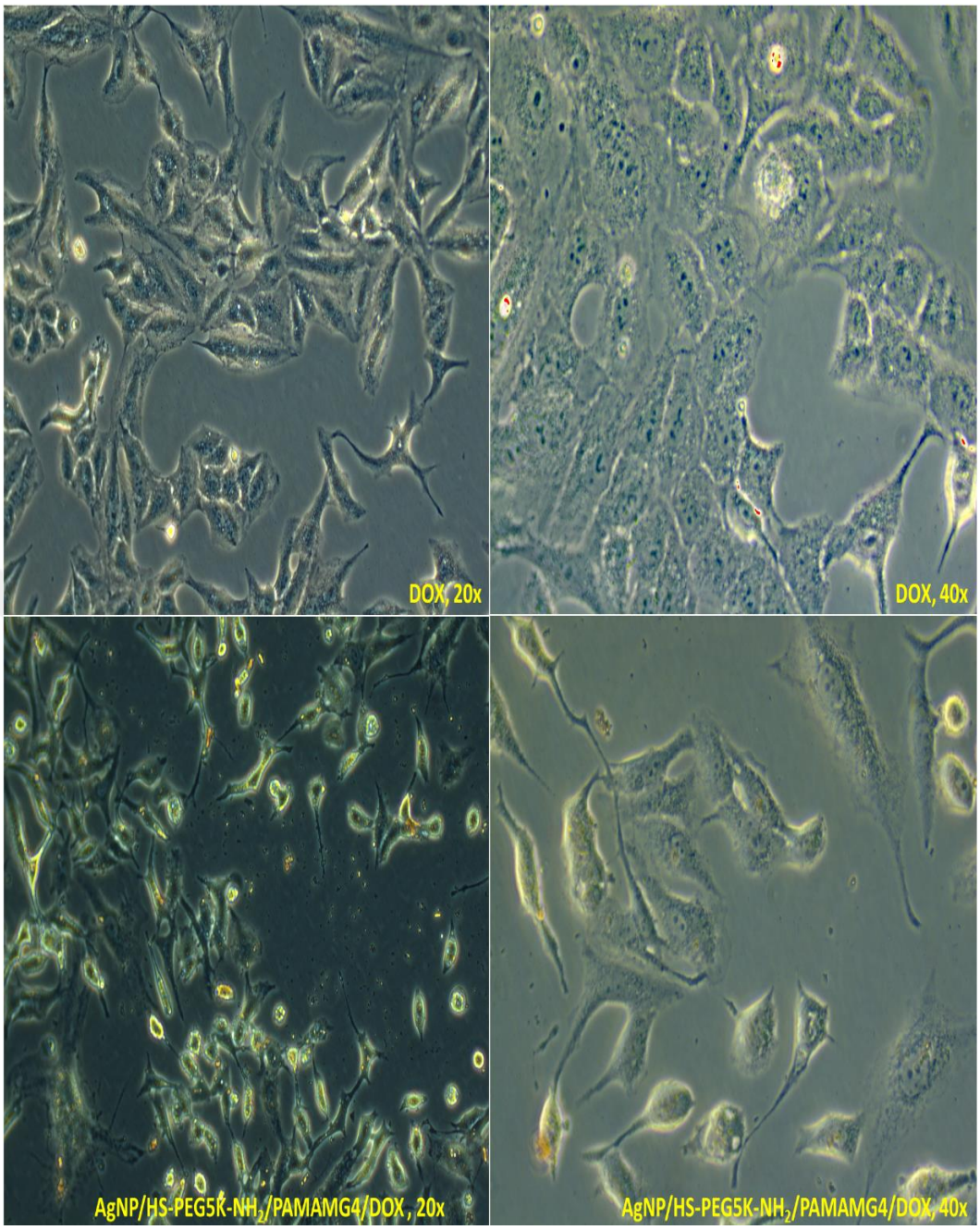

Figure 4.38. Phase contrast images of DOX and AgNP/HS-PEG5K-NH_2/PAMAMG4/DOX with the different magnitudes (20x and 40x)

5. CONCLUSIONS AND SUGGESTIONS

5.1. Conclusions

In this thesis; the efficacy of AgNP/HS-PEG5K-NH_2/PAMAMG4/DOX system was investigated on the treatment of HeLa cells. For this purpose, AgNPs were synthesized by *L. officinalis* leaves extract, primarily. Then, the HS-PEG5K-NH_2 was used for functionalization of the green synthesized AgNPs. After that, PAMAMG4 dendrimer was added into the functionalized nanoparticle system. Lastly, DOX was incorporated into the AgNP/HS-PEG5K-NH_2/PAMAMG4/DOX nano structure. In the next step, characterization of the AgNPs was performed by Uv-Vis, FTIR, AAS, XRD, SEM, TEM and EDS. Also, AgNP/HS-PEG5K-NH_2, AgNP/HS-PEG5K-NH_2/PAMAMG4 and AgNP/HS-PEG5K-NH_2/PAMAMG4/DOX were characterized by UV-Vis, FTIR, SEM, TEM and EDS. Further, the pH and salt test were used for the colloidal stability of the AgNPs, AgNP/HS-PEG5K-NH_2, AgNP/HS-PEG5K-NH_2/PAMAMG4 and AgNP/HS-PEG5K-NH_2/PAMAMG4/DOX in the PBS (pH 4.0, pH 6.6 and pH 7.4). Drug binding study was examined by the absorption of the DOX at 480 nm. The drug release was studied by phosphate buffer solutions (pH 4.0, pH 6.6 and a pH 7.4) and the DOX release was recorded as a function of time up to 10 days. Cytotoxicity tests (WST-8 test) were performed at 24- and 48-hour exposure periods for DOX and AgNP/HS-PEG5K-NH_2/PAMAMG4/DOX. IC10, IC50 and IC90 values of AgNP/HS-PEG5K-NH_2/PAMAMG4/DOX and DOX were calculated by probit-regression analysis. Lastly, statistical analyses were performed ($p<0.05$). To summarize the results obtained,

1 mL E5Y85 and 6 mL 1 mM $AgNO_3$ are the optimized parameters and used for subsequent AgNPs synthesis. The optimized AgNPs were used for further characterization studies. FTIR analysis was studied to identify the presence of functional groups and interaction of *L. officinalis* extract and $AgNO_3$. It was recorded in the region of 4000 – 500 cm^{-1}. The average concentration of the AgNPs in optimized system was found to be 0.2446 mg/L by AAS. Also, four diffraction peaks at 2θ values of 37.98°, 43,72°, 64.73° and 77.71°, which correspond to the reflection of (111), (200), (220), and (311) planes were detected on XRD for the AgNPs. Thus, successful synthesising of AgNPs and crystalline structure were proved by the XRD results. Well distribution of AgNPs with the less aggregation was observed from the SEM images. Besides, the STEM images show the presence of spherically shaped AgNPs supporting

the UV–Vis spectral study. Also, an average mean diameter was found to be 13.40 nm after 3 hours reaction time. The findings are correlated well with the XRD and FTIR analysis.

100 μL of HS-PEG5K-NH_2 aqueous solution was used for the functionalization of the AgNPs. Besides, optimization tests showed that AgNP/HS-PEG5K-NH_2 was stable for 96 hours. The FTIR spectra of AgNP/HS-PEG5K-NH_2 and HS-PEG5K-NH_2 showed that all the data demonstrated the successful functionalization of the HS-PEG5K-NH_2 on the surface of AgNP via the -C-S covalent bonding. The size and surface morphology of AgNPs/HS-PEG5K-NH_2 was studied by SEM and TEM analysis. Results showed that AgNPs/HS-PEG5K-NH_2 were mainly spherical in shape with an average diameter of 21.86 nm.

The surface of AgNPs/HS-PEG5K-NH_2 modified with a carboxylated PAMAMG4 dendrimer through amide linkage with the amine group of AgNPs/HS-PEG5K-NH_2 via an EDC coupling reaction. The stable AgNPs/HS-PEG5K-NH_2/PAMAMG4 nano-structure was obtained with 100 μL, 0.98 $x10^{-8}$ mole of activated PAMAMG4 solution with 48 hours of reaction time. FTIR analysis showed that PAMAMG4 successfully conjugated with HS-PEG5K-NH_2. Besides, STEM images demonstrated spherical agglomerates with size ranging between 20 and 50 nm. The average particle size of AgNP/HS-PEG5K-NH_2/PAMAMG4 was found to be 34.35 nm.

The DOX was bounded to the carboxylic acid group of the PAMAMG4 through amide bonding to get the final AgNP/HS-PEG5K-NH_2/PAMAMG4/DOX pH sensitive drug delivery system. FTIR spectrum indicated the successful conjugation of DOX to the AgNP/HS-PEG5K-NH_2/PAMAMG4. Also, SEM images showed that, AgNP/HS-PEG5K-NH_2/PAMAMG4/DOX were in fine and well disperse form. The average diameter of the AgNP/HS-PEG5K-NH_2/PAMAMG4/DOX was found to be 74.04 nm. 80 % of DOX was loaded into the AgNP/HS-PEG5K-NH_2/PAMAMG4 nano-system.

In vitro drug release studies indicated that 33,28 %, 21,52 % and 7.75 % of the conjugated DOX was released from the nano system for pH 4.0, pH 6.6 and pH 7.4, respectively, in ten days. Whereas, 100 % of free DOX was released in the 24 hours for pH 4.0 and pH 6.6. In the pH 7. 4, only 71.8 % of free-DOX was released at the end of the 10 days.

The AgNP/HS-PEG5K-NH_2, AgNP/HS-PEG5K-NH_2/PAMAMG4 and AgNP/HS-PEG5K-NH_2/PAMAMG4/DOX exhibited higher stability NaCl test. Also, AgNP/HS-PEG5K-NH_2 and AgNP/HS-PEG5K-NH_2/PAMAMG4 had good stability at pH 4.0, pH 6.6 and pH 7.4.

The IC_{50} of AgNP/HS-PEG5K-NH_2/PAMAMG4/DOX was indicated a higher inhibition than free Dox. This is pointing that the final nano-system upgrades the efficacy of the DOX. Besides, The AgNP/HS-PEG5K-NH_2/PAMAMG4/DOX had a 24 hr IC_{50} of 1.66 µg/mL, significantly lower than that of the free DOX which had a 24 hr IC_{50} of 2.58 µg/mL. After 48 hours of exposure, the AgNP/HS-PEG5K-NH_2/PAMAMG4/DOX showed an IC_{50} of 1.04 µg/ml compared to 1.34 µg/mL for the free DOX. Cell inhibition was more profound at 48 hours exposure periods, and AgNP/HS-PEG5K-NH_2/PAMAMG4/DOX was presented again lower IC50 than free DOX. The targeted drug delivery system was significantly altering the speed at which the DOX kills the cell as proof by the differing IC50 values in the 24 hours exposures.

In conclusion, AgNP-SHPEGNH_2-PAMAMG4-DOX pH sensitive nano drug delivery system was developed. The cancer drug DOX was conjugated onto AgNP-SHPEGNH_2-PAMAMG4 nano-system a successful amide bond. TheAgNP-SHPEGNH_2-PAMAMG4-DOX showed a pH sensitive *in vitro* drug release at pH 6.6 and pH 4.0 for 10 days.

5.2. Suggestions

The usage of nanoparticles in the pH responsive drug delivery systems are quite a new technology of our era and, it is extremely possible to avoid harmful side effects of cancer treatment with these novel targeted structures. Drugs including nanoparticles without targeting mechanisms are extremely expensive. Even if they have targeted systems, costs make them unaffordable. Thus, cheap, safe, eco-friendly and system supporter green synthesis applications are getting more attraction for synthesis nanoparticles. In this thesis, it is planned to the design drug delivery system is going to be competitive with familiar examples. The less expensive, less side effects, and also easy production process make it advantageous.

The performed study possesses several scientific outcomes that are needed to be proceed in the future researches. Suggestions for research to be made after the project are given below:

This novel AgNP-SHPEGNH_2-PAMAMG4-DOX targeted drug delivery system could provide a new platform for the intracellular release of DOX at the cancerous area.

This study achieved the applicability of pH responsive targeted drug delivery systems containing AgNPs on drug resistance in cancer cell lines like HeLa cell line.

Moreover, AgNP-SHPEGNH_2-PAMAMG4-DOX showed an excellent toxicity on HeLa cells in a greater extent than free DOX did. Thus, this nano-system appear to be encouraging to reduce the unwanted adverse effects of the free DOX.

Further, promising results make it possible to use AgNP-SHPEGNH_2-PAMAMG4-DOX pH sensitive targeted drug delivery system for the *in vivo* tests. Also, AgNP-SHPEGNH_2-PAMAMG4-DOX nano-system could be a hopeful candidate for enhanced anticancer therapy.

REFERENCES

Ahmed, A., Kim, E., Jeon, S., Kim, J. Y.and Choi, H. (2022). Closed-Loop Temperature-Controlled Magnetic Hyperthermia Therapy with Magnetic Guidance of Superparamagnetic Iron-Oxide Nanoparticles. *Advanced Therapeutics.*

Ahmed, R., Aucamp, M., Ebrahim, N.and Samsodien, H. (2021). Supramolecular assembly of rifampicin and PEGylated PAMAM dendrimer as a novel conjugate for tuberculosis. *Journal of Drug Delivery Science and Technology*, 66.

Alghoraibi, I., Soukkarieh, C., Zein, R., Alahmad, A., Walter, J. G.and Daghestani, M. (2020). Aqueous extract ofEucalyptus camaldulensisleaves as reducing and capping agent in biosynthesis of silver nanoparticles. *Inorganic and Nano-Metal Chemistry, 50*(10), 895-902.

Alkhalaf, M. I., Hussein, R. H.and Hamza, A. (2020). Green synthesis of silver nanoparticles by Nigella sativa extract alleviates diabetic neuropathy through anti-inflammatory and antioxidant effects. *Saudi J Biol Sci, 27*(9), 2410-2419.

Alsehli, M. (2020). Polymeric nanocarriers as stimuli-responsive systems for targeted tumor (cancer) therapy: Recent advances in drug delivery. *Saudi Pharm J, 28*(3), 255-265.

Baghbani, F.and Moztarzadeh, F. (2017). Bypassing multidrug resistant ovarian cancer using ultrasound responsive doxorubicin/curcumin co-deliver alginate nanodroplets. *Colloids Surf B Biointerfaces, 153*, 132-140.

Bahrami, B., Hojjat-Farsangi, M., Mohammadi, H., Anvari, E., Ghalamfarsa, G., Yousefi, M.and Jadidi-Niaragh, F. (2017). Nanoparticles and targeted drug delivery in cancer therapy. *Immunol Lett, 190*, 64-83.

Bahrami, F., Abdekhodaie, M. J., Behroozi, F.and Mehrvar, M. (2020). Nano mesoporous silica for cancer treatment: ROS-responsive and redox-responsive carriers. *Journal of Drug Delivery Science and Technology, 57*, 101510.

Bami, M. S., Raeisi Estabragh, M. A., Khazaeli, P., Ohadi, M.and Dehghannoudeh, G. (2021). pH-responsive drug delivery systems as intelligent carriers for targeted drug therapy: Brief history, properties, synthesis, mechanism and application. *Journal of Drug Delivery Science and Technology*, 102987.

Banala, R. R., Nagati, V. B.and Karnati, P. R. (2015). Green synthesis and characterization of Carica papaya leaf extract coated silver nanoparticles through X-ray diffraction, electron microscopy and evaluation of bactericidal properties. *Saudi J Biol Sci, 22*(5), 637-644.

Bastos, V., Ferreira de Oliveira, J. M., Brown, D., Jonhston, H., Malheiro, E., Daniel-da-Silva, A. L., Duarte, I. F., Santos, C.and Oliveira, H. (2016). The influence of Citrate or PEG coating on silver nanoparticle toxicity to a human keratinocyte cell line. *Toxicol Lett, 249*, 29-41.

Battogtokh, G., Cho, Y. Y., Lee, J. Y., Lee, H. S.and Kang, H. C. (2018). Mitochondrial-Targeting Anticancer Agent Conjugates and Nanocarrier Systems for Cancer Treatment. *Front Pharmacol, 9*, 922.

Behzad, F., Naghib, S. M., kouhbanani, M. A. J., Tabatabaei, S. N., Zare, Y.and Rhee, K. Y. (2021). An overview of the plant-mediated green synthesis of noble metal nanoparticles for antibacterial applications. *Journal of Industrial and Engineering Chemistry, 94*, 92-104.

Bessone, F., Dianzani, C., Argenzian, M., Cangemi, L., Spagnolo, R., Maione, F., Giraudo, E.and Cavalli, R. (2020). Albumin nanoformulations as an innovative solution to overcome doxorubicin chemoresistance. *Cancer Drug Resistance*.

Bilal, M., Qindeel, M., Raza, A., Mehmood, S.and Rahdar, A. (2021). Stimuli-responsive nanoliposomes as prospective nanocarriers for targeted drug delivery. *Journal of Drug Delivery Science and Technology, 66*, 102916.

Blanco, E., Shen, H.and Ferrari, M. (2015). Principles of nanoparticle design for overcoming biological barriers to drug delivery. *Nat Biotechnol, 33*(9), 941-951.

Borker, S.and Pokharkar, V. (2018). Engineering of pectin-capped gold nanoparticles for delivery of doxorubicin to hepatocarcinoma cells: an insight into mechanism of cellular uptake. *Artif Cells Nanomed Biotechnol, 46*(sup2), 826-835.

Bray, F., Ferlay, J., Soerjomataram, I., Siegel, R. L., Torre, L. A.and Jemal, A. (2018). Global cancer statistics 2018: GLOBOCAN estimates of incidence and mortality worldwide for 36 cancers in 185 countries. *CA Cancer J Clin, 68*(6), 394-424.

Caldera, F., Nistico, R., Magnacca, G., Matencio, A., Khazaei Monfared, Y.and Trotta, F. (2022). Magnetic Composites of Dextrin-Based Carbonate Nanosponges and Iron Oxide Nanoparticles with Potential Application in Targeted Drug Delivery. *Nanomaterials (Basel),* 12(5).

Cao, Z., Li, W., Liu, R., Li, X., Li, H., Liu, L., Chen, Y., Lv, C.and Liu, Y. (2019). pH- and enzyme-triggered drug release as an important process in the design of anti-tumor drug delivery systems. *Biomed Pharmacother, 118,* 109340.

Carvalho, J., Paiva, A., Cabral Campello, M. P., Paulo, A., Mergny, J. L., Salgado, G. F., Queiroz, J. A.and Cruz, C. (2019). Aptamer-based Targeted Delivery of a G-quadruplex Ligand in Cervical Cancer Cells. *Sci Rep, 9*(1), 7945.

Chen, C., Ke, J., Zhou, X. E., Yi, W., Brunzelle, J. S., Li, J., Yong, E. L., Xu, H. E.and Melcher, K. (2013). Structural basis for molecular recognition of folic acid by folate receptors. *Nature, 500*(7463), 486-489.

Chen, Q., Jia, C., Xu, Y., Jiang, Z., Hu, T., Li, C.and Cheng, X. (2022). Dual-pH responsive chitosan nanoparticles for improving in vivo drugs delivery and chemoresistance in breast cancer. *Carbohydrate Polymers, 290*, 119518.

Chiang, Y. T., Yen, Y. W.and Lo, C. L. (2015). Reactive oxygen species and glutathione dual redox-responsive micelles for selective cytotoxicity of cancer. *Biomaterials, 61*, 150-161.

Ciolkowski, M., Petersen, J. F., Ficker, M., Janaszewska, A., Christensen, J. B., Klajnert, B.and Bryszewska, M. (2012). Surface modification of PAMAM dendrimer improves its biocompatibility. *Nanomedicine, 8*(6), 815-817.

Constantin, M., Bucatariu, S., Popescu, I., Cosman, B., Ascenzi, P.and Fundueanu, G. (2021). Intelligent micro-vehicles for drug transport and controlled release to cancer cells. *Reactive and Functional Polymers, 165*, 104961.

Corciova, A.and Ivanescu, B. (2018). Biosynthesis, characterisation and therapeutic applications of plant-mediated silver nanoparticles. *Journal of the Serbian Chemical Society, 83*(5), 515-538.

Corma, A., Botella, P.and Rivero-Buceta, E. (2022). Silica-Based Stimuli-Responsive Systems for Antitumor Drug Delivery and Controlled Release. *Pharmaceutics, 14*(1).

Danhier, F., Feron, O.and Preat, V. (2010). To exploit the tumor microenvironment: Passive and active tumor targeting of nanocarriers for anti-cancer drug delivery. *J Control Release, 148*(2), 135-146.

Dare, E. O., Makinde, O. W., Ogundele, K. T., Osinkolu, G. A., Fasasi, Y. A., Sonde, I., Bamgbose, J. T., Maaza, M., Sithole, J., Ezema, F.and Adewoye, O. O. (2012). Zinc-Salt-Mediated Synthesis, Growth Kinetic, and Shaped Evolution of Silver Nanoparticles. *ISRN Nanomaterials, 2012*, 1-8.

Davis, P. H. (1972) Flora of Turkey and East Egean Island, Volume4. Edinburg Universty Press, page 6-8.

De Lazaro, I.and Mooney, D. J. (2021). Obstacles and opportunities in a forward vision for cancer nanomedicine. *Nat Mater, 20*(11), 1469-1479.

Deivanathan, S. K.and Prakash, J. T. J. (2022). Green synthesis of silver nanoparticles using aqueous leaf extract of Guettarda Speciosa and its antimicrobial and anti-oxidative properties. *Chemical Data Collections, 38*, 100831.

Delaney, G., Jacob, S., Featherstone, C.and Barton, M. (2005). The role of radiotherapy in cancer treatment: estimating optimal utilization from a review of evidence-based clinical guidelines. *Cancer, 104*(6), 1129-1137.

Desai, R., Mankad, V., Gupta, S.and Jha, P. (2012). Size Distribution of Silver Nanoparticles: UV-Visible Spectroscopic Assessment. *Nanoscience and Nanotechnology Letters, 4*(1), 30-34.

Díaz-Cruz, C., Alonso Nuñez, G., Espinoza-Gómez, H.and Flores-López, L. Z. (2016). Effect of molecular weight of PEG or PVA as reducing-stabilizing agent in the green synthesis of silver-nanoparticles. *European Polymer Journal, 83*, 265-277.

Diaz-Ruiz, R., Rigoulet, M.and Devin, A. (2011). The Warburg and Crabtree effects: On the origin of cancer cell energy metabolism and of yeast glucose repression. *Biochim Biophys Acta, 1807*(6), 568-576.

Dong, X., Sun, Z., Wang, X., Zhu, D., Liu, L.and Leng, X. (2017). Simultaneous monitoring of the drug release and antitumor effect of a novel drug delivery system-MWCNTs/DOX/TC. *Drug Deliv, 24*(1), 143-151.

Dos Santos, A. l. F., De Almeida, D. R. Q., Terra, L. F., Baptista, M. c. S.and Labriola, L. (2019). Photodynamic therapy in cancer treatment - an update review. *Journal of Cancer Metastasis and Treatment*, 2019.

Dutt, A.and Upadhyay, L. S. B. (2018). Synthesis of Cysteine-Functionalized Silver Nanoparticles Using Green Tea Extract with Application for Lipase Immobilization. *Analytical Letters, 51*(7), 1071-1086.

Dutta, B., Barick, K. C.and Hassan, P. A. (2021). Recent advances in active targeting of nanomaterials for anticancer drug delivery. *Adv Colloid Interface Sci, 296*, 102509.

El-Hammadi, M. M.and Arias, J. L. (2022). Recent Advances in the Surface Functionalization of PLGA-Based Nanomedicines. *Nanomaterials, 12*(3), 354.

El-Naggar, N. E., Hussein, M. H.and El-Sawah, A. A. (2017). Bio-fabrication of silver nanoparticles by phycocyanin, characterization, in vitro anticancer activity against breast cancer cell line and in vivo cytotxicity. *Sci Rep, 7*(1), 10844.

Elemike, E. E., Onwudiwe, D. C., Arijeh, O.and Nwankwo, H. U. (2017). Plant-mediated biosynthesis of silver nanoparticles by leaf extracts of Lasienthra africanum and a study of the influence of kinetic parameters. *Bulletin of Materials Science, 40*(1), 129-137.

Elfiyani, R., Srifiana, Y.and Al Rasyied, F. D. (2018). Curcumin encapsulation using dendrimer PAMAM G4 conjugated with polyethylene glycol to improve the properties of gel dossage form. *Pharmaciana, 8*(1).

Elnair, R., Choate, J.and Jamous, F. (2018). A Poorly Differentiated Lung Malignancy in a Young Adult. *JAMA Oncol, 4*(12), 1773-1774.

EMEA. (2000). Committee for veterinary medicinal products prunus laurocerasus summary report. *e European Agency for the Evaluation of Medicinal Products Veterinary Medicines Evaluation Unit*, mea/mrl/675/99-final.

F. Benyettou, R. R., F. Ravaux, T. Jaber, K. Blumer, M. Jouiad, L. Motte, J.-C. Olsen, C. Platas-Iglesias, M. Magzoub,and A. Trabolsia. (2013). Synthesis of Silver Nanoparticles for the Dual Delivery of Doxorubicin and Alendronate to Cancer Cells. *Journal of Material Chemistry B*.

Fadaka, A., Ajiboye, B., Ojo, O., Adewale, O., Olayide, I.and Emuowhochere, R. (2017). Biology of glucose metabolization in cancer cells. *Journal of Oncological Sciences, 3*(2), 45-51.

Fan Yuan, M. D., Dai Fukumura, Michael Leunig, David A. Berk, Vladimir P. Torchilin, and Rakesh K. Jain. (1995a). Vascular Permeability in a Human Tumor Xenograft: Molecular Size Dependence and Cutoff Size. *Cancer Research, 55*, 3752-3756.

Fan Yuan, M. D., Dai Fukumura, Michael Leunig, David A. Berk, Vladimir P. Torchilin, and Rakesh K. Jain. (1995b). Vascular Permeability in a Human Tumor Xenograft: Molecular Size Dependence and Cutoff Size. *Cancer Research*, 3752-3756.

Felber, A. E., Dufresne, M. H.and Leroux, J. C. (2012). pH-sensitive vesicles, polymeric micelles, and nanospheres prepared with polycarboxylates. *Adv Drug Deliv Rev, 64*(11), 979-992.

Fleige, E., Quadir, M. A.and Haag, R. (2012). Stimuli-responsive polymeric nanocarriers for the controlled transport of active compounds: concepts and applications. *Adv Drug Deliv Rev, 64*(9), 866-884.

Fuentes-García, J. A., Alavarse, A. C., de Castro, C. E., Giacomelli, F. C., Ibarra, M. R., Bonvent, J.-J.and Goya, G. F. (2021). Sonochemical route for mesoporous silica-coated magnetic nanoparticles towards pH-triggered drug delivery system. *Journal of Materials Research and Technology, 15*, 52-67.

Gaffney J. S., N. A. M., andand D.E., J. (2012). Fourier transform infrared (FTIR) spectroscopy. *Characterization of Materials*.

Gao, J., Huang, X., Liu, H., Zan, F.and Ren, J. (2012). Colloidal stability of gold nanoparticles modified with thiol compounds: bioconjugation and application in cancer cell imaging. *Langmuir, 28*(9), 4464-4471.

Gavas, S., Quazi, S.and Karpinski, T. M. (2021). Nanoparticles for Cancer Therapy: Current Progress and Challenges. *Nanoscale Res Lett, 16*(1), 173.

Ghalehkhondabi, V., Fazlali, A.and Soleymani, M. (2022). Folic acid-conjugated pH-responsive poly(methacrylic acid) nanospheres for targeted delivery of anticancer drugs to breast cancer cells. *Journal of Molecular Liquids, 348*, 118028.

Ghassan H. Matar, G. A., Elif Kaymazlar , Muberra Andac. (2022). An Investigation of Green Synthesis of Silver Nanoparticles Using Turkish Honey Against Pathogenic Bacterial Strains. *Biointerface Research in Applied Chemistry, 13*(2), 195.

Ghosh, S., Kundu, M., Dutta, S., Mahalanobish, S., Ghosh, N., Das, J.and Sil, P. C. (2022). Enhancement of anti-neoplastic effects of cuminaldehyde against breast cancer via mesoporous silica nanoparticle based targeted drug delivery system. *Life Sci, 298*, 120525.

Gillet, J. P.and Gottesman, M. M. (2010). Mechanisms of multidrug resistance in cancer. *Methods Mol Biol, 596*, 47-76.

Gocheva, G.and Ivanova, A. (2019). A Look at Receptor-Ligand Pairs for Active-Targeting Drug Delivery from Crystallographic and Molecular Dynamics Perspectives. *Mol Pharm, 16*(8), 3293-3321.

Guan, Z., Ying, S., Ofoegbu, P. C., Clubb, P., Rico, C., He, F.and Hong, J. (2022). Green synthesis of nanoparticles: Current developments and limitations. *Environmental Technology & Innovation*, 102336.

Hanurry, E. Y., Mekonnen, T. W., Andrgie, A. T., Darge, H. F., Birhan, Y. S., Hsu, W. H., Chou, H. Y., Cheng, C. C., Lai, J. Y.and Tsai, H. C. (2020). Biotin-Decorated PAMAM G4.5 Dendrimer Nanoparticles to Enhance the Delivery, Anti-Proliferative, and Apoptotic Effects of Chemotherapeutic Drug in Cancer Cells. *Pharmaceutics, 12*(5).

Hassanpour, M., Jafari, H., Sharifi, S., Rezaie, J., Lighvan, Z. M., Mahdavinia, G. R., Gohari, G.and Akbari, A. (2021). Salicylic acid-loaded chitosan nanoparticles (SA/CTS NPs) for breast cancer targeting: Synthesis, characterization and controlled release kinetics. *Journal of Molecular Structure, 1245*, 131040.

He, Z. Y., Chu, B. Y., Wei, X. W., Li, J., Edwards, C. K., 3rd, Song, X. R., He, G., Xie, Y. M., Wei, Y. Q.and Qian, Z. Y. (2014). Recent development of poly(ethylene glycol)-cholesterol conjugates as drug delivery systems. *Int J Pharm, 469*(1), 168-178.

Hekmat, A., Saboury, A. A.and Divsalar, A. (2012). The effects of silver nanoparticles and doxorubicin combination on DNA structure and its antiproliferative effect against T47D and MCF7 cell lines. *J Biomed Nanotechnol, 8*(6), 968-982.

Hekmati, M., Hasanirad, S., Khaledi, A.and Esmaeili, D. (2020). Green synthesis of silver nanoparticles using extracts of Allium rotundum l, Falcaria vulgaris Bernh, and Ferulago angulate Boiss, and their antimicrobial effects in vitro. *Gene Reports, 19*, 100589.

Helmy, L. A., Abdel-Halim, M., Hassan, R., Sebak, A., Farghali, H. A. M., Mansour, S.and Tammam, S. N. (2021). The other side to the use of active targeting ligands; the case of folic acid in the targeting of breast cancer. *Colloids Surf B Biointerfaces, 211*, 112289.

Hepokur, C., Kariper, I. A., Misir, S., Ay, E., Tunoglu, S., Ersez, M. S., Zeybek, U., Kuruca, S. E.and Yaylim, I. (2019). Silver nanoparticle/capecitabine for breast cancer cell treatment. *Toxicol In Vitro, 61*, 104600.

Heredia-Guerrero, J. A., Benitez, J. J., Dominguez, E., Bayer, I. S., Cingolani, R., Athanassiou, A.and Heredia, A. (2014). Infrared and Raman spectroscopic features of plant cuticles: a review. *Front Plant Sci, 5*, 305.

Hidayat, M. I., Adlim, M., Maulana, I., Suhartono, S., Hayati, Z.and Bakar, N. H. H. A. (2022). Green synthesis of chitosan-stabilized silver-colloidal nanoparticles immobilized on white-silica-gel beads and the antibacterial activities in a simulated-air-filter. *Arabian Journal of Chemistry, 15*(2), 103596.

Huang, D., Sun, L., Huang, L.and Chen, Y. (2021). Nanodrug Delivery Systems Modulate Tumor Vessels to Increase the Enhanced Permeability and Retention Effect. *J Pers Med, 11*(2).

Huckaby, J. T.and Lai, S. K. (2018). PEGylation for enhancing nanoparticle diffusion in mucus. *Adv Drug Deliv Rev, 124*, 125-139.

Huda, S., Alam, M. A.and Sharma, P. K. (2020). Smart nanocarriers-based drug delivery for cancer therapy: An innovative and developing strategy. *Journal of Drug Delivery Science and Technology, 60*, 102018.

Hughes, A. S. (2015). Biosensing on the End of an Optical Fiber.

Hussain, S. M., Hess, K. L., Gearhart, J. M., Geiss, K. T.and Schlager, J. J. (2005). In vitro toxicity of nanoparticles in BRL 3A rat liver cells. *Toxicol In Vitro, 19*(7), 975-983.

Jagpreet Singh, G. K., Pawanpreet Kaur, Rajat Bajaj and Mohit Rawat. (2016). A Review on Green Synthesis and Characterization of Silver Nanoparticles and Their Applications: A Green Nanoworld. *World Journal of Pharmacy and Pharmaceutical Sciences*, 730-762.

Jeffrey S. Gaffney, N. A. M., andand Jones, D. E. (2012). Fourıer transform infrared (FTIR) spectroscopy. *Characterization of Materials*.

Jeong, J. H., An, J. Y., Kwon, Y. T., Rhee, J. G.and Lee, Y. J. (2009). Effects of low dose quercetin: cancer cell-specific inhibition of cell cycle progression. *J Cell Biochem, 106*(1), 73-82.

Jiang, Y. Y., Tang, G. T., Zhang, L. H., Kong, S. Y., Zhu, S. J.and Pei, Y. Y. (2010). PEGylated PAMAM dendrimers as a potential drug delivery carrier: in vitro and in vivo comparative evaluation of covalently conjugated drug and noncovalent drug inclusion complex. *J Drug Target, 18*(5), 389-403.

Jokerst, J. V., Lobovkina, T., Zare, R. N.and Gambhir, S. S. (2011). Nanoparticle PEGylation for imaging and therapy. *Nanomedicine (Lond), 6*(4), 715-728.

Jose, S., A, C. T., Sebastian, R., H, S. M., A, A. N., Durazzo, A., Lucarini, M., Santini, A.and Souto, E. B. (2019). Transferrin-Conjugated Docetaxel-PLGA Nanoparticles for Tumor Targeting: Influence on MCF-7 Cell Cycle. *Polymers (Basel), 11*(11).

Kalyane, D., Raval, N., Maheshwari, R., Tambe, V., Kalia, K.and Tekade, R. K. (2019). Employment of enhanced permeability and retention effect (EPR): Nanoparticle-based precision tools for targeting of therapeutic and diagnostic agent in cancer. *Mater Sci Eng C Mater Biol Appl, 98*, 1252-1276.

Kambale, E. K., Nkanga, C. I., Mutonkole, B. I., Bapolisi, A. M., Tassa, D. O., Liesse, J. I., Krause, R. W. M.and Memvanga, P. B. (2020). Green synthesis of antimicrobial silver nanoparticles using aqueous leaf extracts from three Congolese plant species (Brillantaisia patula, Crossopteryx febrifuga and Senna siamea). *Heliyon, 6*(8), e04493.

Kannan, R. M., Nance, E., Kannan, S.and Tomalia, D. A. (2014). Emerging concepts in dendrimer-based nanomedicine: from design principles to clinical applications. *J Intern Med, 276*(6), 579-617.

Karabegović, I. T., Stojičević, S. S., Veličković, D. T., Nikolić, N. Č.and Lazić, M. L. (2013). Optimization of microwave-assisted extraction and characterization of phenolic compounds in cherry laurel (Prunus laurocerasus) leaves. *Separation and Purification Technology, 120*, 429-436.

Karabegović, I. T., Stojičević, S. S., Veličković, D. T., Todorović, Z. B., Nikolić, N. Č.and Lazić, M. L. (2014). The effect of different extraction techniques on the composition and antioxidant activity of cherry laurel (Prunus laurocerasus) leaf and fruit extracts. *Industrial Crops and Products, 54*, 142-148.

Keles, E., Hazer, B.and Comert, F. B. (2013). Synthesis of antibacterial amphiphilic elastomer based on polystyrene-block-polyisoprene-block-polystyrene via thiol-ene addition. *Mater Sci Eng C Mater Biol Appl, 33*(3), 1061-1066.

Khutale, G. V.and Casey, A. (2017). Synthesis and characterization of a multifunctional gold-doxorubicin nanoparticle system for pH triggered intracellular anticancer drug release. *European Journal of Pharmaceutics and Biopharmaceutics, 119*, 372-380.

Kim, S. H.and Choi, K. C. (2013). Anti-cancer Effect and Underlying Mechanism(s) of Kaempferol, a Phytoestrogen, on the Regulation of Apoptosis in Diverse Cancer Cell Models. *Toxicol Res, 29*(4), 229-234.

Knop, K., Hoogenboom, R., Fischer, D.and Schubert, U. S. (2010). Poly(ethylene glycol) in drug delivery: pros and cons as well as potential alternatives. *Angew Chem Int Ed Engl, 49*(36), 6288-6308.

Krishnaraj, C., Ramachandran, R., Mohan, K.and Kalaichelvan, P. T. (2012). Optimization for rapid synthesis of silver nanoparticles and its effect on phytopathogenic fungi. *Spectrochim Acta A Mol Biomol Spectrosc, 93*, 95-99.

Kumari, P., Ghosh, B.and Biswas, S. (2016). Nanocarriers for cancer-targeted drug delivery. *J Drug Target, 24*(3), 179-191.

Kurtoglu, Y. E., Mishra, M. K., Kannan, S.and Kannan, R. M. (2010). Drug release characteristics of PAMAM dendrimer-drug conjugates with different linkers. *Int J Pharm, 384*(1-2), 189-194.

Li, H., Cheng, Z., Wang, Y., Zhou, D., Su, M., Wang, X., He, P.and Zhang, Y. (2020). Self-Assembled Star-Shaped sPCL–PEG Copolymer Nanomicelles with pH-Sensitivity for Anticancer Drug Delivery. *Macromolecular Chemistry and Physics, 222*(3), 2000379.

Li, S., Dai, W., Yin, Z.-Z., Gao, J., Wu, D.and Kong, Y. (2020). Synthesis of oxidized pullulan coated mesoporous silica for pH-sensitive drug delivery. *European Polymer Journal, 122*, 109399.

Li, Y., He, H., Lu, W.and Jia, X. (2017). A poly(amidoamine) dendrimer-based drug carrier for delivering DOX to gliomas cells. *RSC Advances, 7*(25), 15475-15481.

Litwin, M. S.and Tan, H. J. (2017). The Diagnosis and Treatment of Prostate Cancer: A Review. *JAMA, 317*(24), 2532-2542.

Liu, Y., Wang, W., Yang, J., Zhou, C.and Sun, J. (2013). pH-sensitive polymeric micelles triggered drug release for extracellular and intracellular drug targeting delivery. *Asian Journal of Pharmaceutical Sciences, 8*(3), 159-167.

Liu, Z., Zhang, Y., Shen, N., Sun, J., Tang, Z.and Chen, X. (2022). Destruction of tumor vasculature by vascular disrupting agents in overcoming the limitation of EPR effect. *Adv Drug Deliv Rev, 183*, 114138.

Long, W., Ouyang, H., Zhou, C., Wan, W., Yu, S., Qian, K., Liu, M., Zhang, X., Feng, Y.and Wei, Y. (2020). A novel one-pot strategy for fabrication of PEGylated MoS2 composites for pH responsive controlled drug delivery. *Journal of Molecular Liquids, 307*, 112962.

Lyon, P. C., Gray, M. D., Mannaris, C., Folkes, L. K., Stratford, M., Campo, L., Chung, D. Y. F., Scott, S., Anderson, M., Goldin, R., Carlisle, R., Wu, F., Middleton, M. R., Gleeson, F. V.and Coussios, C. C. (2018). Safety and feasibility of ultrasound-triggered targeted drug delivery of doxorubicin from thermosensitive liposomes in liver tumours (TARDOX): a single-centre, open-label, phase 1 trial. *The Lancet Oncology, 19*(8), 1027-1039.

Lyon, P. C., Griffiths, L. F., Lee, J., Chung, D., Carlisle, R., Wu, F., Middleton, M. R., Gleeson, F. V.and Coussios, C. C. (2017). Clinical trial protocol for TARDOX: a phase I study to investigate the feasibility of targeted release of lyso-thermosensitive liposomal doxorubicin (ThermoDox(R)) using focused ultrasound in patients with liver tumours. *J Ther Ultrasound, 5*, 28.

Ma, H., Zhang, X., Pang, L., Yu, B., Cong, H.and Shen, Y. (2022). Mn-dox metal-organic nanoparticles for cancer therapy and magnetic resonance imaging. *Dyes and Pigments, 199*, 110080.

Ma, J., Lu, X.and Huang, Y. (2011). Genomic analysis of cytotoxicity response to nanosilver in human dermal fibroblasts. *J Biomed Nanotechnol, 7*(2), 263-275.

Maes-Carballo, M., Munoz-Nunez, I., Martin-Diaz, M., Mignini, L., Bueno-Cavanillas, A.and Khan, K. S. (2020). Shared decision making in breast cancer treatment guidelines: Development of a quality assessment tool and a systematic review. *Health Expect, 23*(5), 1045-1064.

Mallick, A., More, P., Ghosh, S., Chippalkatti, R., Chopade, B. A., Lahiri, M.and Basu, S. (2015). Dual drug conjugated nanoparticle for simultaneous targeting of mitochondria and nucleus in cancer cells. *ACS Appl Mater Interfaces, 7*(14), 7584-7598.

Manchun, S., Dass, C. R.and Sriamornsak, P. (2012). Targeted therapy for cancer using pH-responsive nanocarrier systems. *Life Sci, 90*(11-12), 381-387.

Mariadoss, A. V. A., Saravanakumar, K., Sathiyaseelan, A., Karthikkumar, V.and Wang, M. H. (2022). Smart drug delivery of p-Coumaric acid loaded aptamer conjugated starch nanoparticles for effective triple-negative breast cancer therapy. *Int J Biol Macromol, 195*, 22-29.

McGuigan, A., Kelly, P., Turkington, R. C., Jones, C., Coleman, H. G.and McCain, R. S. (2018). Pancreatic cancer: A review of clinical diagnosis, epidemiology, treatment and outcomes. *World J Gastroenterol, 24*(43), 4846-4861.

Mehta, B. K., Chhajlani, M.and Shrivastava, B. D. (2017). Green synthesis of silver nanoparticles and their characterization by XRD. *Journal of Physics: Conference Series, 836*.

Melkamu, W. W.and Bitew, L. T. (2021). Green synthesis of silver nanoparticles using Hagenia abyssinica (Bruce) J.F. Gmel plant leaf extract and their antibacterial and anti-oxidant activities. *Heliyon, 7*(11), e08459.

Miranda, R. R., Sampaio, I.and Zucolotto, V. (2022). Exploring silver nanoparticles for cancer therapy and diagnosis. *Colloids Surf B Biointerfaces, 210*, 112254.

Mishra, P., Nayak, B.and Dey, R. K. (2016). PEGylation in anti-cancer therapy: An overview. *Asian Journal of Pharmaceutical Sciences, 11*(3), 337-348.

Mo, X., Wu, F., Li, Y.and Cai, X. (2021). Hyaluronic acid-functionalized halloysite nanotubes for targeted drug delivery to CD44-overexpressing cancer cells. *Materials Today Communications, 28*, 102682.

Mohamed, N. (2020). Synthesis of Hybrid Chitosan Silver Nanoparticles Loaded with Doxorubicin with Promising Anti-cancer Activity. *BioNanoScience, 10*(3), 758-765.

Nair, G. M., Sajini, T.and Mathew, B. (2022). Advanced green approaches for metal and metal oxide nanoparticles synthesis and their environmental applications. *Talanta Open, 5*, 100080.

Nakhaeepour, Z., Mashreghi, M., Matin, M. M., NakhaeiPour, A.and Housaindokht, M. R. (2019). Multifunctional CuO nanoparticles with cytotoxic effects on KYSE30 esophageal cancer cells, antimicrobial and heavy metal sensing activities. *Life Sci, 234*, 116758.

Nandi, U., Onyesom, I.and Douroumis, D. (2021). Transferrin conjugated Stealth liposomes for sirolimus active targeting in breast cancer. *Journal of Drug Delivery Science and Technology, 66*, 102900.

Nirmala, R., Kang, H. S., Park, H. M., Navamathavan, R., Jeong, I. S.and Kim, H. Y. (2012). Silver-loaded biomimetic hydroxyapatite grafted poly(epsilon-caprolactone) composite nanofibers: a cytotoxicity study. *J Biomed Nanotechnol, 8*(1), 125-132.

Ochekpe N. A., O. P. O. a. N. N. C. (2009). Nanotechnology and Drug Delivery Part 2: Nanostructures for Drug Delivery. *Tropical Journal of Pharmaceutical Research*, 275-287.

Pan, G., Lemmouchi, Y., Akala, E. O.and Bakare, O. (2016). Studies on PEGylated and Drug-Loaded PAMAM Dendrimers. *Journal of Bioactive and Compatible Polymers, 20*(1), 113-128.

Parmar, M.and Sanyal, M. (2022). Extensive study on plant mediated green synthesis of metal nanoparticles and their application for degradation of cationic and anionic dyes. *Environmental Nanotechnology, Monitoring & Management, 17*, 100624.

Pathak, S. (2021). HeLa is not a Cervical Carcinoma but a Human Breast Cancer Cell Line. *American Journal of Biomedical Science & Research, 14*(3), 294-296.

Piechutta, M.and Berghoff, A. S. (2019). New emerging targets in cancer immunotherapy: the role of Cluster of Differentiation 40 (cd40/tnfr5). *Esmo Open, 4*(Suppl 3), e000510.

Pinzaru, I., Coricovac, D., Dehelean, C., Moaca, E. A., Mioc, M., Baderca, F., Sizemore, I., Brittle, S., Marti, D., Calina, C. D., Tsatsakis, A. M.and Soica, C. (2018). Stable PEG-coated silver nanoparticles - A comprehensive toxicological profile. *Food Chem Toxicol, 111*, 546-556.

Prabhuraj, R. S., Bomb, K., Srivastava, R.and Bandyopadhyaya, R. (2020). Selection of superior targeting ligands using PEGylated PLGA nanoparticles for delivery of curcumin in the treatment of triple-negative breast cancer cells. *Journal of Drug Delivery Science and Technology, 57*, 101722.

Raj, S., Khurana, S., Choudhari, R., Kesari, K. K., Kamal, M. A., Garg, N., Ruokolainen, J., Das, B. C.and Kumar, D. (2021). Specific targeting cancer cells with nanoparticles and drug delivery in cancer therapy. *Semin Cancer Biol, 69*, 166-177.

Rajkumar, R., Ezhumalai, G.and Gnanadesigan, M. (2021). A green approach for the synthesis of silver nanoparticles by Chlorella vulgaris and its application in photocatalytic dye degradation activity. *Environmental Technology & Innovation, 21*.

Rapoport, N. (2007). Physical stimuli-responsive polymeric micelles for anti-cancer drug delivery. *Progress in Polymer Science, 32*(8-9), 962-990.

Reboredo, C., Gonzalez-Navarro, C. J., Martinez-Oharriz, C., Martinez-Lopez, A. L.and Irache, J. M. (2021). Preparation and evaluation of PEG-coated zein nanoparticles for oral drug delivery purposes. *Int J Pharm, 597*, 120287.

Reddi, B. A. (2013). Why is saline so acidic (and does it really matter?). *Int J Med Sci, 10*(6), 747-750.

Reshma, P. L., Unnikrishnan, B. S., Preethi, G. U., Syama, H. P., Archana, M. G., Remya, K., Shiji, R., Sreekutty, J.and Sreelekha, T. T. (2019). Overcoming drug-resistance in lung cancer cells by paclitaxel loaded galactoxyloglucan nanoparticles. *Int J Biol Macromol, 136*, 266-274.

Ringhieri, P., Mannucci, S., Conti, G., Nicolato, E., Fracasso, G., Marzola, P., Morelli, G.and Accardo, A. (2017). Liposomes derivatized with multimeric copies of KCCYSL peptide as targeting agents for HER-2-overexpressing tumor cells. *Int J Nanomedicine, 12*, 501-514.

Rolim, W. R., Pelegrino, M. T., de Araújo Lima, B., Ferraz, L. S., Costa, F. N., Bernardes, J. S., Rodigues, T., Brocchi, M.and Seabra, A. B. (2019). Green tea extract mediated biogenic synthesis of silver nanoparticles: Characterization, cytotoxicity evaluation and antibacterial activity. *Applied Surface Science, 463*, 66-74.

Rompicharla, S. V. K., Kumari, P., Bhatt, H., Ghosh, B.and Biswas, S. (2019). Biotin functionalized PEGylated poly(amidoamine) dendrimer conjugate for active targeting of paclitaxel in cancer. *Int J Pharm, 557*, 329-341.

Siavash Iravani, H. K., S.V. Mirmohammadi and B. Zolfaghari. (2014). Synthesis of silver nanoparticles: chemical, physical and biological methods. *Research in Pharmaceutical Sciences, 9(6)*, 385-406.

Saha, T., Makar, S., Swetha, R., Gutti, G.and Singh, S. K. (2019). Estrogen signaling: An emanating therapeutic target for breast cancer treatment. *Eur J Med Chem, 177*, 116-143.

Sakr, T. M., Khowessah, O. M., Motaleb, M. A., Abd El-Bary, A., El-Kolaly, M. T.and Swidan, M. M. (2018). I-131 doping of silver nanoparticles platform for tumor theranosis guided drug delivery. *Eur J Pharm Sci, 122*, 239-245.

Sanna, V., Pala, N.and Sechi, M. (2014). Targeted therapy using nanotechnology: focus on cancer. *Int J Nanomedicine, 9*, 467-483.

Saravanakumar, K., Mariadoss, A. V. A., Sathiyaseelan, A., Venkatachalam, K., Hu, X.and Wang, M.-H. (2021). pH-sensitive release of fungal metabolites from chitosan nanoparticles for effective cytotoxicity in prostate cancer (PC3) cells. *Process Biochemistry, 102*, 165-172.

Scheeren, L. E., Nogueira-Librelotto, D. R., Macedo, L. B., de Vargas, J. M., Mitjans, M., Vinardell, M. P.and Rolim, C. M. B. (2020). Transferrin-conjugated doxorubicin-loaded PLGA nanoparticles with pH-responsive behavior: a synergistic approach for cancer therapy. *Journal of Nanoparticle Research, 22*(3).

Schirrmacher, V. (2019). From chemotherapy to biological therapy: A review of novel concepts to reduce the side effects of systemic cancer treatment (Review). *Int J Oncol, 54*(2), 407-419.

She, W., Li, N., Luo, K., Guo, C., Wang, G., Geng, Y.and Gu, Z. (2013). Dendronized heparin-doxorubicin conjugate based nanoparticle as pH-responsive drug delivery system for cancer therapy. *Biomaterials, 34*(9), 2252-2264.

Siegel, R. L., Miller, K. D., Fuchs, H. E.and Jemal, A. (2021). Cancer Statistics, 2021. *CA Cancer J Clin, 71*(1), 7-33.

Sonju, J. J., Dahal, A., Singh, S. S., Gu, X., Johnson, W. D., Muthumula, C. M. R., Meyer, S. A.and Jois, S. D. (2022). A pH-sensitive liposome formulation of a peptidomimetic-Dox conjugate for targeting HER2 + cancer. *Int J Pharm, 612*, 121364.

Souri, M., Soltani, M., Moradi Kashkooli, F., Kiani Shahvandi, M., Chiani, M., Shariati, F. S., Mehrabi, M. R.and Munn, L. L. (2022). Towards principled design of cancer nanomedicine to accelerate clinical translation. *Mater Today Bio, 13*, 100208.

Sriram, M. I., Kanth, S. B., Kalishwaralal, K.and Gurunathan, S. (2010). Antitumor activity of silver nanoparticles in Dalton's lymphoma ascites tumor model. *Int J Nanomedicine, 5*, 753-762.

Steiger, K., Quigley, N. G., Groll, T., Richter, F., Zierke, M. A., Beer, A. J., Weichert, W., Schwaiger, M., Kossatz, S.and Notni, J. (2021). There is a world beyond alphavbeta3-integrin: Multimeric ligands for imaging of the integrin subtypes alphavbeta6, alphavbeta8, alphavbeta3, and alpha5beta1 by positron emission tomography. *EJNMMI Res, 11*(1), 106.

Stewart, C., Ralyea, C.and Lockwood, S. (2019). Ovarian Cancer: An Integrated Review. *Semin Oncol Nurs, 35*(2), 151-156. doi:10.1016/j.soncn.2019.02.001

Sujit Kumar Ghoshand Pal, T. (2007). nterparticle Coupling Effect on the Surface Plasmon Resonance of Gold Nanoparticles: From Theory to Applications. *Chem. Rev.*, 107, 4797−4862.

Sun, T., Dasgupta, A., Zhao, Z., Nurunnabi, M.and Mitragotri, S. (2020). Physical triggering strategies for drug delivery. *Adv Drug Deliv Rev, 158*, 36-62.

Susan K. Hobbs, W. L. M., Fan Yuan, W. Gregory Roberts, Linda Griffith, Vladamir P. Torchillin, Rakesh K. Jain. (1998). Regulation of transport pathways in tumor vessels: Role of tumor type and microenvironment. *Proc. Natl. Acad. Sci. USA ,, Vol. 95*, pp. 4607–4612.

Swanner, J., Fahrenholtz, C. D., Tenvooren, I., Bernish, B. W., Sears, J. J., Hooker, A., Furdui, C. M., Alli, E., Li, W., Donati, G. L., Cook, K. L., Vidi, P. A.and Singh, R. (2019). Silver nanoparticles selectively treat triple-negative breast cancer cells without affecting non-malignant breast epithelial cells in vitro and in vivo. *FASEB Bioadv, 1*(10), 639-660.

Tailor, G., Yadav, B. L., Chaudhary, J., Joshi, M.and Suvalka, C. (2020). Green synthesis of silver nanoparticles using Ocimum canum and their anti-bacterial activity. *Biochem Biophys Rep, 24*, 100848.

Taleb A., C. Petitand Pileni, M. P. (1998). Optical Properties of Self-Assembled 2D and 3D Superlattices of Silver Nanoparticles. *J. Phys. Chem. B*, 102, 2214-2220.

Tamilarasi, P.and Meena, P. (2020). Green synthesis of silver nanoparticles (AgNPs) using Gomphrena globosa (Globe amaranth) leaf extract and their characterization. *Materials Today: Proceedings, 33*, 2209-2216.

Tavano, L.and Muzzalupo, R. (2016). Multi-functional vesicles for cancer therapy: The ultimate magic bullet. *Colloids Surf B Biointerfaces, 147*, 161-171.

Theek, B., Gremse, F., Kunjachan, S., Fokong, S., Pola, R., Pechar, M., Deckers, R., Storm, G., Ehling, J., Kiessling, F.and Lammers, T. (2014). Characterizing EPR-mediated passive drug targeting using contrast-enhanced functional ultrasound imaging. *J Control Release, 182*, 83-89.

ThermoScientific. (2011). ThermoScientific. Instructions NHS and Sulfo-NHS. Technical Report 24500, PierceBiotechnology, Rockford, IL, 20. ThermoScientific. Instructions NHS and Sulfo-NHS. Technical Report 24500, *PierceBiotechnology, Rockford, IL*, 2011.

Thiagarajan G., R. A., Malugin A. and Ghandehari H. (2010). PAMAM-Camptothecin Conjugate Inhibits Proliferation and Induces Nuclear Fragmentation in Colorectal Carcinoma Cells. *Pharm Res*, 2307–2316.

Thornton, P. D., McConnell, G.and Ulijn, R. V. (2005). Enzyme responsive polymer hydrogel beads. *Chem Commun (Camb)*(47), 5913-5915.

Tian, M., Xin, X., Wu, R., Guan, W.and Zhou, W. (2022). Advances in Intelligent-Responsive Nanocarriers for Cancer Therapy. *Pharmacological Research*, 106184.

Tian, S., Hu, Y., Chen, X., Liu, C., Xue, Y.and Han, B. (2022). Green synthesis of silver nanoparticles using sodium alginate and tannic acid: characterization and anti-S. aureus activity. *Int J Biol Macromol, 195*, 515-522.

Tsujimoto, A., Uehara, H., Yoshida, H., Nishio, M., Furuta, K., Inui, T., Matsumoto, A., Morita, S., Tanaka, M.and Kojima, C. (2021). Different hydration states and passive tumor targeting ability of polyethylene glycol-modified dendrimers with high and low PEG density. *Mater Sci Eng C Mater Biol Appl, 126*, 112159.

Vu, M. T., Bach, L. G., Nguyen, D. C., Ho, M. N., Nguyen, N. H., Tran, N. Q., Nguyen, D. H., Nguyen, C. K.and Hoang Thi, T. T. (2019). Modified Carboxyl-Terminated PAMAM Dendrimers as Great Cytocompatible Nano-Based Drug Delivery System. *Int J Mol Sci, 20*(8).

Waks, A. G.and Winer, E. P. (2019). Breast Cancer Treatment: A Review. *JAMA, 321*(3), 288-300.

Wang, H., Zhu, Y., Hao, C., Fan, J., Liu, Y.and Wang, Y. (2019). Establishment of a drug-resistant human cervical cancer cell line and research on its drug-resistance. *J Cancer Res Ther, 15*(6), 1221-1225.

Wang, J., Li, Y.and Nie, G. (2021). Multifunctional biomolecule nanostructures for cancer therapy. *Nat Rev Mater, 6*(9), 766-783.

Wang, Y., Shim, M. S., Levinson, N. S., Sung, H. W.and Xia, Y. (2014). Stimuli-Responsive Materials for Controlled Release of Theranostic Agents. *Adv Funct Mater, 24*(27), 4206-4220.

Wang, Z., Deng, X., Ding, J., Zhou, W., Zheng, X.and Tang, G. (2018). Mechanisms of drug release in pH-sensitive micelles for tumour targeted drug delivery system: A review. *Int J Pharm, 535*(1-2), 253-260.

Warburg, O. (1956a). On the origin of cancer cells. *Science,* Volume 123, Number 3191.

Warburg, O. (1956b). On the Origin of Cancer Cells. *Science, 123*(3191).

Wike-Hooley J. L., J. H. a. H. S. R. (1984). The relevance of tumour pH to the treatment of malignant disease. *Radiotherapy and Oncology, 2* 343 366.

Wike-Hooley J. L., J. H. a. H. S. R. (1984). The relevance of tumour pH to the treatment of malignant disease. *Radiotherapy and Oncology*, 2, 343-366.

Wicki, A., Witzigmann, D., Balasubramanian, V.and Huwyler, J. (2015). Nanomedicine in cancer therapy: challenges, opportunities, and clinical applications. *J Control Release, 200*, 138-157.

Xie, J., Fan, Z., Li, Y., Zhang, Y., Yu, F., Su, G., Xie, L.and Hou, Z. (2018). Design of pH-sensitive methotrexate prodrug-targeted curcumin nanoparticles for efficient dual-drug delivery and combination cancer therapy. *Int J Nanomedicine, 13*, 1381-1398.

Xie, J., Zhang, Y., Yan, C., Song, L., Wen, S., Zang, F., Chen, G., Ding, Q., Yan, C.and Gu, N. (2014). High-performance PEGylated Mn-Zn ferrite nanocrystals as a passive-targeted agent for magnetically induced cancer theranostics. *Biomaterials, 35*(33), 9126-9136.

Xing, R., Bhirde, A. A., Wang, S., Sun, X., Liu, G., Hou, Y.and Chen, X. (2012). Hollow iron oxide nanoparticles as multidrug resistant drug delivery and imaging vehicles. *Nano Research, 6*(1), 1-9.

Yang, L., Gao, Y., Liu, J., Zhang, Y., Ren, C., Wang, J., Wang, Z., Liu, J., Chu, L., Wang, W.and Huang, F. (2018). Silver-Coated Nanoparticles Combined with Doxorubicin for Enhanced Anticancer Therapy. *J Biomed Nanotechnol, 14*(2), 312-320.

Yang, M., Zhao, H., Zhang, Z., Yuan, Q., Feng, Q., Duan, X., Wang, S.and Tang, Y. (2021). CO/light dual-activatable Ru(ii)-conjugated oligomer agent for lysosome-targeted multimodal cancer therapeutics. *Chem Sci, 12*(34), 11515-11524.

Yang, T., Xu, L., Li, B., Li, W., Ma, X., Fan, L., Lee, R. J., Xu, C.and Xiang, G. (2017). Antitumor activity of a folate receptor-targeted immunoglobulin G-doxorubicin conjugate. *Int J Nanomedicine, 12*, 2505-2515.

Yang, X., Zhai, D., Song, J., Qing, R., Wang, B., Ji, J., Chen, X.and Hao, S. (2020). Rhein-PEG-nHA conjugate as a bone targeted drug delivery vehicle for enhanced cancer chemoradiotherapy. *Nanomedicine, 27,* 102196.

Youbei Qiao, B. L., Yifan Peng, Erlong Ji and Hong Wu. (2018). Preparation and biological evaluation of a novel pH-sensitive poly (β-malic acid) conjugate for antitumor drug delivery. *International Journal of Molecular Medicine, 42:* 3495-3502.

Yousaf, H., Mehmood, A., Ahmad, K. S.and Raffi, M. (2020). Green synthesis of silver nanoparticles and their applications as an alternative antibacterial and antioxidant agents. *Mater Sci Eng C Mater Biol Appl, 112*, 110901.

Yu, X., Trase, I., Ren, M., Duval, K., Guo, X.and Chen, Z. (2016). Design of Nanoparticle-Based Carriers for Targeted Drug Delivery. *J Nanomater*, 2016.

Yuan, L., Tang, Q., Yang, D., Zhang, J. Z., Zhang, F.and Hu, J. (2011). Preparation of pH-Responsive Mesoporous Silica Nanoparticles and Their Application in Controlled Drug Delivery. *The Journal of Physical Chemistry C, 115*(20), 9926-9932.

Zarei, Z., Razmjoue, D.and Karimi, J. (2020). Green Synthesis of Silver Nanoparticles from Caralluma tuberculata Extract and its Antibacterial Activity. *Journal of Inorganic and Organometallic Polymers and Materials, 30*(11), 4606-4614.

Zhai, J., Luwor, R. B., Ahmed, N., Escalona, R., Tan, F. H., Fong, C., Ratcliffe, J., Scoble, J. A., Drummond, C. J.and Tran, N. (2018). Paclitaxel-Loaded Self-Assembled Lipid Nanoparticles as Targeted Drug Delivery Systems for the Treatment of Aggressive Ovarian Cancer. *ACS Appl Mater Interfaces, 10*(30), 25174-25185.

Zhang, M., Zhu, J., Zheng, Y., Guo, R., Wang, S., Mignani, S., Caminade, A. M., Majoral, J. P.and Shi, X. (2018). Doxorubicin-Conjugated PAMAM Dendrimers for pH-Responsive Drug Release and Folic Acid-Targeted Cancer Therapy. *Pharmaceutics, 10*(3).

Zhang, P., Huang, H., Banerjee, S., Clarkson, G. J., Ge, C., Imberti, C.and Sadler, P. J. (2019). Nucleus-Targeted Organoiridium-Albumin Conjugate for Photodynamic Cancer Therapy. *Angew Chem Int Ed Engl, 58*(8), 2350-2354.

Zhang, W.-L., Li, N., Huang, J., Yu, J.-H., Wang, D.-X., Li, Y.-P.and Liu, S.-Y. (2010). Gadolinium-conjugated FA-PEG-PAMAM-COOH nanoparticles as potential tumor-targeted circulation-prolonged macromolecular MRI contrast agents. *Journal of Applied Polymer Science*, n/a-n/a.

Zhao, F.and Li, W. (2011). Dendrimer/inorganic nanomaterial composites: Tailoring preparation, properties, functions, and applications of inorganic nanomaterials with dendritic architectures. *Science China Chemistry, 54*(2), 286-301.

Zhou, X., Shi, K., Hao, Y., Yang, C., Zha, R., Yi, C.and Qian, Z. (2020). Advances in nanotechnology-based delivery systems for EGFR tyrosine kinases inhibitors in cancer therapy. *Asian J Pharm Sci, 15*(1), 26-41.

Zhou, Z.-H., Zhang, R.-Q., Jia, G.-F., Wang, Y.-H., Luo, Y.-L., Xu, F.and Chen, Y.-S. (2020). Controlled release of DOX mediated by glutathione and pH dual-responsive hollow mesoporous silicon coated with polydopamine graft poly(poly(ethylene glycol) methacrylate) nanoparticles for cancer therapy. *Journal of the Taiwan Institute of Chemical Engineers, 115*, 60-70.

Zou, Y., Li, M., Xiong, T., Zhao, X., Du, J., Fan, J.and Peng, X. (2020). A Single Molecule Drug Targeting Photosensitizer for Enhanced Breast Cancer Photothermal Therapy. *Small, 16*(18), e1907677.

CURRICULUM VITAE

Güliz AKYÜZ is graduated from Çanakkale Onsekiz Mart University-Department of Food Engineering in 2011. She has completed the Master program at Ordu University-Department of Food Engineering in 2016.

Contact information:

ORCID ID : *0000-0002-3522-9716*

Publications:

1. G. AKYÜZ, E. KAYMAZLAR, H. AY, M. ANDAC & Ö. ANDAC, Extending the shelf-life of fruits by edible coating with silver nanoparticles loaded locust bean gum, Biointerface Research in Applied Chemistry, Journal, 2023.Volume 13, Issue 3, 2023, 289.

2. G.H. MATAR, G. AKYÜZ, E. KAYMAZLAR & M. ANDAC, An investigation of green synthesis of silver nanoparticles using Turkish honey against pathogenic bacterial strains, Biointerface Research in Applied Chemistry, Journal, 2022. ISSN: 2069-5837.

3. A. ELMAS, G. AKYÜZ, A. BERGAL, M. ANDAC & Ö. ANDAC, Enhanced Analytic Approach for Describing pH Triggered Fast Drug Release Systems, Current Drug Delivery, 2021,Vol:18Iss:8,1118-1124.

4. G. AKYÜZ, A. ELMAS, M. ANDAÇ & Ö. ANDAÇ, Evaluation of nano sized Mg@BTC metal organic framework as a drug carrier: A long term experimental and predictive theoretical study, The International Journal of Research on Engineering Structures and Materials (RESM), 2020, p-ISSN:2148-9807; o-ISSN:2149-4088, Vol. 7 Iss.135-156.

5. A. ELMAS, G. AKYÜZ, A. BERGAL, M. ANDAÇ & Ö. ANDAÇ, Mathematical Modelling of Drug Release, Research on Engineering Structures and Materials, 2020, p-ISSN:2148-9807; o-ISSN:2149-4088, Vol. 6 Iss.4, 327-350.

6. G. AKYÜZ & B. G. MAZI, Physicochemical and sensory characterization of bread produced from different dough formulations by *Kluyveromyces lactis*, Journal of food processing and preservation, 2020, 1745-4549, Volume 44, Issue 5, 1-10.

7. A. BERGAL, A. ELMAS & G. AKYÜZ, A New Type and Effective Approach for Anti-Cancer Drug Delivery Application: Nanosponge, Nano Research & Applications, 2019, 2471-9838, Vol.5, No.3:1, 1-10.

8. Muberra ANDAC, Cigdem DIKBAS, Guliz AKYUZ, Synthesis and Characterization Techniques of Nanoparticles, Turkish Clinics Scientific Book Chapter, 2022.

9. G. AKYÜZ, M. ANDAÇ, Ö. ANDAÇ & S. YENİGÜN, Green Synthesis of Silver Nanoparticles and Their Antimicrobial Effect on Strawberries' Shelf Life, Gıda Kimyası Kongresi, 2022, Antalya, Türkiye.

10. H. KAYACI, G. AKYÜZ, M. E. GÜRSOY, G. MATAR & M. ANDAÇ, Green Synthesis of Silver Nanoparticles by Fresh *Ginkgo Biloba* Leaf Extract, Gıda Kimyası Kongresi, 2022, Antalya, Türkiye.

11. S. YAMAN, G. AKYÜZ, M. E. GÜRSOY & M. ANDAÇ, Antifungal Activity of the Green Synthesised Silver Nanoparticles by *Quercus ithaburensis* subsp. *macrolepis*, Gıda Kimyası Kongresi, 2022, Antalya, Türkiye.

12. M. MORAL, G. AKYÜZ, M. ANDAÇ & Ö. ANDAÇ, Metal-Organic Frameworks Design and Synthesis for Cancer Therapy and Diagnosis, Oral Presentation, International Congress on Multidisciplinary Natural Sciences and Engineering, December 2021, Ankara, Türkiye.

13. E. KAYMAZLAR, G. AKYÜZ, H. AY, M. ANDAÇ & Ö. ANDAÇ, Antimicrobial Activity of The Silver Nanoparticles Loaded Locust Bean Gum Hydrogel, Poster Presentation, Uluslararası Veteriner Bilimleri Kongresi, 25-27 June 2021, Samsun, Türkiye.

14. A. GENÇ, G. AKYÜZ & S. BAYRAKTAR, The relationship between vitamin-D and athlete performance in current nanotechnological applications, Oral Presentation, 18th International Sport Sciences Congress, November 2020, Türkiye.

15. G. AKYÜZ, M. ANDAÇ & Ö. ANDAÇ, Yumurta akından elde edilen gümüş nanoparçacıkların antibakteriyel aktivitelerinin değerlendirilmesi, Poster Presentation, Türkiye 13. Gıda Kongresi, October, 2020.

16. G. AKYÜZ, A. ELMAS, E. KAYMAZLAR, M. ANDAÇ & Ö. ANDAÇ, Nanocarriers Used in Drug Delivery Systems, Oral Presentation, ISAS 2018-Winter 2nd International Symposium on Innovative Approaches in Scientific Studies, December 2018, 2618-6446, p84.

17. M. ÇİL, E. KAYMAZLAR, G. AKYÜZ, M. ANDAÇ & Ö. ANDAÇ, Synthesis and Characterization of Iron Ion Imprinted Polymer, Poster Presentation, ISAS 2018-Winter 2nd International Symposium on Innovative Approaches in Scientific Studies, November 2018, 02 December 2018.

18. G. AKYÜZ, A. ELMAS, M. ANDAÇ & Ö. ANDAÇ, Nanotechnology in Food Safety, Oral Presentation, 2nd International Unidokap Black Sea Symposium, November 2018, p146.

19. G. AKYÜZ, A. ELMAS, Ç. DİKBAŞ, M. ANDAÇ & Ö. ANDAÇ, Synthesis and Evaluation of Silver Nanoparticles by The Green Chemistry Method, Poster Presentation, 4th Nanoscience and Nanotechnology Conference, September 2018, p284.

20. G. AKYÜZ, S. TURHAN & N. Ş. ÜSTÜN, A Short Review of Üvez (rowanberry), Poster Presentation, The 4th International Symposium On traditional Foods from Adriatic To Caucasus 19-21 April 2018 Kyrenia / Northern Cyprus, April 2018, p295.

21. G. AKYÜZ & S. TURHAN, A Traditional Taste: tirit, Poster Presentation, The 4th International Symposium On traditional Foods from Adriatic To Caucasus Kyrenia / Northern Cyprus, April 2018, p346.

22. G. AKYÜZ & S. TURHAN, Sarambula With Anchovy, Poster Presentation, The 4th International Symposium On traditional Foods from Adriatic To Caucasus Kyrenia / Northern Cyprus, April 2018, p345.

23. G. AKYÜZ & B. G. MAZI, Evaluation of *Kluyveromyces Lactis* As Baker's Yeast, Poster Presentation, 1st International Tourism and Microbial Food Safety Congress, April 2016, p3.

24. G. AKYÜZ & B. G. MAZI, Farkl Formüllerdeki Roll-ekmeklerin Baz Fiziksel Ve Kimyasal Özelliklerinin Tespiti, Poster Presentation, 9. Gıda Mühendisliği Kongresi, November 2015, p80.

25. G. AKYÜZ & B. G. MAZI, Textural and Sensory Properties of Bafra Turkish Delight, Poster Presentation, The 3rd International Symposium on Traditional Foods from Adriatic To Caucasus, November 2015, p441.

26. G. AKYÜZ & B. G. MAZI, Farkl Formüllerde Hazrlanan Roll-ekmeklerin Tekstürel Ve Duyusal Olarak Değerlendirilmesi, Poster Presentation, Iç Anadolu Bölgesi 2. Tarım Ve Gıda Kongresi, April 2015, p358.

Won Awards, Incentives and Scholarships

1. 100/2000 YOK National PhD Scholarship Program in the field of Targeted Drugs.
2. 2211-C TUBITAK National PhD Scholarship Program in the Priority Fields in Science and Technology.
3. Erasmus+ exchange program at Coimbra University, Faculty of Pharmacy, Portugal.